

Response to reviews

Reviewer comments are in **bold**. Author responses are in plain text. Excerpts from the manuscript are in *italics*. Modifications to the manuscript are in *blue italics*. Page and line numbers in the responses correspond to those in the ACPD paper.

Review #1

In this work, de Sa et al. presented measurements of isoprene-derived secondary organic aerosol in central Amazonia. Specifically, using positive matrix factorization of aerosol mass spectrometry data, they isolated SOA from isoprene epoxydiol (IEPOXSOA) and showed the complex dependence of this factor on anthropogenic emissions from nearby urban area (sulfate, nitrogen oxides). This work uses field measurements to highlight some aspects of isoprene chemistry that has been shown first in laboratory and then in other field studies. I believe this work is important and should be published in ACP. I have minor comments only:

We appreciate the feedback provided by the reviewer. The revised manuscript takes into account their comments and questions. Detailed responses to each question are given below.

1. It is a little puzzling that total PM does not trend with IEPOX SOA. Given the location, I would imagine that in this area the SOA chemistry is dominated by IEPOX SOA. I understand that there will be another manuscript addressing the full PMF work, but it seems like if there is any location in the world where IEPOX SOA is most dominant, it would be in the Amazon. It seems like the remaining OA dampens some of the variations in IEPOX-SOA, leading to the rather constant total OA. Perhaps the authors can consider just briefly address why in the manuscript?

We thank the reviewer for pointing out this aspect. The manuscript has been revised to highlight this point as follows:

Line 415:

These ranges shifted to [0.35, 0.40] and [0.07, 0.18] for high sulfate concentration. ~~The magnitude of the decrease~~ As a limiting statement, for the most favorable conditions with respect to the production of IEPOX-derived PM in central Amazonia (i.e., lowest NO_y and highest sulfate), f exceeded 0.40 at 25% frequency. The implication is that at all times significant additional pathways for PM production were active. This conclusion is subject to the accuracy of the IEPOX-SOA factor loading as a scalar proxy of IEPOX-derived PM concentration (cf. discussion of Figure 1 in Section 3.1). The magnitude of the decrease in f for high sulfate concentrations suggests that IEPOX-derived PM shifted from being a major to a minor component of the PM. ~~, although the caveats related to under- and~~

~~overestimates connected to the IEPOX-SOA factor should be kept in mind (vide supra).~~

2. How is the observed sulfate produced? Are they direct emissions from Manaus, or SO₂ emitted from Manaus and converted to sulfate in the few hours of transit to the field site? In the conclusions (Ln 534-542) the discussion seems to assume that SO₂ and sulfate are equivalent. They might not be if the sulfate is coming from SO₂ oxidation in transit.

We cannot determine based on our dataset whether sulfate from Manaus is mostly primary or secondary in origin. This point is clarified in the revised manuscript in the following manner:

Line 331:

The figure shows that the distribution at T3 did not differ greatly from those of the upwind sites even though the air masses over T3 regularly transported Manaus pollution, ~~indicating that Manaus did not constitute a dominant sulfate source in the region.~~ Elevated. The implication is that Manaus sulfate sources, whether primary or secondary, had small contributions relative to background sources when averaged over time. In short, elevated sulfate concentrations on any one afternoon at the T3 site might have arisen because of elevated background concentrations on that day rather than the influence of the Manaus pollution plume.

Line 539:

Based on the findings presented herein, a reduction in sulfate sources from Manaus, ~~whether primary or secondary~~, would not be expected to considerably affect the mass concentration of IEPOX-derived species in forest regions affected by the plume.

3. Just another thought about sulfate: could sulfate just be an indicator of degree of oxidation? Since sulfate is a secondary product, it is possible that the variation in sulfate is driven by degree of processing, rather than variation in source strength. Have the authors looked at other indicators of oxidation (e.g. odd oxygen, NO_y/NO_x ratio, hydrocarbon clocks) to isolate this effect?

We appreciate the thoughtful suggestion made by the reviewer. The analysis of indicators of oxidation were complicated by several factors. Absence of NO_x, NO₂, and SO₂ data as well as low signal-to-noise ratio in toluene and benzene measurements precluded a systematic analysis on degree of processing by the several methods mentioned.

Nevertheless, the positive correlation found between IEPOX-SOA factor loadings and sulfate concentrations can be taken as an indication that sulfate variability was not prevalently associated with degree of oxidation. Hu et al. (2015) showed an inverse relationship between *f*₄₄ (the AMS marker for degree of oxidation) and *f*₈₂ (the AMS

marker for IEPOX-SOA). Therefore, if sulfate concentration was mostly an indicator of degree of oxidation and not source strength, IEPOX-SOA factor loading would be expected to decrease with sulfate concentration, which is opposite to what was observed.

4. a) As the author stated, this environment is different from SE US, in that sulfate levels are generally lower and reduced sulfur can contribute to total sulfate.

Our intent was to mention reduced sulfur species in the Amazon as precursors to particle sulfate, and not as particle phase components themselves. The text was revised to clarify this point:

Line 316:

*Background concentrations of sulfate in Amazonia, distinguished from sulfate tied to the urban Manaus plume, originated from in-basin emissions of **gas-phase precursors such as dimethyl sulfide (DMS) and hydrogen sulfide (H₂S)** from the forest as well as from out-of-basin marine emissions from the Atlantic Ocean (...)*

b) Are there any indications that reduced sulfur species would be measured as SO₄ in the AMS?

If present as particle phase components, reduced sulfur species could be detected by the AMS (DeWitt et al., 2010). They have not, however, been reported in ambient particles to our knowledge, and we do not see any indication of such reduced sulfur species in the AMS spectra.

5. Are there any estimates of HO₂ concentrations? The switch from IEPOX production (under HO₂ dominated chemistry) to high NO_x chemistry happens at around HO₂/NO = 1 (since RO₂+NO and RO₂+HO₂ rate constants are quite close). From the data, it appears that the switch happens at around 0.5 ppb NO, which would suggest that HO₂ levels are also around 0.5 ppb. That seems reasonable, but perhaps the authors can explain that in the manuscript to solidify this point.

The reviewer raises an excellent question about the gas phase chemistry of isoprene. In fact, Liu et al. (2016a) reported calculated HO₂ concentrations at the T3 site and simulated the fate of ISOPOO radicals as a function of NO. The manuscript has been revised as to emphasize the relevance of the findings of Liu et al. (2016a) to this study, as follows.

Line 389:

The greatest changes in factor loading were in the region of 1 ppb NO_y. This region of greatest sensitivity coincided with the transition from background to polluted

~~conditions. For the same time period, a change was reported in the gas phase from a dominance of ISOPOOH to MVK/MACR products across this transition in NO_y concentration (Liu et al., 2016a).~~

For the same time period of these PM analyses of IEPOX-SOA factor loading, Liu et al. (2016a) observed a shift in dominant isoprene gas-phase products from ISOPOOH to MVK/MACR across the transition in NO_y concentration. Liu et al. (2016a) further simulated the dependence on NO concentration of the ratio of the production rate of ISOPOOH to that of MVK + MACR. The highest ratios (0.6 to 0.9) were obtained for background concentrations of NO_y. The calculated HO₂ concentration was < 4 × 10⁸ cm⁻³ (0.016 ppb). The simulated transition for the dominant fate of the ISOPOO radicals occurred for an NO concentration of < 0.05 ppb.

6. The authors have largely focused on R2 when looking at regressions and demonstrated that, for example, IEPOX-SOA and SO4 are correlated. It would be interesting to also look at the slopes, and compare the sensitivity of IEPOX-SOA to SO4 across the different field studies (and maybe even lab studies). There are, of course, many other factors that would affect this sensitivity (pH, NO_x, aerosol liquid water content etc.). But maybe some simple relationships will emerge that would help construct simplified models to represent these complex chemical systems.

We agree with the reviewer that a comprehensive cross comparison of relationships between IEPOX-SOA and sulfate found in many different studies/locations is valuable, but that is out of the scope of present paper. As demonstrated in this manuscript, even in one location only, the relationship between IEPOX-SOA factor loadings and sulfate concentrations can be dissected by using NO_y concentrations to yield subsets of different slopes (Table 1).

7. In Section 3.1, the authors compared the IEPOX-SOA factor to that observed in other studies. Listing the fractions is useful, but it would be even better to compare the mass spectra (like the authors did with the factor from previous study in the same location). That way it would be more convincing to argue IEPOX-SOA factor is ubiquitous.

The reviewer's curiosity is well justified. Hu et al. (2015) addressed the ubiquity and characteristic spectral features of the IEPOX-SOA factor, and the manuscript has been revised as follows.

Line 190:

(...), and in AMAZE-08 ($f = 0.34$) (Chen et al., 2015). A further review on the ubiquity and characteristics of the IEPOX-SOA factor is presented in Hu et al. (2015).

Review #2

This is compelling and well written paper, describing observations to elucidate the role of anthropogenic nitrogen oxides and sulfate on the formation of biogenic “IEPOX SOA”. The measurements are robust: the identification of IEPOX SOA from PMF factors is grounded in isoprene oxidation tracers. The analysis is carefully considered, and two golden days in which the Manaus plume intercepted the Amazonian field site are used to evaluate the impacts of anthropogenic pollution on the development of SOA over the rainforest. The authors find that IEPOX-SOA increases with sulfate, but once that is controlled for by binning into ‘high’ versus ‘low’ sulfate, IEPOX SOA also decreases with NO_x exposure. This is consistent with our mechanistic understanding of isoprene oxidation and SOA formation in low NO_x environments. Finally, the authors use a Lagrangian model to demonstrate that the effect of NO_x is really to reduce IEPOX SOA production, rather than to increase loss rates. I recommend publication with very minor corrections. A few points for the authors to consider:

We acknowledge the reviewer for the valuable questions and comments that were provided. These aspects are considered in the revision, and detailed replies to each question are given below.

8. The authors describe that sulfate has both background and urban sources, while NO_x has just urban sources, complicating the use of sulfate as an anthropogenic tracer (line 374). To what extent do background sources really impact sulfate? (i.e. can the authors quantify this?). I am surprised that sulfate formation from MSA and such would be enough to actually complicate the analysis.

As the reviewer brings up, sulfate sources in the Amazon forest are indeed a very interesting theme. Chen et al. (2009) investigated this topic, and reported that background contributions other than from DMS or H₂S precursors may also be present to a large extent (Section 3.3, lines 316-319). We now see that it would be helpful in Section 3.4 to refer the reader to the relevant section and figures, so we have revised the manuscript as follows.

Line 374:

In relation to the influence of Manaus pollution, sulfate concentration was affected by a mixture of background and urban sources (cf. discussion in Section 3.3) whereas NO_y concentration largely had urban sources (cf. Figures 5b and 6b).

9. The premise of the paper is the relative rate for the ISOP_{OO} radical (an RO₂ radical) to react with HO₂ versus NO. It may be useful to actually calculate that ratio (so $k_{RO_2+HO_2} [HO_2]$ versus $k_{RO_2+NO} [NO]$) as a function of NO_x. I

would anticipate that this ratio maximizes IEPOX SOA formation at the same NO_x concentration as the observations show.

The reviewer brings up an excellent point, and we agree that this analysis is important. Fortunately, a co-located study by Liu et al. (2016a) investigated the gas-phase chemistry of isoprene and addressed this question. The manuscript has been revised to include this aspect. Please see answer to comment 5.

Technical comment:

Line 459. I think you mean “model” instead of “mode”.

Our intent here was to refer to the statistical mode of transport time values generated from air mass backtrajectory analysis. This transport time was an input to the model, as opposed to output. To clarify this point, the manuscript was revised as follows.

Line 459:

*The **statistical** mode value for τ_{tr} ~~is~~ of 4 h based on trajectory analysis **is used in the model**
(...)*

References

- Chen, Q., Farmer, D. K., Schneider, J., Zorn, S. R., Heald, C. L., Karl, T. G., Guenther, A., Allan, J. D., Robinson, N., Coe, H., Kimmel, J. R., Pauliquevis, T., Borrmann, S., Pöschl, U., Andreae, M. O., Artaxo, P., Jimenez, J. L., and Martin, S. T.: Mass spectral characterization of submicron biogenic organic particles in the Amazon Basin, *Geophys. Res. Lett.*, 36, L20806, 2009, 10.1029/2009GL039880.
- Chen, Q., Farmer, D. K., Rizzo, L. V., Pauliquevis, T., Kuwata, M., Karl, T. G., Guenther, A., Allan, J. D., Coe, H., Andreae, M. O., Pöschl, U., Jimenez, J. L., Artaxo, P., and Martin, S. T.: Submicron particle mass concentrations and sources in the Amazonian wet season (AMAZE-08), *Atmos. Chem. Phys.*, 15, 3687-3701, 2015, 10.5194/acp-15-3687-2015.
- DeWitt, H.L., Hasenkopf, C.A., Trainer, M.G., Farmer, D.K., Jimenez, J.L., McKay, C.P., Toon, O.B., and Tolbert, M.A.: The formation of sulfate and elemental sulfur aerosols under varying laboratory conditions: implications for early Earth, *Astrobiology*, 10, 773-781, 2010, 10.1089/ast.2009.9455.
- Hu, W. W., Campuzano-Jost, P., Palm, B. B., Day, D. A., Ortega, A. M., Hayes, P. L., Krechmer, J. E., Chen, Q., Kuwata, M., Liu, Y. J., de Sá, S. S., McKinney, K., Martin, S. T., Hu, M., Budisulistiorini, S. H., Riva, M., Surratt, J. D., St. Clair, J. M., Isaacman-Van Wertz, G., Yee, L. D., Goldstein, A. H., Carbone, S., Brito, J., Artaxo, P., de Gouw, J. A., Koss, A., Wisthaler, A., Mikoviny, T., Karl, T., Kaser, L., Jud, W., Hansel, A., Docherty, K. S., Alexander, M. L., Robinson, N. H., Coe, H., Allan, J. D., Canagaratna, M. R., Paulot, F., and

Jimenez, J. L.: Characterization of a real-time tracer for isoprene epoxydiols-derived secondary organic aerosol (IEPOX-SOA) from aerosol mass spectrometer measurements, *Atmos. Chem. Phys.*, 15, 11807-11833, 2015, 10.5194/acp-15-11807-2015.

Liu, Y., Brito, J., Dorris, M. R., Rivera-Rios, J. C., Seco, R., Bates, K. H., Artaxo, P., Duvoisin, S., Keutsch, F. N., Kim, S., Goldstein, A. H., Guenther, A. B., Manzi, A. O., Souza, R. A. F., Springston, S. R., Watson, T. B., McKinney, K. A., and Martin, S. T.: Isoprene photochemistry over the Amazon rain forest, *Proc. Natl. Acad. Sci. USA*, 113, 6125-6130, 2016a, 10.1073/pnas.1524136113.

Influence of urban pollution on the production of organic particulate matter from isoprene epoxydiols in central Amazonia

Suzane S. de Sá (1), Brett B. Palm (2), Pedro Campuzano-Jost (2), Douglas A. Day (2), Matthew K. Newburn (3), Weiwei Hu (2), Gabriel Isaacman-VanWertz^a (4), Lindsay D. Yee (4), Ryan Thalman (5), Joel Brito^b (6), Samara Carbone (6), Paulo Artaxo (6), Allen H. Goldstein (4), Antonio O. Manzi (7), Rodrigo A.F. Souza (8), Fan Mei (9), John E. Shilling (3,9), Stephen R. Springston (5), Jian Wang (5), Jason D. Surratt (10), M. Lizabeth Alexander (3), Jose L. Jimenez (2), Scot T. Martin* (1, 11)

- (1) School of Engineering and Applied Sciences, Harvard University, Cambridge, Massachusetts, USA
- (2) Department of Chemistry & Biochemistry and Cooperative Institute for Research in Environmental Sciences, University of Colorado, Boulder, Colorado, USA
- (3) Environmental Molecular Sciences Laboratory, Pacific Northwest National Laboratory, Richland, Washington, USA
- (4) Dept. of Environmental Science, Policy, and Management, University of California, Berkeley, California, USA
- (5) Brookhaven National Laboratory, Upton, New York, USA
- (6) Departamento de Física Aplicada, Universidade de São Paulo, São Paulo, Brasil
- (7) Instituto Nacional de Pesquisas da Amazonia, Manaus, Amazonas, Brasil
- (8) Escola Superior de Tecnologia, Universidade do Estado do Amazonas, Manaus, Amazonas, Brasil
- (9) Atmospheric- Sciences and Global Change Division, Pacific Northwest National Laboratory, Richland, WA, USA
- (10) Department of Environmental Sciences and Engineering, Gillings School of Global Public Health, The University of North Carolina at Chapel Hill, Chapel Hill, North Carolina, USA
- (11) Department of Earth and Planetary Sciences, Harvard University, Cambridge, Massachusetts, USA

^a Now at Massachusetts Institute of Technology, Cambridge, Massachusetts, USA

^b Now at: Laboratory for Meteorological Physics (LaMP), University Blaise Pascal, Aubière, France

Submitted: November 2016

Atmospheric Chemistry and Physics

*To Whom Correspondence Should be Addressed

E-mail: scot_martin@harvard.edu

1 Abstract

2 The atmospheric chemistry of isoprene contributes to the production of a substantial mass
3 fraction of the particulate matter (PM) over tropical forests. Isoprene epoxydiols (IEPOX)
4 produced in the gas phase by the oxidation of isoprene under HO₂-dominant conditions are
5 subsequently taken up by particles, thereby leading to production of secondary organic PM. The
6 present study investigates possible perturbations to this pathway by urban pollution. The
7 measurement site in central Amazonia was located 4 to 6 ~~hoursh~~ downwind of Manaus, Brazil.
8 Measurements took place from February through March 2014 of the wet season, as part of the
9 GoAmazon2014/5 experiment. Mass spectra of organic PM collected with an Aerodyne Aerosol
10 Mass Spectrometer were analyzed by positive-matrix factorization. One resolved statistical
11 factor (“IEPOX-SOA factor”) was associated with PM production by the IEPOX pathway.
12 ~~Loadings of this~~The IEPOX-SOA factor loadings correlated with independently measured mass
13 concentrations of tracers of IEPOX-derived PM, namely C₅-alkene triols and 2-methyltetrols (R
14 = 0.96 and 0.78, respectively). ~~Factor~~The factor loading, as well as the ratio f of the ~~factor~~
15 loading to organic PM mass concentration, decreased under polluted compared to background
16 conditions. ~~For the study period~~For an increase in NO_y concentration from 0.5 to 2 ppb, the
17 factor loading and f decreased by two- to three-fold. Overall, sulfate concentration explained
18 37% of the variability in the factor loading. After segregation of ~~the data set by~~factor loading
19 into subsets based on NO_y concentration, the sulfate concentration explained up to 75% of the
20 variability ~~in factor loading within~~. Considering both factors, the data sets show that the NO_y
21 subsets. The sulfate-detrended IEPOX-SOA factor loading decreased by two- to three-fold for an
22 increase in NO_y concentration from 0.5 to 2 ppb. The suppressing effects of elevated
23 NOincreased NO concentrations dominated over the enhancing effects of higher sulfate with
24 respect to the production of IEPOX-derived PM. Relative to background conditions, the Manaus
25 concentrations. The pollution contributed from Manaus elevated NO_y concentrations more

26 significantly ~~to NO_y~~ than ~~to sulfate~~ sulfate concentrations relative to background conditions. In
27 this light, increased emissions of nitrogen oxides, as anticipated for some scenarios of
28 Amazonian economic development, could significantly alter pathways of PM production that
29 presently prevail over the tropical forest, implying changes to air quality and regional climate.

30 **1. Introduction**

31 Organic compounds comprise up to 90% of the mass concentration of submicron organic
32 particulate matter (PM) over tropical forests (Kanakidou et al., 2005). Submicron PM has
33 adverse effects on human health (Nel, 2005; Pope III and Dockery, 2006) and influences air
34 quality and climate by scattering radiation and acting as cloud condensation nuclei (Ramanathan
35 et al., 2001; Kaufman et al., 2002). A significant fraction of the submicron organic material
36 originates from secondary processes, mainly by the atmospheric oxidation of volatile organic
37 compounds (VOCs) emitted as part of natural and human activities (Zhang et al., 2007; Hallquist
38 et al., 2009; Jimenez et al., 2009). The particle life cycle over Amazonia is in particular strongly
39 influenced by secondary processes that produce organic PM (Martin et al., 2010a; Pöschl et al.,
40 2010). Biogenic emissions from tropical forests are high, and environmental conditions favor
41 photooxidation reactions. The reactive chemistry and the relative importance of pathways
42 leading to PM production can be strongly guided by regulating species, such as sulfate and nitric
43 oxide (Surratt et al., 2007a; Worton et al., 2013; Liu et al., 2016a). The concentrations of these
44 species depend on their background occurrence, pollution sources, and the relative mix of
45 background and polluted air masses.

46 Over tropical forests such as Amazonia, the atmospheric chemistry of isoprene produces
47 a substantial fraction of the submicron organic PM (Chen et al., 2009; Robinson et al., 2011;
48 Chen et al., 2015; Isaacman-VanWertz et al., 2016). Isoprene (2-methyl-1,3-butadiene, C_5H_8) is
49 the non-methane VOC most abundantly emitted by tropical forests (Guenther et al., 2012), and
50 isoprene epoxydiols (IEPOX) have been identified as important intermediates in the production
51 of PM from isoprene (Paulot et al., 2009; Surratt et al., 2010; Lin et al., 2012). A chemical
52 sequence for the production of IEPOX-derived PM from the photooxidation of isoprene in the

53 atmosphere is represented in Figure 1. The sequence is initiated when isoprene peroxy radicals
54 (ISOPOO) are produced in the gas phase by reactions between isoprene and photochemically
55 generated hydroxyl radicals (OH). The reactive fate of the ISOPOO radicals can differ under
56 background compared to polluted conditions (Surratt et al., 2010; Crouse et al., 2011; Worton et
57 al., 2013).

58 Under background conditions, meaning that HO₂ pathways are favorable in the absence
59 of extensive NO pollution (Wennberg, 2013; Liu et al., 2016a), the ISOPOO radicals continue in
60 large part through the series of species highlighted in yellow in Figure 1. Through HO_x-
61 facilitated reaction steps, the ISOPOO radicals produce hydroperoxides (ISOPOOH) as major
62 first-generation products and subsequently isoprene epoxydiols (IEPOX) as major second-
63 generation products (Carlton et al., 2009; Paulot et al., 2009; Liu et al., 2013; St. Clair et al.,
64 2015; Liu et al., 2016a). Some of the produced IEPOX undergoes reactive uptake to particles, as
65 facilitated by hydronium ions at the surface (Surratt et al., 2007a; Lin et al., 2012; Gaston et al.,
66 2014; Kuwata et al., 2015; Lewandowski et al., 2015). This chemical sequence can contribute a
67 significant fraction of submicron PM mass concentration over tropical forests (Claeys et al.,
68 2004; Hu et al., 2015). Laboratory studies indicate that about half of the PM produced by
69 isoprene photooxidation under HO₂-dominant conditions in the presence of acidic sulfate
70 particles is associated with IEPOX production and uptake (Liu et al., 2015). Interaction of
71 IEPOX with cloud waters warrants investigation (Lim et al., 2005; Ervens et al., 2011;
72 Budisulistiorini et al., 2015; Chen et al., 2015). In addition to IEPOX pathways, laboratory
73 studies suggest that multifunctional hydroperoxides produced in the gas phase can contribute to
74 isoprene-derived PM production (Krechmer et al., 2015; Liu et al., 2016b; Riva et al., 2016b).

75 After reactive uptake of IEPOX, particle-phase reactions can produce several different
76 families of species. These species are collectively labeled “IEPOX-derived PM” and represent a
77 subset of the ambient organic PM, as labeled in Figure 1. The presence of 2-methyltetrols, C₅-
78 alkene triols, 3-methyltetrahydrofuran-3,4-diols, organosulfates, and related oligomers in
79 ambient PM is an indicator of PM production by IEPOX uptake under atmospheric conditions
80 (Claeys et al., 2004; Surratt et al., 2006; Surratt et al., 2007b; Surratt et al., 2010; Robinson et al.,
81 2011; Lin et al., 2012; Lin et al., 2014). Even though these species may differ in some cases from
82 the actual compounds in the atmospheric PM due to thermal decomposition during analysis
83 (Lopez-Hilfiker et al., 2016), they serve as chemical tracers for the atmospheric concentration of
84 IEPOX-derived PM (Hu et al., 2015; Isaacman-VanWertz et al., 2016). The analytical methods
85 highlighted in Figure 1, including that of the “IEPOX-SOA factor” of the AMS analysis used
86 herein, can lead to over- and underestimated IEPOX-derived PM concentrations. This
87 uncertainty is represented in the figure by the brown dashed lines that approximately but not
88 exactly correspond to IEPOX-derived PM.

89 Under polluted conditions, the reactive sequence of isoprene and ultimately PM
90 production can become significantly altered (Figure 1). NO concentrations can be sufficiently
91 high that ISOPROO radicals react almost entirely with NO in place of HO₂, thereby largely
92 producing methacrolein (MACR) and methyl vinyl ketone (MVK) in place of ISOPROOH (Liu et
93 al., 2016a). As a result, IEPOX production can be greatly decreased, ultimately reducing PM
94 production by IEPOX pathways. A minor channel along the NO pathway can still produce
95 IEPOX, although much less efficiently (Jacobs et al., 2014). Under NO-dominant conditions,
96 alternative pathways of PM production not involving IEPOX can become active, though in lower
97 yields. MACR can be oxidized to produce peroxyethylacrylic nitric anhydride (MPAN), which

98 is a precursor to methacrylic acid epoxide (MAE) and hydroxymethylmethyl- α -lactone
99 (HMML), and these compounds can undergo reactive uptake to produce PM (Kjaergaard et al.,
100 2012; Lin et al., 2013; Worton et al., 2013; Nguyen et al., 2015). Glyoxal produced from
101 isoprene oxidation can contribute to PM production (Volkamer et al., 2007; Ervens and
102 Volkamer, 2010; McNeill et al., 2012; Marais et al., 2016).

103 Another possible mechanism affecting PM production by IEPOX uptake under polluted
104 conditions is altered particle composition, especially particle acidity, largely driven by sulfate.
105 Laboratory studies show that IEPOX uptake increases with increasing acidity (Gaston et al.,
106 2014; Kuwata et al., 2015; Liu et al., 2015). A proposed reaction during uptake is the acid-
107 catalyzed ring opening of the IEPOX molecule (Surratt et al., 2010). The subsequent particle-
108 phase reactions include the addition of available nucleophiles, such as water to produce tetrols or
109 sulfate to produce organosulfates as well as their oligomers (Surratt et al., 2010; Lin et al., 2014;
110 Nguyen et al., 2014). In support of this proposed mechanism, analyses by positive-matrix
111 factorization (PMF) of mass spectra collected in the southeastern USA identified PMF factors
112 associated with IEPOX-derived PM, and these factors correlated positively with sulfate mass
113 concentrations (Budisulistiorini et al., 2013; Hu et al., 2015; Xu et al., 2015). In short, different
114 regimes of NO:HO₂ concentration ratios and different possible PM compositions between
115 polluted and background conditions can lead to different product distributions and different
116 production rates of IEPOX-derived PM.

117 The extent to which pollution may shift the production pathways of IEPOX-derived PM
118 over tropical forests remains to be elucidated. The study described herein is based on data sets
119 collected in the wet season downwind of Manaus, Brazil, during the *Observations and Modeling*
120 *of the Green Ocean Amazon* Experiment (GoAmazon2014/5) (Martin et al., ~~2016e~~2016a). The

121 research site was influenced at times and to variable extents by the pollution outflow from the
122 Manaus metropolitan area. Compared to the background environment in Amazonia, the Manaus
123 plume had high number concentrations of particles and enhanced concentrations of pollutants,
124 including oxides of nitrogen and sulfate (Kuhn et al., 2010; Martin et al., ~~2016~~2016a). The
125 reactive gas-phase chemistry was strongly guided by the relative mix of background and polluted
126 air masses (Trebs et al., 2012; Liu et al., 2016a). The analysis herein focuses on how the
127 pollution perturbed IEPOX-derived PM production relative to background conditions.

128 **2. Methodology**

129 Data sets were collected at the “T3” site (3.2133 °S, 60.5987 °W) located 70 km to the
130 west of Manaus, Brazil, in central Amazonia (Martin et al., ~~2016~~2016a). The site was situated in
131 a pasture (2.5 km × 2 km) surrounded by forest. The analysis herein focuses on data sets
132 collected during the wet season period of February 1 to March 31, 2014, corresponding to the
133 first Intensive Operating Period (IOP1) of the GoAmazon2014/5 experiment.

134 A High-Resolution Time-of-Flight Aerosol Mass Spectrometer (HR-ToF-AMS, hereafter
135 AMS; Aerodyne, Inc., Billerica, Massachusetts, USA) recorded the primary data set of this
136 study. The AMS provided quantitative bulk characterization of the atmospheric PM ~~at a time~~
137 ~~resolution of minutes~~. The design principles and capabilities of this instrument are described in
138 the literature (DeCarlo et al., 2006; Canagaratna et al., 2007). The instrument was housed within
139 a temperature-controlled research container, and the inlet to the instrument sampled from 5 m
140 above ground level. Detailed aspects of AMS operation are presented in the Supplement (Section
141 S1). In brief, ambient measurements were obtained ~~for every~~ other 4 ~~of 8~~-min. Organic, sulfate,
142 ammonium, nitrate, and chloride PM mass concentrations were obtained from “V-mode” data.
143 The choice of ions to fit was aided by the “W-mode” data, which were collected once every five

144 days. Data analysis was performed using *SQUIRREL* (1.56D) and *PIKA* (1.14G) of the AMS
145 software suite.

146 Positive-matrix factorization was applied to the time series of the organic component of
147 the high-resolution mass spectra (Ulbrich et al., 2009). The present study focuses on one of the
148 resolved statistical factors, referred to as the “IEPOX-SOA factor” (Hu et al., 2015). Diagnostics
149 of the PMF analysis, especially as related to the resolved IEPOX-SOA factor, are presented in
150 the Supplement (Section S2). A separate account is forthcoming to present the other PMF factors
151 (de Sá, in preparation). Herein, “factor profile” and “factor loading” refer to the mathematical
152 products of the multivariate statistical analysis, whereas “mass spectrum” and “mass
153 concentration” refer to measurements.

154 In complement to the AMS data sets, mass concentrations of molecular and tracer organic
155 species were measured using a Semi-Volatile Thermal Desorption Aerosol Gas Chromatograph
156 (SV-TAG) at a time resolution of one hour. The instrument collected gas and particle samples,
157 followed by thermal desorption, derivatization, and gas chromatography coupled to mass
158 spectrometry (Isaacman et al., 2014). A summary of operational details for GoAmazon2014/5 is
159 presented in the Supplement (Section S1), and the main account is presented in Isaacman-
160 VanWertz et al. (2016).

161 Additional data sets used in the analysis were collected at the T3 site by instruments
162 housed in the research container of the Mobile Aerosol Observing System (MAOS) of the ARM
163 Climate Research Facility (ACRF) operated by the USA Department of Energy (Mather and
164 Voyles, 2013; Martin et al., ~~2016~~[2016a](#)). A temperature-controlled inlet was mounted at 10 m
165 above ground level. Measurements of nitrogen oxides were made using a chemiluminescence-
166 based instrument (Air Quality Design). The measured odd-nitrogen family “NO_y”, meaning NO_x

167 + reservoir species, included NO, NO₂, HNO₃, organonitrates, particle nitrate, and peroxyacetyl
168 nitrates. Further details of the NO_y measurements are presented in the Supplement (Section S1).
169 Ozone concentrations were measured by an Ozone Analyzer (Thermo Fisher, model 49i).
170 Particle number concentrations were measured by a Condensation Particle Counter (TSI, model
171 3772). Meteorological variables provided by the ARM Mobile Facility (AMF-1), which was also
172 part of the ACRF, included wind direction, solar irradiance, and precipitation rate. Measurements
173 of NO_y and particle number concentration onboard the G-1 aircraft of the ARM Aerial Facility
174 (AAF) were also used in the analysis (Schmid et al., 2014; Martin et al., ~~2016~~2016a).

175 **3. Results and Discussion**

176 The organization of the presentation herein is as follows. The factor profile obtained from
177 AMS PMF analysis is ~~presented~~discussed (Section 3.1), a case study comparing factor loading
178 under background to polluted conditions is ~~discussed~~presented (Section 3.2), the roles of sulfate
179 (Section 3.3) and nitric oxide (Section 3.4) in affecting factor loading are explored, and the
180 influence of NO on production and loss processes of IEPOX-derived PM is considered (Section
181 3.5).

182 **3.1 Statistical IEPOX-SOA factor**

183 Positive-matrix factorization was carried out on the time series of AMS organic mass
184 spectra. One statistical factor had a similar ~~pattern~~profile of peak intensities as the “IEPOX-SOA
185 factor” identified in other studies (Figure S1) (Robinson et al., 2011; Slowik et al., 2011;
186 Budisulistiorini et al., 2013; Budisulistiorini et al., 2015; Chen et al., 2015; Xu et al., 2015). The
187 Pearson correlation coefficient R between this factor and the one obtained ~~for a data set~~ in the
188 2008 wet season in central Amazonia as part of the AMAZE-08 experiment was 0.99 (Chen et
189 al., 2015). The ratio f of the factor loading to the mass concentration of submicron organic PM

190 for the present study was 0.17 ± 0.09 (mean \pm standard deviation). The IEPOX-SOA factor has
191 been identified previously over the maritime tropical forest of Borneo ($f = 0.23$) (Robinson et al.,
192 2011), in a rural area in Canada 70 km north of Toronto ($f = 0.17$) (Slowik et al., 2011), across
193 several locations in the summertime southeastern USA ($f = 0.17$ to 0.41) (Budisulistiorini et al.,
194 2013; Budisulistiorini et al., 2015; Hu et al., 2015; Xu et al., 2015; Budisulistiorini et al., 2016;
195 Marais et al., 2016), and in AMAZE-08 ($f = 0.34$) (Chen et al., 2015). [A further review on the
196 ubiquity and characteristics of the IEPOX-SOA factor is presented in Hu et al. \(2015\).](#)

197 The IEPOX-SOA factor reported herein had prominent peaks at m/z 53.04 and m/z 82.04
198 (Figure S1). The ion at m/z 82.04, corresponding to $C_5H_6O^+$, has been attributed to 3-methylfuran
199 (3-MF). The thermal degradation of isoprene-derived PM upon mass spectral analysis was
200 suggested as the source of 3-MF (Robinson et al., 2011). Lin et al. (2012) proposed that
201 sequential dehydrations upon mass spectral analysis of 3-methyltetrahydrofuran-3,4-diols, which
202 are an identified component of IEPOX-derived PM, can produce 3-MF. Other IEPOX-derived
203 species as well as non-IEPOX species might also contribute to the production of $C_5H_6O^+$ ions
204 (Surratt et al., 2010; Hu et al., 2015; Liu et al., 2016c).

205 Laboratory studies show that a mass spectrum having a pattern of peak intensities similar
206 to that of the IEPOX-SOA factor is produced both by the uptake of IEPOX into aqueous acidic
207 sulfate particles as well as by the photooxidation of isoprene under HO_2 -dominant conditions in
208 the presence of acidic sulfate particles (Budisulistiorini et al., 2013; Nguyen et al., 2014; Kuwata
209 et al., 2015; Liu et al., 2015). The possibility of similar uptake by a broader range of liquid media
210 remains to be fully tested, such as other acidic solutions as well as cloud waters. Compared to the
211 laboratory spectra of (Liu et al., 2015),- representing about 4 h of OH exposure at atmospheric
212 concentrations (1.7×10^6 molec cm^{-3}), the main difference was the relative intensity of the m/z

213 44 peak. For the IEPOX-SOA factor of the present study, this peak was four times more intense
214 (Figure S1), suggesting that the atmospheric PM was more oxidized. Hu et al. (2016) showed
215 that heterogeneous aging of IEPOX-SOA can result in increased relative signal at m/z 44.

216 By contrast, laboratory studies show that a significantly different mass spectrum from
217 that of the IEPOX-SOA factor is obtained for PM produced from isoprene photooxidation in the
218 absence of aqueous particles (Krechmer et al., 2015; Kuwata et al., 2015). Under these
219 conditions, chemical pathways other than IEPOX uptake into a liquid medium appear to be
220 active, such as the condensation of low-volatility, multifunctional compounds produced by
221 additional oxidation of ISOPOOH (Krechmer et al., 2015; Liu et al., 2016b; Riva et al., 2016b).
222 This non-IEPOX pathway, however, is not expected to contribute a large fraction of the
223 produced PM during the study period because of the high RH conditions in Amazonia and the
224 prevalence of liquid particles for the prevailing atmospheric conditions (Bateman et al., 2016; de
225 Sá, in preparation).

226 The SV-TAG measurements of the concentrations of C₅-alkene triols and 2-methyltetrols
227 support the interpretation of the IEPOX-SOA factor as an indicator that PM was being produced,
228 at least in significant part, from the reactive uptake of IEPOX (Claeys et al., 2004; Wang et al.,
229 2005; Surratt et al., 2010). The factor loading strongly correlated with the concentrations of C₅-
230 alkene triols ($R = 0.96$) and 2-methyltetrols ($R = 0.78$) (Figure 2). These species have been
231 associated with the IEPOX reaction pathway in several laboratory studies (Surratt et al., 2010;
232 Riedel et al., 2016). The R value with respect to C₅-alkene triols was independent of the f_{peak}
233 value of the PMF solution, demonstrating the robustness of the relative time trend of factor
234 loading even though the factor profile and absolute loadings changed across f_{peak} values (Figure
235 S2d).

236 The loading of the IEPOX-SOA factor may be an overestimate or an underestimate of the
237 atmospheric concentration of the IEPOX-derived PM (Supplement, Section S2). The IEPOX-
238 SOA factor can be understood as the net result of (i) produced IEPOX-derived PM, (ii) less that
239 portion of the carbon that gets further oxidized and mixed into other PMF factors, and (iii) plus
240 that portion of non-IEPOX-derived PM that gives rise to a similar AMS mass spectral pattern as
241 the IEPOX-derived PM (Supplement, Section S2). Processes of type ii contribute to
242 underestimates and processes of type iii lead to overestimates when using IEPOX-SOA factor
243 loading as a surrogate for IEPOX-derived PM concentration. These uncertainties are
244 qualitatively represented in Figure 1 by the brown dashed lines that enclose the fraction of
245 particle material statistically captured by the factor analysis. The further analysis herein is based
246 on using the loading of the IEPOX-SOA factor as a scalar proxy for the mass concentration of
247 IEPOX-derived PM in a sampled air mass.

248 **3.2 Background compared to polluted conditions**

249 Under background conditions in the wet season, remote areas of the Amazon forest
250 constitute one of the least polluted continental regions on Earth (Martin et al., 2010a). Nitric
251 oxide (NO) concentrations characteristic of central Amazonia range from 20 to 70 ppt (Torres
252 and Buchan, 1988; Bakwin et al., 1990; Levine et al., 2015). Daytime maximum ozone
253 concentrations are 10 to 15 ppb (Rummel et al., 2007). Sulfate mass concentrations associated
254 with in-basin processes are on average $< 0.1 \mu\text{g m}^{-3}$, and total background sulfate concentrations
255 contributed by in- and out-of-basin processes rarely exceed $0.5 \mu\text{g m}^{-3}$ (Andreae et al., 1990;
256 Chen et al., 2009).

257 In the wet season, Manaus emissions were the most important anthropogenic influence on
258 observations at the T3 research site (Martin et al., ~~2016a~~2017). The afternoons of March 3 and

259 13, 2014, are presented herein as representative cases of background and polluted conditions,
260 respectively. Both days were sunny, and major precipitation events were absent. Particle number
261 concentrations measured onboard the G-1 aircraft within the atmospheric boundary layer show
262 the position of the pollution plume on these two afternoons (Figure 3). NO_y concentrations
263 measured during the same flight are shown in Figure S3. The visualization in Figure 3 shows that
264 on March 3 the Manaus plume passed south of the T3 site. By comparison, on March 13 the
265 central portion of the plume passed over T3. Aircraft-based observations to track the Manaus
266 plume were available for 16 afternoons of the two-month study period. ~~Ground site diagnostics
267 of the urban pollution reaching the T3 site were therefore also needed.~~

268 Measurements at ground level at the T3 site are plotted in Figure 4 for the afternoons of
269 March 3 (left panel) and March 13 (right panel). Based on wind speeds, the research site was 4 to
270 6 h downwind of Manaus (Martin et al., [2016a](#)). Anthropogenic-biogenic interactions
271 affecting the production of IEPOX-derived PM were driven in large part by atmospheric
272 photochemistry at daybreak. Morning urban emissions followed by atmospheric processing
273 arrived at the T3 site during the local afternoon. The afternoon period, in addition to the
274 connection to the Manaus plume, was also characterized by reduced variability in other possible
275 confounding variables, such as temperature, radiation, and relative humidity. Figure 4 shows that
276 on the afternoon of March 3 ozone concentrations were below 10 ppb, particle number
277 concentrations were below 1000 cm^{-3} , NO_y concentrations were less than 1 ppb, and sulfate
278 concentrations were 0.3 to $0.4 \mu\text{g m}^{-3}$. Species concentrations were stable throughout the
279 afternoon. On March 13, ozone concentrations exceeded 30 ppb for most of the afternoon,
280 particle concentrations reached $10,000 \text{ cm}^{-3}$, NO_y concentrations consistently exceeded 1 ppb,
281 and sulfate concentrations were 0.3 to $0.6 \mu\text{g m}^{-3}$. Concentrations fluctuated markedly

282 throughout the afternoon on March 13, reflecting different levels of pollution influence in the air
283 passing over the T3 site during that period.

284 Elevated concentrations of ozone, particle number, and NO_y were reliable markers of
285 pollution influence over the course of the study period (Supplement, Section S3). Pollution was
286 associated with stronger relative enhancements in NO_y concentrations than in sulfate
287 concentrations (Sections 3.3 and 3.4). With respect to the IEPOX-SOA factor, Figure 4 shows
288 that the absolute and relative loadings decreased for the polluted compared to background
289 conditions. Relative loadings are expressed by the ratio f of IEPOX-SOA factor loading to the
290 organic PM mass concentration. Decreased absolute and relative factor loadings under polluted
291 conditions, presented in Figure 4 as a case study, also characterized the data sets of the entire
292 study period. Other examples are presented in the Supplement (Figure S4).

293 **3.3 Sulfate as a driver of IEPOX-derived PM production**

294 A scatter plot between sulfate mass concentrations and IEPOX-SOA factor loadings for
295 all afternoon periods is shown in Figure 5a. Background and polluted conditions are represented
296 in the data set. For further visualization, the data set was organized into six subsets based on
297 sulfate concentration. The medians and the means of the subsets are plotted in the figure. The
298 visualization shows that sulfate concentration served as a first-order predictor of the IEPOX-
299 SOA factor loading in central Amazonia in the wet season. The explanation can be a
300 combination of increased acidity, greater reaction volume including by enhanced hygroscopic
301 growth, and possibly a nucleophilic role for sulfate (Xu et al., 2015; Marais et al., 2016). An
302 analysis of the relative importance of each is out of the scope of the present study (Supplement,
303 Section S4).

304 For Figure 5a, the coefficient R^2 of determination between sulfate mass concentration and
305 factor loading was 0.37, meaning that 37% of the variance of the IEPOX-SOA factor loading
306 was explained by sulfate mass concentration. As a point of comparison, R^2 varied between 0.4
307 and 0.6 for observations in the southeastern USA, which seasonally is a region of high isoprene
308 emissions (Budisulistiorini et al., 2013; Budisulistiorini et al., 2015; Hu et al., 2015; Xu et al.,
309 2015). A chemical transport model that predicted IEPOX-derived PM mass
310 ~~concentrations~~concentration for the southeastern USA obtained R^2 of 0.4 for the relationship to
311 predicted sulfate mass concentration (Marais et al., 2016). The model attributed the correlation to
312 the acidity and particle volume provided by sulfate, both of which favored IEPOX uptake.
313 Central Amazonia and the southeastern USA differ considerably in terms of meteorology,
314 chemistry, and levels of regional pollution, yet they have in common an important role of sulfate
315 concentration as a predictor of IEPOX-derived PM concentration, even as the sulfate
316 concentrations themselves differ by an order of magnitude. Sulfate concentrations typically had
317 an interquartile range of [1.5, 3.0] $\mu\text{g m}^{-3}$ in the studies in the southeastern USA, which can be
318 compared to a range of [0.11, 0.36] $\mu\text{g m}^{-3}$ under background conditions during the wet season in
319 central Amazonia.

320 A key difference between the southeastern USA and central Amazonia is the role of
321 sulfate concentration as a clear or ambiguous indicator, respectively, of urban influence. For the
322 relatively low sulfate mass concentrations ($<0.5 \mu\text{g m}^{-3}$) characteristic of the study period,
323 background air in central Amazonia contributed significantly to the variability in sulfate
324 concentration measured at the T3 site. Background concentrations of sulfate in Amazonia,
325 distinguished from sulfate tied to the urban Manaus plume, originated from in-basin emissions of
326 gas-phase precursors such as dimethyl sulfide (DMS) and hydrogen sulfide (H_2S) from the forest

327 as well as from out-of-basin marine emissions from the Atlantic Ocean (Andreae et al., 1990;
328 Chen et al., 2009; Martin et al., 2010a). In the wet season, biomass burning from Africa and to a
329 lesser extent from South America also episodically contributed significantly to sulfate
330 concentrations in the Manaus region. In addition, emissions from large cities on the eastern coast
331 of Brazil were important at times when rare meteorological events shifted the northeasterlies
332 typical of the wet season to easterlies (Martin et al., ~~2016a~~2017). Manaus contributions to sulfate
333 mass concentrations in an air mass were in addition to these various background sources.

334 The relative importance of Manaus contributions to the sulfate concentrations in the air
335 masses that passed over T3 was assessed by comparison of the probability density function of
336 sulfate concentration at T3 to those of sites upwind of Manaus (Figure 5b). The distributions of
337 the two upwind sites had a central tendency of 0.05 to 0.3 $\mu\text{g m}^{-3}$, suggesting the range of natural
338 concentrations, and a rightside skewness up to 0.6 $\mu\text{g m}^{-3}$, suggesting the importance of episodic
339 long-range transport (Chen et al., 2009). The figure shows that the distribution at T3 did not
340 differ greatly from those of the upwind sites even though the air masses over T3 regularly
341 transported Manaus pollution, ~~indicating that Manaus did not constitute a dominant sulfate~~
342 ~~source in the region. Elevated. The implication is that Manaus sulfate sources, whether primary~~
343 ~~or secondary, had small contributions relative to background sources when averaged over time.~~
344 In short, elevated sulfate concentrations on any one afternoon at the T3 site might have arisen
345 because of elevated background concentrations on that day rather than the influence of the
346 Manaus pollution plume. The implications are that (i) sulfate concentration was an ambiguous
347 indicator of urban influence at the T3 site and (ii) increases in sulfate concentrations in pollution
348 events were moderate relative to background concentrations.

349 3.4 NO as a modulator of IEPOX-derived PM production

350 In the transport from Manaus to the T3 research site, NO concentration ~~is~~was not
351 conserved, in part because of reactions with ozone and organic peroxy radicals (Martin et al.,
352 ~~2016a~~2017). In this case, the instantaneous NO concentrations measured at the T3 site ~~do~~did not
353 directly provide information about the fate of ISOPOO radicals along the transport time of 4 to 6
354 h from Manaus to the T3 site. The collective contributions of NO, NO₂, and their oxidation
355 products ~~are~~were, however, reflected in measurements of NO_y concentrations at the T3 site. The
356 NO_y family is expected to have a longer lifetime than the transport time from Manaus to the T3
357 site (Romer et al., 2016). The NO_y concentration measured at T3 therefore served as a surrogate
358 for the integrated exposure of the air mass to NO chemistry between Manaus and T3 (Liu et al.,
359 2016a).

360 Unlike the ambiguity associated with the sulfate concentration, an elevated NO_y
361 concentration served as a clear indicator of anthropogenic influence in an air mass passing over
362 the T3 site. For background conditions over the forest, NO_y ~~originated~~originates from NO
363 emitted from soils and other natural sources such as lightning (Bakwin et al., 1990; Jacob and
364 Wofsy, 1990). The probability density function of NO_y concentration under background
365 conditions in the wet season of the central Amazon basin is shown in Figure 6b (Bakwin et al.,
366 1990). The distribution for measurements at T3 is also shown. Relative to the narrow distribution
367 around 0.5 ppb for background conditions, there is high-side skewness extending up to 4 ppb for
368 the T3 measurements, indicating the clear influence of Manaus emissions on NO_y concentrations.

369 NO_y concentration was incorporated into the analysis by segregation of the dataset of
370 Figure 5a into five subsets (Supplement, Section S5). Linear fits to the NO_y-segregated data
371 subsets are plotted in Figure 6a. Each subset is represented by a different color. Parameter values

372 of the associated fits are listed in Table 1. In conjunction with sulfate concentration, the
373 visualization presented in Figure 6a shows that NO_y concentration further explained the
374 variability in IEPOX-SOA factor loadings. The R^2 values, representing the extent to which
375 sulfate was able to explain variability in IEPOX-SOA factor loading once isolated for NO_y
376 concentration, were higher for the data subsets having lower and higher extremes of NO_y
377 concentrations (Table 1). These conditions represent the limiting cases of fully background
378 conditions for the former and the strongest effects of Manaus pollution for the latter. By
379 comparison, intermediate NO_y concentrations could arise from air masses that mixed together
380 background air with Manaus pollution during the transport to T3 (e.g., by entrainment) and thus
381 represent complex processing. Single or multiple mixing points could occur anywhere along the
382 path from Manaus to T3, thus introducing variability into the effective photochemical age of the
383 air mass arriving at T3 and resulting in lower R^2 values for intermediate NO_y concentrations. In
384 caveat, this explanation assumes that NO emissions from Manaus had low day-to-day variability.

385 In relation to the influence of Manaus pollution, sulfate concentration was affected by a
386 mixture of background and urban sources [\(cf. discussion in Section 3.3\)](#) whereas NO_y
387 concentration largely had urban sources: [\(cf. Figures 5b and 6b\)](#). As an approximation to keeping
388 the sulfate concentration constant and thus focusing on the role of NO in the urban pollution, the
389 visualization of the dependence of IEPOX-SOA factor loading on NO_y concentration was further
390 refined by taking data subsets segregated by low ($< 0.1 \mu\text{g m}^{-3}$) and high ($> 0.3 \mu\text{g m}^{-3}$) sulfate
391 concentrations. Figures 7a, 7b, and 7c show the factor loading, organic PM mass concentration,
392 and the ratio f of the IEPOX-SOA factor loading to the organic PM mass concentration,
393 respectively, plotted against NO_y concentration for low and high sulfate concentrations.

394 Figure 7a shows that for both low and high sulfate concentrations an increase in NO_y
395 concentration from background to polluted concentrations was associated with a decrease in the
396 IEPOX-SOA factor loading by two to three times. For low sulfate concentration, the interquartile
397 range of the factor loading decreased from [0.037, 0.093] to [0.022, 0.039] μg m⁻³ for an increase
398 in NO_y concentration from 0.5 to 2 ppb. For high sulfate concentration, the factor loading
399 decreased from [0.57, 0.95] to [0.21, 0.35] μg m⁻³ for the same transition in NO_y concentration.
400 The greatest changes in factor loading were in the region of 1 ppb NO_y. This region of greatest
401 sensitivity coincided with the transition from background to polluted conditions. ~~For the same~~
402 ~~time period, a change was reported in the gas phase from a dominance of ISOPOOH to~~
403 ~~MVK/MACR products across this transition in NO_y concentration (Liu et al., 2016a).~~

404 For the same time period of these PM analyses of IEPOX-SOA factor loading, Liu et al.
405 (2016a) observed a shift in dominant isoprene gas-phase products from ISOPOOH to
406 MVK/MACR across the transition in NO_y concentration. Liu et al. (2016a) further simulated the
407 dependence on NO concentration of the ratio of the production rate of ISOPOOH to that of MVK
408 + MACR. The highest ratios (0.6 to 0.9) were obtained for background concentrations of NO_y.
409 The calculated HO₂ concentration was < 4 × 10⁸ cm⁻³ (0.016 ppb). The simulated transition for
410 the dominant fate of the ISOPOO radicals occurred for an NO concentration of < 0.05 ppb.

411 Figure 7b shows that for both low and high sulfate concentrations the organic PM mass
412 concentration M_{org} and the IEPOX-SOA factor loading had opposite trends for low compared to
413 intermediate NO_y concentrations, even though the trend in M_{org} was less steep. The factor
414 loadings decreased by 60% whereas the M_{org} increased by 25% for 0.5 to 2 ppb NO_y (Figures 7a
415 and 7b). Increases in M_{org} can include contributions from secondary PM produced by enhanced
416 concentrations of hydroxyl radicals and ozone in the pollution plume as well as from primary

417 PM emitted from the Manaus urban region (Martin et al., ~~2016a~~2017; de Sá, in preparation). For
418 higher NO_y concentrations (> 2 ppb), however, Figure 7b shows that M_{org} decreased after a peak
419 value, approaching values close to background under the most polluted conditions. The
420 chemistry can become sufficiently shifted that more-volatile gas-phase products can be produced
421 (Pandis et al., 1991; Kroll et al., 2005; Carlton et al., 2009). In addition, hydroxyl radical
422 concentrations can also decrease because of titration by NO_2 (Valin et al., 2013; Rohrer et al.,
423 2014). An increase in total organic mass concentration could possibly contribute to a decrease in
424 IEPOX-derived PM production by kinetically limiting the uptake of IEPOX (Gaston et al., 2014;
425 Lin et al., 2014; Riva et al., 2016a). The dominant effect of the urban plume, however, seems to
426 be that of shifting the fate of ISOPOO radicals through the increase in NO , thereby significantly
427 decreasing the production of ISOPOOH (Liu et al., 2016a) (Section 3.5).

428 The combined trends of Figures 7a and 7b for increasing NO_y are represented in Figure
429 7c as the ratio f . The figure shows that f decreased for increasing NO_y concentration for both low
430 and high sulfate concentrations. The greatest decrease occurred across the range of NO_y/NO_y
431 concentrations that represented the shift from background to polluted conditions. For low sulfate
432 concentration, the interquartile range of f decreased from [0.09, 0.18] to [0.04, 0.09] for an
433 increase in NO_y concentration from 0.5 to 2 ppb. These ranges shifted to [0.35, 0.40] and [0.07,
434 0.18] for high sulfate concentration. ~~The magnitude of the decrease~~As a limiting statement, for
435 the most favorable conditions with respect to the production of IEPOX-derived PM in central
436 Amazonia (i.e., lowest NO_y and highest sulfate), f exceeded 0.40 at 25% frequency. The
437 implication is that at all times significant additional pathways for PM production were active.
438 This conclusion is subject to the accuracy of the IEPOX-SOA factor loading as a scalar proxy of
439 IEPOX-derived PM concentration (cf. discussion of Figure 1 in Section 3.1). The magnitude of

440 ~~the decrease in f~~ for high sulfate concentrations suggests that IEPOX-derived PM shifted from
441 being a major to a minor component of the PM, ~~although the caveats related to under- and~~
442 ~~overestimates connected to the IEPOX-SOA factor should be kept in mind (vide supra).~~ Taken
443 together, the results shown in Figure 7 demonstrate how urban pollution affected the production
444 and composition of regional IEPOX-derived PM.

445 The data sets presented in Figures 5, 6, and 7 lead to the conclusion that the additional
446 NO concentrations contributed by Manaus emissions typically suppress the production of
447 IEPOX-derived PM to a greater extent than the additional sulfate concentrations enhance it.
448 Figure 8 presents a systematic visualization. The factor loadings at T3 are represented as
449 contours for axes of sulfate and NO_y concentrations. Higher factor loadings are favored for
450 higher sulfate and lower NO_y concentrations. Factor loadings are most sensitive to changing
451 concentration in the high-sulfate, low-NO_y region. The gray dashed line in Figure 8 represents a
452 qualitative divisor between domains of typical background and polluted conditions downwind of
453 Manaus.

454 **3.5 Influence of NO on production and loss processes of IEPOX-derived PM**

455 Elevated NO may affect both the production and loss processes of IEPOX-derived PM.
456 On the one hand, production may be reduced because of increased scavenging of ISOPOO by
457 NO, thus obviating production of IEPOX and consequently of IEPOX-derived PM. Production
458 may also be reduced because of more rapid gas-phase loss of IEPOX in response to elevated OH
459 and O₃ concentrations. On the other hand, loss of IEPOX-derived PM may be enhanced due to
460 faster processing of its characteristic compounds by the elevated oxidant concentrations.

461 A Lagrangian model is employed to help delineate the relative importance of reduced
462 production compared to enhanced loss on the observed IEPOX-derived PM concentrations. The

463 model is initialized by background air that passes over Manaus in the mid-morning. The
 464 evolution of IEPOX-derived PM in that air mass is modeled under either polluted or background
 465 conditions for arrival at the T3 site in the afternoon. The governing differential equation of the
 466 model represents the sum of production and loss processes affecting the concentrations of
 467 IEPOX-derived PM, as follows:

$$468 \quad \frac{dM}{dt} = -\alpha_L k_L M + \alpha_P k_P \quad (1)$$

469 where M designates the IEPOX-derived PM mass concentration, t designates time, and the first
 470 and second terms on the right-hand side represent loss and production processes, respectively.
 471 Table 2 lists other symbol definitions and units.

472 The analytic solution of Equation 1 for time t is presented in the Supplement (Section
 473 S6). From this solution, characteristic times τ for production and loss processes for polluted
 474 compared to background conditions are as follows: $\tau_{P,pol} = M_0 / (\alpha_P k_P)$, $\tau_{P,bg} = M_0 / k_P$, $\tau_{L,pol} = 1 /$
 475 $(\alpha_L k_L)$, and $\tau_{L,bg} = 1 / k_L$ (Supplement, Section S6). The term M_0 represents the IEPOX-derived
 476 PM mass concentration just upwind of Manaus. Under background conditions, the enhancement
 477 factors α_L and α_P are unity by definition. Under polluted conditions, $\alpha_L = 2$ and $\alpha_P = 0.1$ to reflect
 478 enhanced loss and decreased production, respectively. Further descriptions of the model and
 479 assumptions are presented in the Supplement (Section S6).

480 The analysis strategy is to compare τ_P and τ_L to the transport time τ_{tr} under polluted and
 481 background conditions to assess the relative importance of altered production and loss processes
 482 for IEPOX-derived PM from Manaus to T3. The statistical mode value for τ_{tr} ~~is of~~ 4 h based on
 483 trajectory analysis is used in the model (Martin et al., ~~2016~~2016a). Intervals for the
 484 characteristic times τ_P and τ_L are constrained by the T3 afternoon data sets. Concentration ratios
 485 ξ , defined as $\xi = M_{pol} / M_{bg}$, are used to constrain the model (Table 3). The quantities M_{pol} and

486 M_{bg} denote $M(t = \tau_{tr})$, meaning the mass concentration at T3 under polluted or background
487 conditions, respectively. The use of the ratio quantity ζ in the analysis, rather than absolute
488 concentrations, provides increased robustness because of low variability in ζ across the observed
489 range of sulfate concentrations, even as M_{pol} and M_{bg} vary greatly (Table 3). The possible impact
490 of over- or underestimates of IEPOX-derived PM mass concentration, as a consequence of using
491 IEPOX-SOA factor loading as a surrogate, is also mitigated by the use of ζ .

492 Two cases of the model (1 and 2) are presented, respectively focusing on constraining k_P
493 or k_L and consequently τ_P or τ_L (Table 4). The results for Case 1 of the analysis are shown in
494 Figure 9a. The value of k_P is varied from 0 to $0.2 \mu\text{g m}^{-3} \text{h}^{-1}$ while the other model parameters are
495 held constant. The loss rate coefficient k_L is fixed at 0.015 h^{-1} , corresponding to a characteristic
496 time of 2.8 days (Supplement, Section S6). Based on observed values of ζ (gray shaded area in
497 Figure 9a), an interval for k_P of $[0.07, 0.13] \mu\text{g m}^{-3} \text{h}^{-1}$ is obtained, as indicated by the vertical
498 dashed lines. Across this interval, M_{bg} and M_{pol} vary from 0.49 to $0.72 \mu\text{g m}^{-3}$ and 0.23 to $0.25 \mu\text{g}$
499 m^{-3} , respectively, which are consistent with the observed IEPOX-SOA factor loadings (Table 3).
500 The modeled production times have intervals of $[1.8, 3.3] \text{ h}$ for $\tau_{P,bg}$ and $[18, 33] \text{ h}$ for $\tau_{P,pol}$.

501 Case 2 of the analysis evaluates constraints on the loss rate coefficient k_L , and results are
502 shown in Figure 9b. Loss processes can include chemistry, such as heterogeneous oxidation or
503 other in-particle reactions that reduce the IEPOX-SOA factor loading, as well as physical
504 mechanisms, such as particle deposition and particle dilution by entrainment that reduce mass
505 concentrations of IEPOX-derived PM (Supplement, Section S6). The value of k_L is varied over
506 three orders of magnitude, representing characteristic times of hours to weeks, while the other
507 model parameters are held constant (Table 4). The production rate coefficient k_P is fixed at 0.10
508 $\mu\text{g m}^{-3} \text{h}^{-1}$, corresponding to the interval midpoint of Case 1. The observed values of ζ (gray

509 shaded area) in intersection with the modeled values of ζ imply an upper limit on k_L at 0.043 h^{-1} ,
510 corresponding to characteristic times of a day to weeks (Figure 9b). Correspondingly, $\tau_{L,bg} > 24$
511 h under background conditions, and $\tau_{L,pol} > 12$ h under polluted conditions.

512 The analyses of Cases 1 and 2 constrain the values of $\tau_{P,pol}$, $\tau_{P,bg}$, $\tau_{L,pol}$, and $\tau_{L,bg}$ based on
513 the observed values of ζ . The lower limits of the characteristic times for loss, meaning $\tau_{L,bg} > 24$
514 h and $\tau_{L,pol} > 12$ h, are considerably longer than the transport time of 4 h under both background
515 and polluted conditions. Enhanced loss, therefore, does not explain alone the observed values of
516 ζ . By comparison, the observed values of ζ imply a shift in the characteristic time for production
517 from [1.8, 3.3] h under background conditions to [18, 33] h under pollution conditions. The shift
518 in timescale is significant in light of the transport time of 4 h. Therefore, reduced production,
519 rather than enhanced loss, is consistent with the lower IEPOX-derived PM concentrations under
520 polluted conditions. A few afternoon hours of altered isoprene chemistry is sufficient to
521 significantly shift the atmospheric concentration of IEPOX-derived PM.

522 **4. Summary and conclusions**

523 The influence of anthropogenic emissions on the production of organic particulate matter
524 from isoprene epoxydiols was studied during the wet season of the tropical forest in central
525 Amazonia. The IEPOX-derived PM concentration at the T3 site, as indicated by the IEPOX-
526 SOA factor loading, was lower under polluted compared to background conditions. Sulfate
527 concentration was an important first-order predictor of the IEPOX-SOA factor loading,
528 corroborating the understanding of the role of sulfate in the production of IEPOX-derived PM
529 that has been developed in laboratory studies as well as in investigations in the southeastern USA
530 (Surratt et al., 2007b; Budisulistiorini et al., 2013; Budisulistiorini et al., 2015; Hu et al., 2015;
531 Kuwata et al., 2015; Xu et al., 2015). Unlike the southeastern USA, however, where

532 anthropogenic influences dominated variability in sulfate concentrations, contributions by the
533 Manaus urban region to sulfate concentrations were of approximately equal magnitude to the
534 background variability in central Amazonia. By comparison, Manaus urban emissions of NO
535 dominated over background concentrations, and the NO_y concentration measured 4 to 6 h
536 downwind of Manaus at the T3 site was an important predictor of the IEPOX-SOA factor
537 loading. In net effect, the suppression of IEPOX production because of elevated NO
538 concentrations in the pollution plume dominated over any enhancements in IEPOX uptake
539 because of greater sulfate concentrations.

540 The dependence of the IEPOX-SOA factor loadings on both sulfate and NO_y
541 concentrations, as shown in Figure 8, suggests that altered net anthropogenic effects may be
542 expected for different geographic regions, even within Amazonia, and different time periods,
543 such as the wet and dry seasons. The T3 site experienced a wide range of NO_y concentrations,
544 allowing for the systematic demonstration of the dependence of IEPOX-derived PM
545 concentrations on NO_y concentrations. The results show that the transition in isoprene
546 photochemistry related to the production of IEPOX-derived PM is most sensitive precisely at the
547 transition between background and polluted conditions, around 1 ppb of NO_y, at least for central
548 Amazonia in the wet season. These findings suggest that the fraction of PM derived from IEPOX
549 might be lower and have lower variability for other geographic regions characterized by higher
550 NO_y baseline concentrations (e.g., upward of 1 to 2 ppb). For regions further downwind of the
551 urban center, the effects of the plume are expected to phase out both due to dilution and to
552 consumption of NO, and a gradual transition to background chemistry is expected to take place.
553 Adequately representing background conditions and the transition to polluted conditions within
554 models, including the dependence of the production of IEPOX-derived PM not only on sulfate

555 but also on NO concentration, is thus important for making accurate predictions of PM
556 concentrations, both in Amazonia and around the globe.

557 The findings herein can be considered in the context of Amazonia in transition (Davidson
558 et al., 2012). In the past 50 years, the metropolitan area of Manaus, today at more than 2 million
559 inhabitants, has experienced rapid economic and population growth (Martin et al., ~~2016~~2016a).
560 Changes in the fuel matrix, such as the ongoing shift from high-sulfur to low-sulfur oil in the
561 vehicle fleet as well as from fuel oil to natural gas in many power plants (Medeiros et al., in
562 preparation), are changing the composition of the Manaus pollution plume. Based on the findings
563 presented herein, a reduction in sulfate sources from Manaus, whether primary or secondary,
564 would not be expected to considerably affect the mass concentration of IEPOX-derived species
565 in forest regions affected by the plume. Background sources independent of Manaus appear
566 sufficient to sustain sulfate concentrations regionally. On the other hand, in the absence of
567 pollution control technologies, NO emissions can be expected to increase in coming years due to
568 the development of more efficient (i.e., higher temperature) sources of electricity associated with
569 the development of natural gas resources in the basin, as well as from growth in transportation
570 associated with increased population. Increased NO concentrations can be expected to reduce the
571 mass concentration of IEPOX-derived species in forest regions affected by the plume. Changes
572 in the atmospheric particle population can have follow-on effects on cloud type, duration, and
573 rainfall (Pöschl et al., 2010). In addition to PM derived from IEPOX as discussed herein, a better
574 understanding of other pathways that also contribute to organic PM, as well as possible changes
575 to those pathways with increasing pollution in the region, warrants further study so as to achieve
576 sufficient knowledge for decision-making related to air quality and climate in Amazonia.

Acknowledgments. Institutional support was provided by the Central Office of the Large Scale Biosphere Atmosphere Experiment in Amazonia (LBA), the National Institute of Amazonian Research (INPA), and Amazonas State University (UEA). We acknowledge support from the Atmospheric Radiation Measurement (ARM) Climate Research Facility, a user facility of the United States Department of Energy (DOE), Office of Science, sponsored by the Office of Biological and Environmental Research, and support from the Atmospheric System Research (ASR) program of that office. Additional funding was provided by the Amazonas State Research Foundation (FAPEAM), the São Paulo State Research Foundation (FAPESP), the USA National Science Foundation (NSF), and the Brazilian Scientific Mobility Program (CsF/CAPES). S. de Sá acknowledges support by the Schlumberger Foundation, Faculty for the Future Fellowship. The research was conducted under scientific license 001030/2012-4 of the Brazilian National Council for Scientific and Technological Development (CNPq).

References

- Andreae, M., Berresheim, H., Bingemer, H., Jacob, D. J., Lewis, B., Li, S. M., and Talbot, R. W.: The atmospheric sulfur cycle over the Amazon Basin: 2. Wet season, *J. Geophys. Res. Atmos.*, 95, 16813-16824, 1990, 10.1029/JD095iD10p16813.
- Andreae, M. O., Acevedo, O. C., Araùjo, A., Artaxo, P., Barbosa, C. G. G., Barbosa, H. M. J., Brito, J., Carbone, S., Chi, X., Cintra, B. B. L., da Silva, N. F., Dias, N. L., Dias-Júnior, C. Q., Ditas, F., Ditz, R., Godoi, A. F. L., Godoi, R. H. M., Heimann, M., Hoffmann, T., Kesselmeier, J., Könemann, T., Krüger, M. L., Lavric, J. V., Manzi, A. O., Lopes, A. P., Martins, D. L., Mikhailov, E. F., Moran-Zuloaga, D., Nelson, B. W., Nölscher, A. C., Santos Nogueira, D., Piedade, M. T. F., Pöhlker, C., Pöschl, U., Quesada, C. A., Rizzo, L. V., Ro, C. U., Ruckteschler, N., Sá, L. D. A., de Oliveira Sá, M., Sales, C. B., dos Santos, R. M. N., Saturno, J., Schöngart, J., Sörgel, M., de Souza, C. M., de Souza, R. A. F., Su, H., Targhetta, N., Tóta, J., Trebs, I., Trumbore, S., van Eijck, A., Walter, D., Wang, Z., Weber, B., Williams, J., Winderlich, J., Wittmann, F., Wolff, S., and Yáñez-Serrano, A. M.: The Amazon Tall Tower Observatory (ATTO): overview of pilot measurements on ecosystem ecology, meteorology, trace gases, and aerosols, *Atmos. Chem. Phys.*, 15, 10723-10776, 2015, 10.5194/acp-15-10723-2015.
- Bakwin, P. S., Wofsy, S. C., Fan, S. M., Keller, M., Trumbore, S. E., and Da Costa, J. M.: Emission of nitric oxide (NO) from tropical forest soils and exchange of NO between the forest canopy and atmospheric boundary layers, *J. Geophys. Res. Atmos.*, 95, 16755-16764, 1990, 10.1029/JD095iD10p16755.
- Bateman, A. P., Gong, Z., Liu, P., Sato, B., Cirino, G., Zhang, Y., Artaxo, P., Bertram, A. K., Manzi, A. O., Rizzo, L. V., Souza, R. A. F., Zaveri, R. A., and Martin, S. T.: Sub-

- micrometre particulate matter is primarily in liquid form over Amazon rainforest, *Nature Geosci.*, 9, 34-37, 2016, 10.1038/ngeo2599
<http://www.nature.com/ngeo/journal/v9/n1/abs/ngeo2599.html#supplementary-information>.
- Budisulistiorini, S. H., Canagaratna, M. R., Croteau, P. L., Marth, W. J., Baumann, K., Edgerton, E. S., Shaw, S. L., Knipping, E. M., Worsnop, D. R., Jayne, J. T., Gold, A., and Surratt, J. D.: Real-time continuous characterization of secondary organic aerosol derived from isoprene epoxydiols in downtown Atlanta, Georgia, using the Aerodyne Aerosol Chemical Speciation Monitor, *Environ. Sci. Technol.*, 47, 5686-5694, 2013, 10.1021/es400023n.
- Budisulistiorini, S. H., Li, X., Bairai, S. T., Renfro, J., Liu, Y., Liu, Y. J., McKinney, K. A., Martin, S. T., McNeill, V. F., Pye, H. O. T., Nenes, A., Neff, M. E., Stone, E. A., Mueller, S., Knote, C., Shaw, S. L., Zhang, Z., Gold, A., and Surratt, J. D.: Examining the effects of anthropogenic emissions on isoprene-derived secondary organic aerosol formation during the 2013 Southern Oxidant and Aerosol Study (SOAS) at the Look Rock, Tennessee ground site, *Atmos. Chem. Phys.*, 15, 8871-8888, 2015, 10.5194/acp-15-8871-2015.
- Budisulistiorini, S. H., Baumann, K., Edgerton, E. S., Bairai, S. T., Mueller, S., Shaw, S. L., Knipping, E. M., Gold, A., and Surratt, J. D.: Seasonal characterization of submicron aerosol chemical composition and organic aerosol sources in the southeastern United States: Atlanta, Georgia, and Look Rock, Tennessee, *Atmos. Chem. Phys.*, 16, 5171-5189, 2016, 10.5194/acp-16-5171-2016.
- Canagaratna, M. R., Jayne, J. T., Jimenez, J. L., Allan, J. D., Alfarra, M. R., Zhang, Q., Onasch, T. B., Drewnick, F., Coe, H., Middlebrook, A., Delia, A., Williams, L. R., Trimborn, A.

- M., Northway, M. J., DeCarlo, P. F., Kolb, C. E., Davidovits, P., and Worsnop, D. R.: Chemical and microphysical characterization of ambient aerosols with the aerodyne aerosol mass spectrometer, *Mass Spectrom. Rev.*, 26, 185-222, 2007, 10.1002/mas.20115.
- Carlton, A., Wiedinmyer, C., and Kroll, J.: A review of secondary organic aerosol (SOA) formation from isoprene, *Atmos. Chem. Phys.*, 9, 4987-5005, 2009, 10.5194/acp-9-4987-2009.
- Chen, Q., Farmer, D. K., Schneider, J., Zorn, S. R., Heald, C. L., Karl, T. G., Guenther, A., Allan, J. D., Robinson, N., Coe, H., Kimmel, J. R., Pauliquevis, T., Borrmann, S., Pöschl, U., Andreae, M. O., Artaxo, P., Jimenez, J. L., and Martin, S. T.: Mass spectral characterization of submicron biogenic organic particles in the Amazon Basin, *Geophys. Res. Lett.*, 36, L20806, 2009, 10.1029/2009GL039880.
- Chen, Q., Farmer, D. K., Rizzo, L. V., Pauliquevis, T., Kuwata, M., Karl, T. G., Guenther, A., Allan, J. D., Coe, H., Andreae, M. O., Pöschl, U., Jimenez, J. L., Artaxo, P., and Martin, S. T.: Submicron particle mass concentrations and sources in the Amazonian wet season (AMAZE-08), *Atmos. Chem. Phys.*, 15, 3687-3701, 2015, 10.5194/acp-15-3687-2015.
- Claeys, M., Graham, B., Vas, G., Wang, W., Vermeylen, R., Pashynska, V., Cafmeyer, J., Guyon, P., Andreae, M. O., Artaxo, P., and Maenhaut, W.: Formation of secondary organic aerosols through photooxidation of isoprene, *Science*, 303, 1173-1176, 2004, 10.1126/science.1092805.
- Crouse, J. D., Paulot, F., Kjaergaard, H. G., and Wennberg, P. O.: Peroxy radical isomerization in the oxidation of isoprene, *Phys. Chem. Chem. Phys.*, 13, 13607-13613, 2011, 10.1039/C1CP21330J.

- Davidson, E. A., de Araújo, A. C., Artaxo, P., Balch, J. K., Brown, I. F., Bustamante, M. M., Coe, M. T., DeFries, R. S., Keller, M., and Longo, M.: The Amazon basin in transition, *Nature*, 481, 321-328, 2012.
- de Sá, S. S.: ~~Sources~~Anthropogenic emissions affect the sources and composition of submicron particulate matter in central Amazonia ~~as affected by anthropogenic emissions during~~in the wet ~~and dry~~ season, in preparation.
- DeCarlo, P. F., Kimmel, J. R., Trimborn, A., Northway, M. J., Jayne, J. T., Aiken, A. C., Gonin, M., Fuhrer, K., Horvath, T., Docherty, K. S., Worsnop, D. R., and Jimenez, J. L.: Field-deployable, high-resolution, time-of-flight aerosol mass spectrometer, *Anal. Chem.*, 78, 8281-8289, 2006, 10.1021/ac061249n.
- Ervens, B. and Volkamer, R.: Glyoxal processing by aerosol multiphase chemistry: towards a kinetic modeling framework of secondary organic aerosol formation in aqueous particles, *Atmos. Chem. Phys.*, 10, 8219-8244, 2010, 10.5194/acp-10-8219-2010.
- Ervens, B., Turpin, B., and Weber, R.: Secondary organic aerosol formation in cloud droplets and aqueous particles (aqSOA): a review of laboratory, field and model studies, *Atmos. Chem. Phys.*, 11, 11069-11102, 2011, 10.5194/acp-11-11069-2011.
- Fu, T. M., Jacob, D. J., Wittrock, F., Burrows, J. P., Vrekoussis, M., and Henze, D. K.: Global budgets of atmospheric glyoxal and methylglyoxal, and implications for formation of secondary organic aerosols, *J. Geophys. Res. Atmos.*, 113, D15303, 2008, 10.1029/2007JD009505.
- Gaston, C. J., Riedel, T. P., Zhang, Z., Gold, A., Surratt, J. D., and Thornton, J. A.: Reactive uptake of an isoprene-derived epoxydiol to submicron aerosol particles, *Environ. Sci. Technol.*, 48, 11178-11186, 2014, 10.1021/es5034266.

Guenther, A., Jiang, X., Heald, C., Sakulyanontvittaya, T., Duhl, T., Emmons, L., and Wang, X.:

The Model of Emissions of Gases and Aerosols from Nature version 2.1 (MEGAN2. 1): an extended and updated framework for modeling biogenic emissions, *Geosci. Model Dev.*, 5, 1471–1492, 2012, 10.5194/gmd-5-1471-2012.

Hallquist, M., Wenger, J. C., Baltensperger, U., Rudich, Y., Simpson, D., Claeys, M., Dommen,

J., Donahue, N. M., George, C., Goldstein, A. H., Hamilton, J. F., Herrmann, H.,

Hoffmann, T., Iinuma, Y., Jang, M., Jenkin, M. E., Jimenez, J. L., Kiendler-Scharr, A.,

Maenhaut, W., McFiggans, G., Mentel, T. F., Monod, A., Prévôt, A. S. H., Seinfeld, J.

H., Surratt, J. D., Szmigielski, R., and Wildt, J.: The formation, properties and impact of secondary organic aerosol: current and emerging issues, *Atmos. Chem. Phys.*, 9, 5155-5236, 2009, 10.5194/acp-9-5155-2009.

Hu, W. W., Campuzano-Jost, P., Palm, B. B., Day, D. A., Ortega, A. M., Hayes, P. L.,

Krechmer, J. E., Chen, Q., Kuwata, M., Liu, Y. J., de Sá, S. S., McKinney, K., Martin, S.

T., Hu, M., Budisulistiorini, S. H., Riva, M., Surratt, J. D., St. Clair, J. M., Isaacman-Van

Wertz, G., Yee, L. D., Goldstein, A. H., Carbone, S., Brito, J., Artaxo, P., de Gouw, J. A.,

Koss, A., Wisthaler, A., Mikoviny, T., Karl, T., Kaser, L., Jud, W., Hansel, A., Docherty,

K. S., Alexander, M. L., Robinson, N. H., Coe, H., Allan, J. D., Canagaratna, M. R.,

Paulot, F., and Jimenez, J. L.: Characterization of a real-time tracer for isoprene

epoxydiols-derived secondary organic aerosol (IEPOX-SOA) from aerosol mass

spectrometer measurements, *Atmos. Chem. Phys.*, 15, 11807-11833, 2015, 10.5194/acp-15-11807-2015.

Hu, W. W., Palm, B., Day, D., Campuzano-Jost, P., Krechmer, J., Peng, Z., De Sá, S. S., Martin,

S. T., Alexander, M. L., Baumann, K., Hacker, L., Kiendler-Scharr, A., Koss, A., De

- Gouw, J., Goldstein, A. H., Seco, R., Sjostedt, S., Park, J.-H., Guenther, A., Kim, S., Canonaco, F., Prevot, A., Brune, W., and Jimenez, J. L.: Long lifetime of ambient isoprene epoxydiols-derived Secondary Organic Aerosol (IEPOX-SOA) against OH oxidation and evaporation, *Atmos. Chem. Phys. Disc.*, 2016, doi: 10.5194/acp-2016-418.
- Isaacman-VanWertz, G., Yee, L. D., Kreisberg, N. M., Wernis, R., Moss, J. A., Hering, S. V., de Sá, S. S., Martin, S. T., Alexander, M. L., Palm, B. B., Hu, W., Campuzano-Jost, P., Day, D. A., Jimenez, J. L., Riva, M., Surratt, J. D., Viegas, J., Manzi, A., Edgerton, E., Baumann, K., Souza, R., Artaxo, P., and Goldstein, A. H.: Ambient Gas-Particle Partitioning of Tracers for Biogenic Oxidation, *Env. Sci. Technol.*, 2016, 10.1021/acs.est.6b01674.
- Isaacman, G., Kreisberg, N., Yee, L., Worton, D., Chan, A., Moss, J., Hering, S., and Goldstein, A.: Online derivatization for hourly measurements of gas-and particle-phase semi-volatile oxygenated organic compounds by thermal desorption aerosol gas chromatography (SV-TAG), *Atmos. Meas. Tech.*, 7, 4417-4429, 2014, 10.5194/amt-7-4417-2014.
- Jacob, D. J. and Wofsy, S. C.: Budgets of reactive nitrogen, hydrocarbons, and ozone over the Amazon forest during the wet season, *J. Geophys. Res. Atmos.*, 95, 16737-16754, 1990, 10.1029/JD095iD10p16737.
- Jacobs, M. I., Burke, W., and Elrod, M. J.: Kinetics of the reactions of isoprene-derived hydroxynitrates: gas phase epoxide formation and solution phase hydrolysis, *Atmos. Chem. Phys.*, 14, 8933-8946, 2014, 10.5194/acp-14-8933-2014.
- Jimenez, J. L., Canagaratna, M. R., Donahue, N. M., Prevot, A. S. H., Zhang, Q., Kroll, J. H., DeCarlo, P. F., Allan, J. D., Coe, H., Ng, N. L., Aiken, A. C., Docherty, K. S., Ulbrich, I. M., Grieshop, A. P., Robinson, A. L., Duplissy, J., Smith, J. D., Wilson, K. R., Lanz, V.

- A., Hueglin, C., Sun, Y. L., Tian, J., Laaksonen, A., Raatikainen, T., Rautiainen, J., Vaattovaara, P., Ehn, M., Kulmala, M., Tomlinson, J. M., Collins, D. R., Cubison, M. J., Dunlea, J., Huffman, J. A., Onasch, T. B., Alfarra, M. R., Williams, P. I., Bower, K., Kondo, Y., Schneider, J., Drewnick, F., Borrmann, S., Weimer, S., Demerjian, K., Salcedo, D., Cottrell, L., Griffin, R., Takami, A., Miyoshi, T., Hatakeyama, S., Shimojo, A., Sun, J. Y., Zhang, Y. M., Dzepina, K., Kimmel, J. R., Sueper, D., Jayne, J. T., Herndon, S. C., Trimborn, A. M., Williams, L. R., Wood, E. C., Middlebrook, A. M., Kolb, C. E., Baltensperger, U., and Worsnop, D. R.: Evolution of organic aerosols in the atmosphere, *Science*, 326, 1525-1529, 2009, 10.1126/science.1180353.
- Kanakidou, M., Seinfeld, J. H., Pandis, S. N., Barnes, I., Dentener, F. J., Facchini, M. C., Van Dingenen, R., Ervens, B., Nenes, A., Nielsen, C. J., Swietlicki, E., Putaud, J. P., Balkanski, Y., Fuzzi, S., Horth, J., Moortgat, G. K., Winterhalter, R., Myhre, C. E. L., Tsigaridis, K., Vignati, E., Stephanou, E. G., and Wilson, J.: Organic aerosol and global climate modelling: a review, *Atmos. Chem. Phys.*, 5, 1053-1123, 2005, 10.5194/acp-5-1053-2005.
- Kaufman, Y. J., Tanré, D., and Boucher, O.: A satellite view of aerosols in the climate system, *Nature*, 419, 215-223, 2002.
- Kjaergaard, H. G., Knap, H. C., Ørnsø, K. B., Jørgensen, S., Crouse, J. D., Paulot, F., and Wennberg, P. O.: Atmospheric Fate of Methacrolein. 2. Formation of Lactone and Implications for Organic Aerosol Production, *J. Phys. Chem. A*, 116, 5763-5768, 2012, 10.1021/jp210853h.
- Krechmer, J. E., Coggon, M. M., Massoli, P., Nguyen, T. B., Crouse, J. D., Hu, W., Day, D. A., Tyndall, G. S., Henze, D. K., Rivera-Rios, J. C., Nowak, J. B., Kimmel, J. R., Mauldin,

- R. L., Stark, H., Jayne, J. T., Sipilä, M., Junninen, H., Clair, J. M. S., Zhang, X., Feiner, P. A., Zhang, L., Miller, D. O., Brune, W. H., Keutsch, F. N., Wennberg, P. O., Seinfeld, J. H., Worsnop, D. R., Jimenez, J. L., and Canagaratna, M. R.: Formation of low volatility organic compounds and secondary organic aerosol from isoprene hydroxyhydroperoxide low-NO oxidation, *Environ. Sci. Technol.*, 49, 10330-10339, 2015, 10.1021/acs.est.5b02031.
- Kroll, J. H., Ng, N. L., Murphy, S. M., Flagan, R. C., and Seinfeld, J. H.: Secondary organic aerosol formation from isoprene photooxidation under high-NO_x conditions, *Geophys. Res. Lett.*, 32, 2005, 10.1029/2005GL023637.
- Kuhn, U., Ganzeveld, L., Thielmann, A., Dindorf, T., Schebeske, G., Welling, M., Sciare, J., Roberts, G., Meixner, F. X., Kesselmeier, J., Lelieveld, J., Kolle, O., Ciccioli, P., Lloyd, J., Trentmann, J., Artaxo, P., and Andreae, M. O.: Impact of Manaus City on the Amazon Green Ocean atmosphere: ozone production, precursor sensitivity and aerosol load, *Atmos. Chem. Phys.*, 10, 9251-9282, 2010, 10.5194/acp-10-9251-2010.
- Kuwata, M., Liu, Y., McKinney, K., and Martin, S. T.: Physical state and acidity of inorganic sulfate can regulate the production of secondary organic material from isoprene photooxidation products, *Phys. Chem. Chem. Phys.*, 17, 5670-5678, 2015, 10.1039/C4CP04942J.
- Levine, J. G., MacKenzie, A. R., Squire, O. J., Archibald, A. T., Griffiths, P. T., Abraham, N. L., Pyle, J. A., Oram, D. E., Forster, G., Brito, J. F., Lee, J. D., Hopkins, J. R., Lewis, A. C., Bauguitte, S. J. B., Demarco, C. F., Artaxo, P., Messina, P., Lathièrre, J., Hauglustaine, D. A., House, E., Hewitt, C. N., and Nemitz, E.: Isoprene chemistry in pristine and polluted Amazon environments: Eulerian and Lagrangian model frameworks and the strong

- bearing they have on our understanding of surface ozone and predictions of rainforest exposure to this priority pollutant, *Atmos. Chem. Phys. Disc.*, 15, 24251-24310, 2015, doi: 10.5194/acpd-15-24251-2015.
- Lewandowski, M., Jaoui, M., Offenberg, J., Krug, J., and Kleindienst, T.: Atmospheric oxidation of isoprene and 1, 3-butadiene: influence of aerosol acidity and relative humidity on secondary organic aerosol, *Atmos. Chem. Phys.*, 15, 3773-3783, 2015, 10.5194/acp-15-3773-2015.
- Lim, H.-J., Carlton, A. G., and Turpin, B. J.: Isoprene forms secondary organic aerosol through cloud processing: Model simulations, *Environ. Sci. Technol.*, 39, 4441-4446, 2005, 10.1021/es048039h.
- Lin, Y.-H., Zhang, Z., Docherty, K. S., Zhang, H., Budisulistiorini, S. H., Rubitschun, C. L., Shaw, S. L., Knipping, E. M., Edgerton, E. S., Kleindienst, T. E., Gold, A., and Surratt, J. D.: Isoprene epoxydiols as precursors to secondary organic aerosol formation: acid-catalyzed reactive uptake studies with authentic compounds, *Environ. Sci. Technol.*, 46, 250-258, 2012, 10.1021/es202554c.
- Lin, Y.-H., Zhang, H., Pye, H. O. T., Zhang, Z., Marth, W. J., Park, S., Arashiro, M., Cui, T., Budisulistiorini, S. H., Sexton, K. G., Vizuete, W., Xie, Y., Luecken, D. J., Piletic, I. R., Edney, E. O., Bartolotti, L. J., Gold, A., and Surratt, J. D.: Epoxide as a precursor to secondary organic aerosol formation from isoprene photooxidation in the presence of nitrogen oxides, *Proc. Natl. Acad. Sci. USA*, 110, 6718-6723, 2013, 10.1073/pnas.1221150110.
- Lin, Y.-H., Budisulistiorini, S. H., Chu, K., Siejack, R. A., Zhang, H., Riva, M., Zhang, Z., Gold, A., Kautzman, K. E., and Surratt, J. D.: Light-absorbing oligomer formation in secondary

organic aerosol from reactive uptake of isoprene epoxydiols, *Environ. Sci. Technol.*, 48, 12012-12021, 2014, 10.1021/es503142b.

~~Liu, Y., Herdlinger-Blatt, I., McKinney, K., and Martin, S.: Production of methyl vinyl ketone and methacrolein via the hydroperoxyl pathway of isoprene oxidation, *Atmos. Chem. Phys.*, 13, 5715-5730, 2013, 10.5194/acp-13-5715-2013J., D'Ambro, E. L., Lee, B. H., Lopez-Hilfiker, F. D., Zaveri, R. A., Rivera-Rios, J. C., Keutsch, F. N., Iyer, S., Kurten, T., Zhang, Z., Gold, A., Surratt, J. D., Shilling, J. E., and Thornton, J. A.: Efficient Isoprene Secondary Organic Aerosol Formation from a Non-IEPOX Pathway, *Environ. Sci. Technol.*, 2016a, 10.1021/acs.est.6b01872.~~

~~Liu, Y., Herdlinger-Blatt, I., McKinney, K., and Martin, S.: Production of methyl vinyl ketone and methacrolein via the hydroperoxyl pathway of isoprene oxidation, *Atmos. Chem. Phys.*, 13, 5715-5730, 2013, 10.5194/acp-13-5715-2013.~~

Liu, Y., Kuwata, M., Strick, B. F., Geiger, F. M., Thomson, R. J., McKinney, K. A., and Martin, S. T.: Uptake of epoxydiol isomers accounts for half of the particle-phase material produced from isoprene photooxidation via the HO₂ pathway, *Environ. Sci. Technol.*, 49, 250-258, 2015, 10.1021/es5034298.

Liu, Y., Brito, J., Dorris, M. R., Rivera-Rios, J. C., Seco, R., Bates, K. H., Artaxo, P., Duvoisin, S., Keutsch, F. N., Kim, S., Goldstein, A. H., Guenther, A. B., Manzi, A. O., Souza, R. A. F., Springston, S. R., Watson, T. B., McKinney, K. A., and Martin, S. T.: Isoprene photochemistry over the Amazon rain forest, *Proc. Natl. Acad. Sci. USA*, 113, 6125-6130, ~~2016b~~2016a, 10.1073/pnas.1524136113.

Liu, J., D'Ambro, E. L., Lee, B. H., Lopez-Hilfiker, F. D., Zaveri, R. A., Rivera-Rios, J. C., Keutsch, F. N., Iyer, S., Kurten, T., Zhang, Z., Gold, A., Surratt, J. D., Shilling, J. E., and

Thornton, J. A.: Efficient Isoprene Secondary Organic Aerosol Formation from a Non-IEPOX Pathway, Environ. Sci. Technol., 2016b, 10.1021/acs.est.6b01872.

Liu, Y., Kuwata, M., McKinney, K. A., and Martin, S. T.: Uptake and release of gaseous species accompanying the reactions of isoprene photo-oxidation products with sulfate particles, *Phys. Chem. Chem. Phys.*, 18, 1595-1600, 2016c, 10.1039/C5CP04551G.

Lopez-Hilfiker, F. D., Mohr, C., D'Ambro, E. L., Lutz, A., Riedel, T. P., Gaston, C. J., Iyer, S., Zhang, Z., Gold, A., Surratt, J. D., Lee, B. H., Kurten, T., Hu, W. W., Jimenez, J., Hallquist, M., and Thornton, J. A.: Molecular composition and volatility of organic aerosol in the Southeastern US: implications for IEPOX derived SOA, *Environ. Sci. Technol.*, 2200–2209, 2016, 10.1021/acs.est.5b04769.

Marais, E. A., Jacob, D. J., Jimenez, J. L., Campuzano-Jost, P., Day, D. A., Hu, W., Krechmer, J., Zhu, L., Kim, P. S., Miller, C. C., Fisher, J. A., Travis, K., Yu, K., Hanisco, T. F., Wolfe, G. M., Arkinson, H. L., Pye, H. O. T., Froyd, K. D., Liao, J., and McNeill, V. F.: Aqueous-phase mechanism for secondary organic aerosol formation from isoprene: application to the southeast United States and co-benefit of SO₂ emission controls, *Atmos. Chem. Phys.*, 16, 1603-1618, 2016, 10.5194/acp-16-1603-2016.

Martin, S. T., Andreae, M. O., Artaxo, P., Baumgardner, D., Chen, Q., Goldstein, A. H., Guenther, A., Heald, C. L., Mayol-Bracero, O. L., McMurry, P. H., Pauliquevis, T., Pöschl, U., Prather, K. A., Roberts, G. C., Saleska, S. R., Silva Dias, M. A., Spracklen, D. V., Swietlicki, E., and Trebs, I.: Sources and properties of Amazonian aerosol particles, *Rev. Geophys.*, 48, RG2012, 2010a, 10.1029/2008RG000280.

Martin, S. T., Andreae, M. O., Althausen, D., Artaxo, P., Baars, H., Borrmann, S., Chen, Q., Farmer, D. K., Guenther, A., Gunthe, S. S., Jimenez, J. L., Karl, T., Longo, K., Manzi,

A., Müller, T., Pauliquevis, T., Petters, M. D., Prenni, A. J., Pöschl, U., Rizzo, L. V., Schneider, J., Smith, J. N., Swietlicki, E., Tota, J., Wang, J., Wiedensohler, A., and Zorn, S. R.: An overview of the Amazonian aerosol characterization experiment 2008 (AMAZE-08), *Atmos. Chem. Phys.*, 10, 11415-11438, 2010b, [10.5194/acp-10-11415-2010](https://doi.org/10.5194/acp-10-11415-2010).

Martin, S. T., Artaxo, P., Machado, L. [A. T., Manzi, A. O., Souza, R. A. F., Schumacher, C., Wang, J., Andreae, M. O., Barbosa, H. M. J., Fan, J., Fisch, G., Goldstein, A. H., Guenther, A., Jimenez, J. L., Pöschl, U., Silva Dias, M. A., Smith, J. N., and Wendisch, M.: Introduction: observations and modeling of the green ocean Amazon \(GoAmazon2014/5\), *Atmos. Chem. Phys.*, 16, 4785-4797, 2016a, \[10.5194/acp-16-4785-2016\]\(https://doi.org/10.5194/acp-16-4785-2016\).](#)

[Martin, S. T., Artaxo, P. E., Chen, Q., Guenther, A. B., Gunthe, S. S., Jimenez, J. L., Manzi, A., Prenni, K. L., Pöschl, U., Schneider, J., and Swietlicki, E.: AMAZE-08 Aerosol Characterization and Meteorological Data, Central Amazon Basin: 2008. ORNL Distributed Active Archive Center, 2016b.](#)

[Martin, S. T., Artaxo, P., Machado, L., Manzi, A. O., Souza, R. A. F., Schumacher, C., Wang, J., Biscaro, T., Brito, J., Calheiros, A., Jardine, K., Medeiros, A., Portela, B., Sá, S. S. d., Adachi, K., Aiken, A. C., Albrecht, R., Alexander, L., Andreae, M. O., Barbosa, H. M. J., Buseck, P., Chand, D., Comstock, J. M., Day, D. A., Dubey, M., Fan, J., Fast, J., Fisch, G., Fortner, E., Giangrande, S., Gilles, M., Goldstein, A. H., Guenther, A., Hubbe, J., Jensen, M., Jimenez, J. L., Keutsch, F. N., Kim, S., Kuang, C., Laskin, A., McKinney, K., Mei, F., Miller, M., Nascimento, R., Pauliquevis, T., Pekour, M., Peres, J., Petäjä, T., Pöhlker, C., Pöschl, U., Rizzo, L., Schmid, B., Shilling, J. E., Dias, M. A. S., Smith, J.](#)

N., Tomlinson, J. M., Tóta, J., and Wendisch, M.: The Green ocean Amazon Experiment (GoAmazon2014/5) observes pollution affecting gases, aerosols, clouds, and rainfall over the rain forest, B. Am. Meteorol. Soc., [2016a](#)[2017](#), doi:10.1175/BAMS-D-15-00221.1.

~~Martin, S. T., Artaxo, P. E., Chen, Q., Guenther, A. B., Gunthe, S. S., Jimenez, J. L., Manzi, A., Prenni, K. L., Poschl, U., Schneider, J., and Swietlicki, E.: AMAZE-08 Aerosol Characterization and Meteorological Data, Central Amazon Basin: 2008. ORNL Distributed Active Archive Center, 2016b.~~

~~Martin, S. T., Artaxo, P., Machado, L. A. T., Manzi, A. O., Souza, R. A. F., Schumacher, C., Wang, J., Andreae, M. O., Barbosa, H. M. J., Fan, J., Fisch, G., Goldstein, A. H., Guenther, A., Jimenez, J. L., Pöschl, U., Silva Dias, M. A., Smith, J. N., and Wendisch, M.: Introduction: observations and modeling of the green ocean Amazon (GoAmazon2014/5), Atmos. Chem. Phys., [16](#), 4785–4797, 2016c, [10.5194/acp-16-4785-2016](#).~~

Mather, J. H. and Voyles, J. W.: The ARM Climate Research Facility: A review of structure and capabilities, B. Am. Meteorol. Soc., 94, 377-392, 2013, <http://dx.doi.org.ezp-prod1.hul.harvard.edu/10.1175/BAMS-D-11-00218.1>.

McNeill, V. F., Woo, J. L., Kim, D. D., Schwier, A. N., Wannell, N. J., Sumner, A. J., and Barakat, J. M.: Aqueous-phase secondary organic aerosol and organosulfate formation in atmospheric aerosols: a modeling study, Environ. Sci. Technol., 46, 8075-8081, 2012, [10.1021/es3002986](#).

Medeiros, A., Souza, R. A. F., and Martin, S. T., in preparation.

Nel, A.: Air pollution-related illness: effects of particles, Science, 308, 804-806, 2005.

- Nguyen, T. B., Coggon, M. M., Bates, K. H., Zhang, X., Schwantes, R. H., Schilling, K. A., Loza, C. L., Flagan, R. C., Wennberg, P. O., and Seinfeld, J. H.: Organic aerosol formation from the reactive uptake of isoprene epoxydiols (IEPOX) onto non-acidified inorganic seeds, *Atmos. Chem. Phys.*, 14, 3497-3510, 2014, 10.5194/acp-14-3497-2014.
- Nguyen, T. B., Bates, K. H., Crouse, J. D., Schwantes, R. H., Zhang, X., Kjaergaard, H. G., Surratt, J. D., Lin, P., Laskin, A., Seinfeld, J. H., and Wennberg, P. O.: Mechanism of the hydroxyl radical oxidation of methacryloyl peroxyxynitrate (MPAN) and its pathway toward secondary organic aerosol formation in the atmosphere, *Phys. Chem. Chem. Phys.*, 17, 17914-17926, 2015, 10.1039/C5CP02001H.
- Pandis, S. N., Paulson, S. E., Seinfeld, J. H., and Flagan, R. C.: Aerosol formation in the photooxidation of isoprene and β -pinene, *Atmos. Environ., Part A*, 25, 997-1008, 1991, 10.1016/0960-1686(91)90141-S.
- Paulot, F., Crouse, J. D., Kjaergaard, H. G., Kürten, A., Clair, J. M. S., Seinfeld, J. H., and Wennberg, P. O.: Unexpected epoxide formation in the gas-phase photooxidation of isoprene, *Science*, 325, 730-733, 2009, 10.1126/science.1172910.
- Pope III, C. A. and Dockery, D. W.: Health effects of fine particulate air pollution: lines that connect, *J Air Waste Manag Assoc*, 56, 709-742, 2006.
- Pöschl, U., Martin, S. T., Sinha, B., Chen, Q., Gunthe, S. S., Huffman, J. A., Borrmann, S., Farmer, D. K., Garland, R. M., Helas, G., Jimenez, J. L., King, S. M., Manzi, A., Mikhailov, E., Pauliquevis, T., Petters, M. D., Prenni, A. J., Roldin, P., Rose, D., Schneider, J., Su, H., Zorn, S. R., Artaxo, P., and Andreae, M. O.: Rainforest aerosols as biogenic nuclei of clouds and precipitation in the Amazon, *Science*, 329, 1513-1516, 2010, 10.1126/science.1191056.

- Ramanathan, V., Crutzen, P., Kiehl, J., and Rosenfeld, D.: Aerosols, climate, and the hydrological cycle, *Science*, 294, 2119-2124, 2001.
- Riedel, T., Lin, Y.-H., Zhang, Z., Chu, K., Thornton, J., Vizuete, W., Gold, A., and Surratt, J.: Constraining condensed-phase formation kinetics of secondary organic aerosol components from isoprene epoxydiols, *Atmos. Chem. Phys.*, 16, 1245-1254, 2016, DOI: 10.5194/acp-16-1245-2016.
- Riva, M., Bell, D. M., Hansen, A.-M. K., Drozd, G. T., Zhang, Z., Gold, A., Imre, D., Surratt, J. D., Glasius, M., and Zelenyuk, A.: Effect of organic coatings, humidity and aerosol acidity on multiphase chemistry of isoprene epoxydiols, *Environ. Sci. Technol.*, 50, 5580-5588, 2016a, 10.1021/acs.est.5b06050.
- Riva, M., Budisulistiorini, S. H., Chen, Y., Zhang, Z., D'Ambro, E. L., Zhang, X., Gold, A., Turpin, B. J., Thornton, J. A., Canagaratna, M. R., and Surratt, J. D.: Chemical characterization of secondary organic aerosol from oxidation of isoprene hydroxyhydroperoxides, *Environ. Sci. Technol.*, 2016b, 10.1021/acs.est.6b02511.
- Robinson, N. H., Hamilton, J. F., Allan, J. D., Langford, B., Oram, D. E., Chen, Q., Docherty, K., Farmer, D. K., Jimenez, J. L., Ward, M. W., Hewitt, C. N., Barley, M. H., Jenkin, M. E., Rickard, A. R., Martin, S. T., McFiggans, G., and Coe, H.: Evidence for a significant proportion of Secondary Organic Aerosol from isoprene above a maritime tropical forest, *Atmos. Chem. Phys.*, 11, 1039-1050, 2011, 10.5194/acp-11-1039-2011.
- Rohrer, F., Lu, K., Hofzumahaus, A., Bohn, B., Brauers, T., Chang, C.-C., Fuchs, H., Haseler, R., Holland, F., Hu, M., Kita, K., Kondo, Y., Li, X., Lou, S., Oebel, A., Shao, M., Zeng, L., Zhu, T., Zhang, Y., and Wahner, A.: Maximum efficiency in the hydroxyl-radical-

- based self-cleansing of the troposphere, *Nat. Geosci.*, 7, 559-563, 2014,
10.1038/ngeo2199.
- Romer, P. S., Duffey, K. C., Wooldridge, P. J., Allen, H. M., Ayres, B. R., Brown, S. S., Brune,
W. H., Crouse, J. D., de Gouw, J., Draper, D. C., Feiner, P. A., Fry, J. L., Goldstein, A.
H., Koss, A., Misztal, P. K., Nguyen, T. B., Olson, K., Teng, A. P., Wennberg, P. O.,
Wild, R. J., Zhang, L., and Cohen, R. C.: The lifetime of nitrogen oxides in an isoprene-
dominated forest, *Atmos. Chem. Phys.*, 16, 7623-7637, 2016, 10.5194/acp-16-7623-2016.
- Rummel, U., Ammann, C., Kirkman, G., Moura, M., Foken, T., Andreae, M., and Meixner, F.:
Seasonal variation of ozone deposition to a tropical rain forest in southwest Amazonia,
Atmos. Chem. Phys., 7, 5415-5435, 2007, 10.5194/acp-7-5415-2007.
- Schmid, B., Tomlinson, J. M., Hubbe, J. M., Comstock, J. M., Mei, F., Chand, D., Pekour, M. S.,
Kluzek, C. D., Andrews, E., Biraud, S. C., and McFarquhar, G. M.: The DOE ARM
aerial facility, *B. Am. Meteorol. Soc.*, 95, 723-742, 2014, 10.1175/BAMS-D-13-00040.1.
- Slowik, J. G., Brook, J., Chang, R. Y. W., Evans, G. J., Hayden, K., Jeong, C. H., Li, S. M.,
Liggio, J., Liu, P. S. K., McGuire, M., Mihele, C., Sjostedt, S., Vlasenko, A., and Abbatt,
J. P. D.: Photochemical processing of organic aerosol at nearby continental sites: contrast
between urban plumes and regional aerosol, *Atmos. Chem. Phys.*, 11, 2991-3006, 2011,
10.5194/acp-11-2991-2011.
- St. Clair, J. M., Rivera-Rios, J. C., Crouse, J. D., Knap, H. C., Bates, K. H., Teng, A. P.,
Jørgensen, S., Kjaergaard, H. G., Keutsch, F. N., and Wennberg, P. O.: Kinetics and
products of the reaction of the first-generation isoprene hydroxy hydroperoxide
(ISOPOOH) with OH, *J. Phys. Chem. A*, 2015, 10.1021/acs.jpca.5b06532.

- Surratt, J. D., Murphy, S. M., Kroll, J. H., Ng, N. L., Hildebrandt, L., Sorooshian, A., Szmigielski, R., Vermeylen, R., Maenhaut, W., Claeys, M., Flagan, R. C., and Seinfeld, J. H.: Chemical composition of secondary organic aerosol formed from the photooxidation of isoprene, *J. Phys. Chem. A*, 110, 9665-9690, 2006, 10.1021/jp061734m.
- Surratt, J. D., Lewandowski, M., Offenberg, J. H., Jaoui, M., Kleindienst, T. E., Edney, E. O., and Seinfeld, J. H.: Effect of acidity on secondary organic aerosol formation from isoprene, *Environ. Sci. Technol.*, 41, 5363-5369, 2007a, 10.1021/es0704176.
- Surratt, J. D., Kroll, J. H., Kleindienst, T. E., Edney, E. O., Claeys, M., Sorooshian, A., Ng, N. L., Offenberg, J. H., Lewandowski, M., Jaoui, M., Flagan, R. C., and Seinfeld, J. H.: Evidence for organosulfates in secondary organic aerosol, *Environ. Sci. Technol.*, 41, 517-527, 2007b, 10.1021/es062081q.
- Surratt, J. D., Chan, A. W., Eddingsaas, N. C., Chan, M., Loza, C. L., Kwan, A. J., Hersey, S. P., Flagan, R. C., Wennberg, P. O., and Seinfeld, J. H.: Reactive intermediates revealed in secondary organic aerosol formation from isoprene, *Proc. Natl. Acad. Sci. USA*, 107, 6640-6645, 2010, 10.1073/pnas.0911114107.
- Torres, A. and Buchan, H.: Tropospheric nitric oxide measurements over the Amazon Basin, *J. Geophys. Res. Atmos.*, 93, 1396-1406, 1988, 10.1029/JD093iD02p01396.
- Trebs, I., Mayol-Bracero, O. L., Pauliquevis, T., Kuhn, U., Sander, R., Ganzeveld, L., Meixner, F. X., Kesselmeier, J., Artaxo, P., and Andreae, M. O.: Impact of the Manaus urban plume on trace gas mixing ratios near the surface in the Amazon Basin: Implications for the NO-NO₂-O₃ photostationary state and peroxy radical levels, *J. Geophys. Res. Atmos.*, 117, D05307, 2012, doi:10.1029/2011JD016386.

- Ulbrich, I., Canagaratna, M., Zhang, Q., Worsnop, D., and Jimenez, J.: Interpretation of organic components from Positive Matrix Factorization of aerosol mass spectrometric data, *Atmos. Chem. Phys.*, 9, 2891-2918, 2009, 10.5194/acp-9-2891-2009.
- Valin, L., Russell, A., and Cohen, R.: Variations of OH radical in an urban plume inferred from NO₂ column measurements, *Geophys. Res. Lett.*, 40, 1856-1860, 2013, 10.1002/grl.50267.
- Volkamer, R., San Martini, F., Molina, L. T., Salcedo, D., Jimenez, J. L., and Molina, M. J.: A missing sink for gas-phase glyoxal in Mexico City: Formation of secondary organic aerosol, *Geophys. Res. Lett.*, 34, L19807, 2007, 10.1029/2007GL030752.
- Wang, W., Kourtchev, I., Graham, B., Cafmeyer, J., Maenhaut, W., and Claeys, M.: Characterization of oxygenated derivatives of isoprene related to 2-methyltetrols in Amazonian aerosols using trimethylsilylation and gas chromatography/ion trap mass spectrometry, *Rap. Commun. Mass Spectrom.*, 19, 1343-1351, 2005, 10.1002/rcm.1940.
- Wennberg, P.: Let's abandon the "high NO_x" and "low NO_x" terminology, *IGAC news*, 50, 3-4, 2013.
- Worton, D. R., Surratt, J. D., LaFranchi, B. W., Chan, A. W. H., Zhao, Y., Weber, R. J., Park, J.-H., Gilman, J. B., de Gouw, J., Park, C., Schade, G., Beaver, M., Clair, J. M. S., Crouse, J., Wennberg, P., Wolfe, G. M., Harrold, S., Thornton, J. A., Farmer, D. K., Docherty, K. S., Cubison, M. J., Jimenez, J.-L., Frossard, A. A., Russell, L. M., Kristensen, K., Glasius, M., Mao, J., Ren, X., Brune, W., Browne, E. C., Pusede, S. E., Cohen, R. C., Seinfeld, J. H., and Goldstein, A. H.: Observational insights into aerosol formation from isoprene, *Environ. Sci. Technol.*, 47, 11403-11413, 2013, 10.1021/es4011064.

Xu, L., Guo, H., Boyd, C. M., Klein, M., Bougiatioti, A., Cerully, K. M., Hite, J. R., Isaacman-VanWertz, G., Kreisberg, N. M., Knote, C., Olson, K., Koss, A., Goldstein, A. H., Hering, S. V., de Gouw, J., Baumann, K., Lee, S.-H., Nenes, A., Weber, R. J., and Ng, N. L.: Effects of anthropogenic emissions on aerosol formation from isoprene and monoterpenes in the southeastern United States, *Proc. Natl. Acad. Sci. USA*, 112, 37-42, 2015, [10.1073/pnas.1417609112](https://doi.org/10.1073/pnas.1417609112).

Zhang, Q., Jimenez, J. L., Canagaratna, M. R., Allan, J. D., Coe, H., Ulbrich, I., Alfarra, M. R., Takami, A., Middlebrook, A. M., Sun, Y. L., Dzepina, K., Dunlea, E., Docherty, K., DeCarlo, P. F., Salcedo, D., Onasch, T., Jayne, J. T., Miyoshi, T., Shimojo, A., Hatakeyama, S., Takegawa, N., Kondo, Y., Schneider, J., Drewnick, F., Borrmann, S., Weimer, S., Demerjian, K., Williams, P., Bower, K., Bahreini, R., Cottrell, L., Griffin, R. J., Rautiainen, J., Sun, J. Y., Zhang, Y. M., and Worsnop, D. R.: Ubiquity and dominance of oxygenated species in organic aerosols in anthropogenically-influenced Northern Hemisphere midlatitudes, *Geophys. Res. Lett.*, 34, L13801, 2007, [10.1029/2007GL029979](https://doi.org/10.1029/2007GL029979).

List of Tables

| Group | NO _y range (ppb) | Fit slope | Fit intercept | Fit R^2 |
|-------|-----------------------------|-----------|---------------|-----------|
| 1 | < 0.66 | 2.16 | -0.13 | 0.75 |
| 2 | 0.66 – 0.92 | 1.48 | -0.04 | 0.64 |
| 3 | 0.92 – 1.55 | 0.78 | 0.06 | 0.24 |
| 4 | 1.55 – 2.45 | 0.71 | -0.01 | 0.44 |
| 5 | > 2.45 | 0.55 | -0.02 | 0.62 |

Table 1. Parameters associated with NO_y groupings in Figure 6. Listed are the NO_y concentrations and the parameters for least-squares linear fits to each group. R^2 represents the coefficient of determination.

| Symbol | Description | Unit |
|-----------------|---|------------------------------------|
| M | mass concentration of IEPOX-derived PM | $\mu\text{g m}^{-3}$ |
| t | time | h |
| k_P | zero-order rate coefficient for production under background conditions | $\mu\text{g m}^{-3} \text{h}^{-1}$ |
| k_L | first-order rate coefficient for loss under background conditions | h^{-1} |
| α | multiplicative factor representing the effects of Manaus pollution on rate coefficients | |
| τ | characteristic time of a process (e.g., production, loss, or transport) | h |
| Subscript tr | Refers to transport | |
| Subscript bg | Refers to background conditions | |
| Subscript pol | Refers to polluted conditions | |
| Subscript 0 | Refers to an initial state (i.e., just upwind of Manaus) | |
| Subscript P | Refers to production processes | |
| Subscript L | Refers to loss processes | |

Table 2. Descriptions and units of symbols in the model.

| | Loading ($\mu\text{g m}^{-3}$) for background conditions | | Loading ($\mu\text{g m}^{-3}$) for polluted conditions | | Ratio ζ | |
|----------------------|--|-----------------|--|-----------------|---------------|---------|
| | Low | High | Low | High | Low | High |
| | sulfate | sulfate | sulfate | sulfate | sulfate | sulfate |
| IEPOX- SOA factor | [0.037, 0.093] | [0.57, 0.95] | [0.022, 0.039] | [0.21, 0.35] | 0.47 | 0.35 |

Table 3. Interquartile intervals of IEPOX-SOA factor loadings observed for background and polluted conditions. Background and polluted conditions correspond to approximately 0.5 ppb and 2 ppb of NO_y , respectively. The table also lists the resulting ratio ζ of the median factor loading under polluted compared to background conditions.

| Model case | Parameter values | | | | Initial condition |
|---------------|------------------|------------|------------|------------|-------------------|
| | k_P | k_L | α_P | α_L | M_0 |
| 1. Vary k_P | 0 to 0.2 | 0.018 | 0.1 | 3 | 0.23 |
| 2. Vary k_L | 0.065 | 0.001 to 1 | 0.1 | 3 | 0.23 |

Table 4. Parameter values and initial conditions used in model cases. Descriptions and units are listed in Table 2. The M_0 value is based on the mean IEPOX-SOA factor loading that was measured from 14:00-16:00 UTC (10:00-12:00 local time) at a regional background site during two months of the wet season in 2008 (Chen et al., 2015). For comparison, a similar value of $0.19 \mu\text{g m}^{-3}$ was obtained during the present study as the mean value observed at the T3 site for $\text{NO}_y < 1$ ppb (14:00-16:00 UTC).

List of Figures

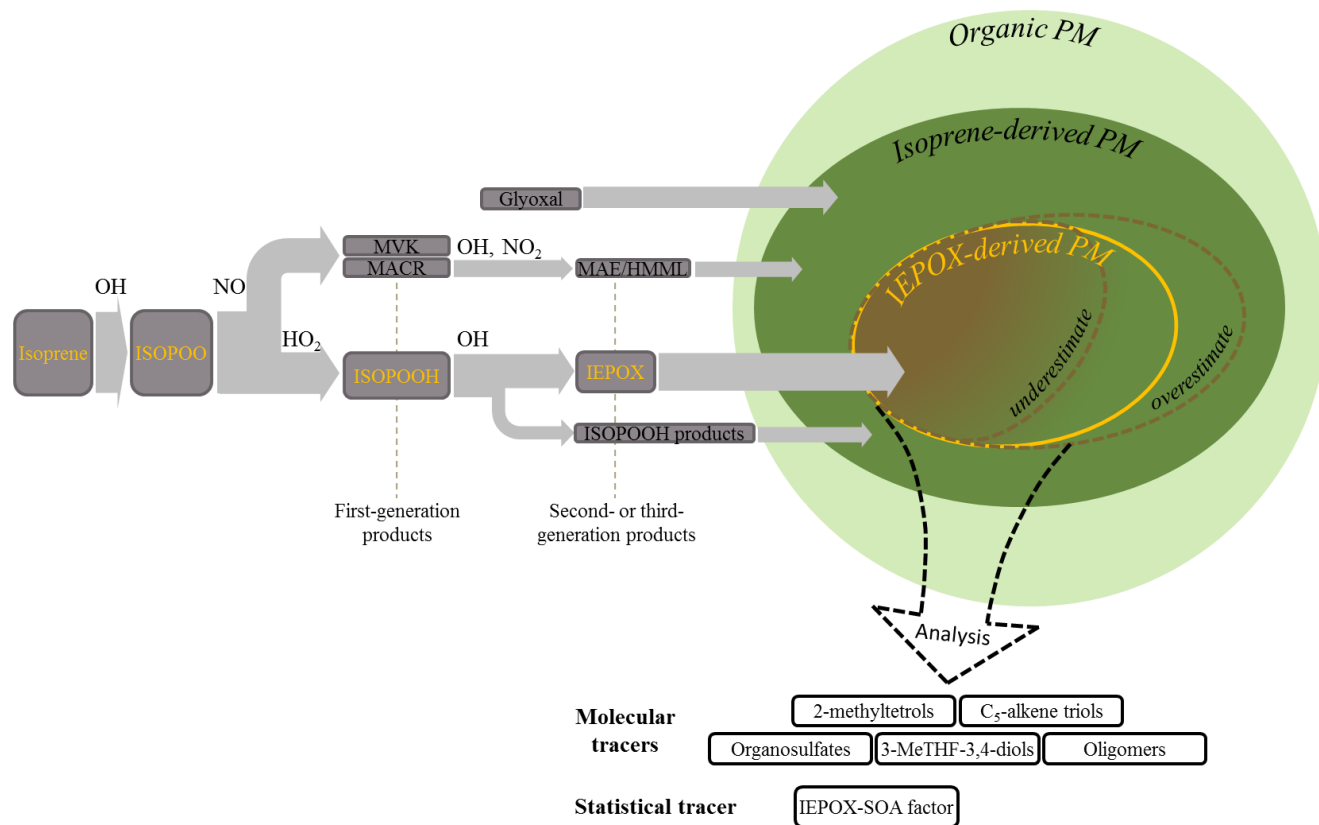


Figure 1. Schematic diagram for the production of IEPOX-derived PM from the photooxidation of isoprene. Organic peroxy radicals (ISOPOO), produced by OH attack and O₂ addition to isoprene, are scavenged along NO or HO₂ pathways. By the HO₂ pathway, organic hydroperoxides (ISOPOOH) are first-generation products that react with additional OH to produce isoprene epoxydiols (IEPOX). The IEPOX species undergo reactive uptake into particles, ultimately producing IEPOX-derived particulate matter. Arrow thickness qualitatively illustrates the relative importance (i.e., mass flux) of a reaction channel under background conditions. Gray and green background colors indicate species in the gas and particle phases, respectively. The light-green disk represents the total organic PM. Within that disk, the contribution by isoprene-derived PM, including compounds produced both IEPOX and non-IEPOX pathways, is represented by the dark-green oval. Inside that oval, the contribution by IEPOX-derived PM is represented by the yellow oval region. The color gradient between brown and dark green illustrates the chemical modification of the IEPOX-derived PM over time. The large dashed black arrow represents the analytical methods that use different types of molecular and statistical tracers (listed in the boxes) to quantify the IEPOX-derived PM mass concentrations. For simplicity, the figure omits the many routes leading to the production of glyoxal (Fu et al., 2008), possible ISOPOO isomerization when NO and HO₂ concentrations are sufficiently low (Crouse et al., 2011; Liu et al., 2016a), second-generation production of peroxyacetic nitric anhydride (Lin et al., 2013; Nguyen et al., 2015), and particle water and other inorganic components. 3-methyltetrahydrofuran-3,4-diols are abbreviated as 3-MeTHF-3,4-diols. Other abbreviations are provided in the main text.

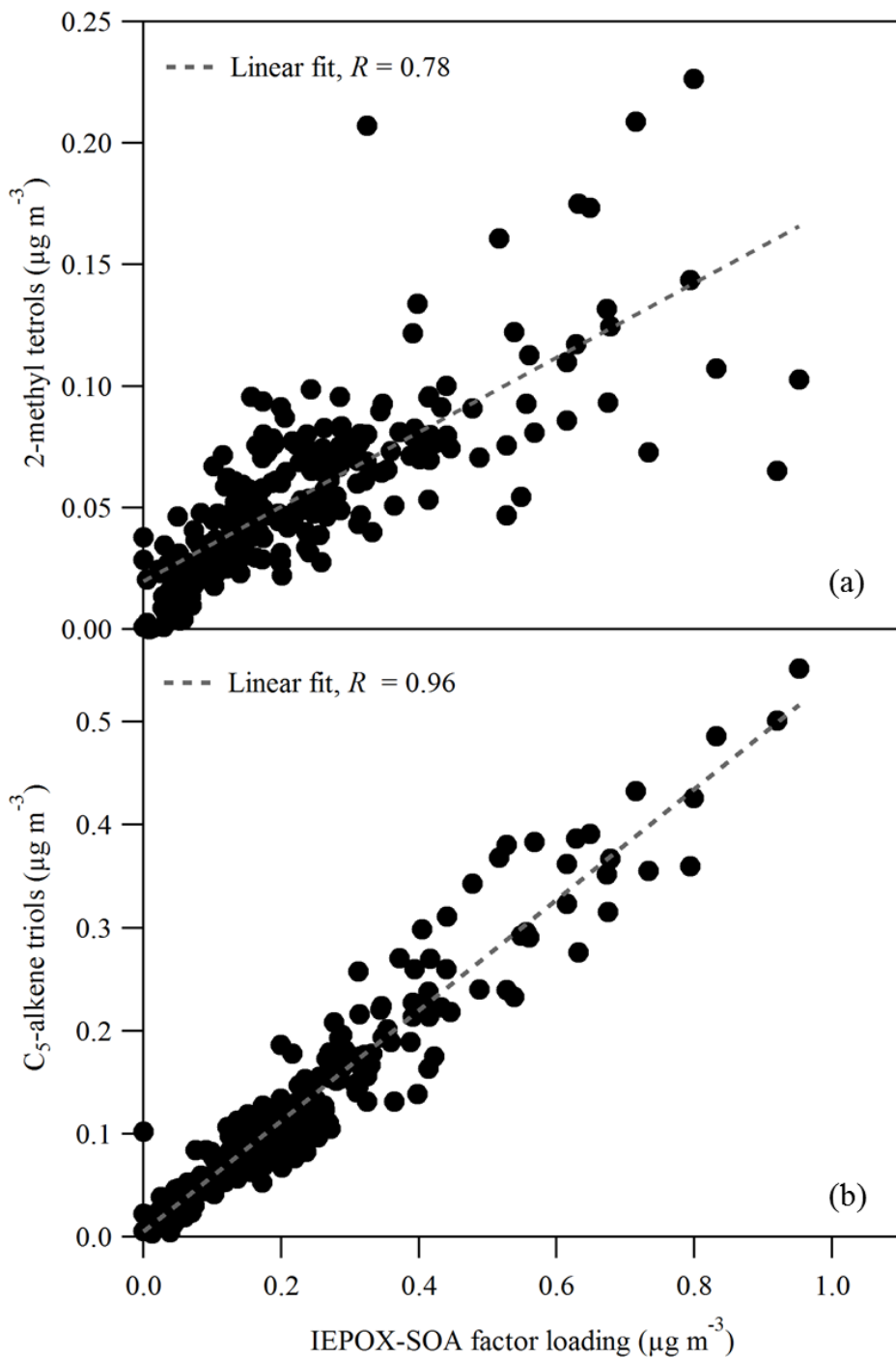


Figure 2. Scatter plot of the loading of the IEPOX-SOA factor derived from analysis of the AMS data set and the mass concentrations of C_5 -alkene triols and 2-methyltetrols measured by SV-TAG. All data collected during IOP1 are included, meaning that the plotted data are not limited to afternoon time periods.

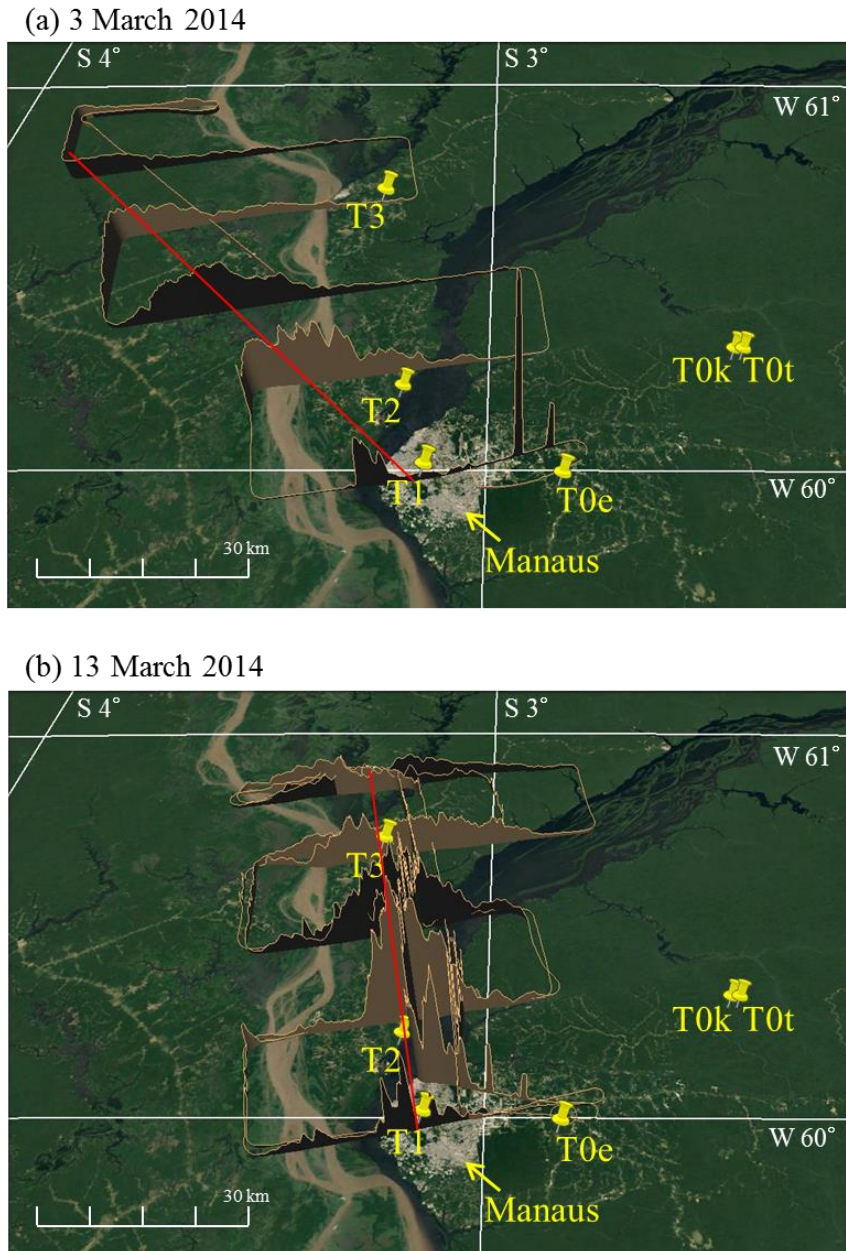


Figure 3. Visualization of the Manaus pollution plume by plotting particle number concentrations in the vertical axis. Observations took place on flights from late morning to early afternoon on (a) March 3, 2014, 17:45 – 19:26 UTC, and (b) March 13, 2014, 14:14 – 17:21 UTC. Local time is UTC minus 4 h. The red lines guide the eye through the central axis of the plume. The direction and extent of the plume was observed by the G-1 aircraft within the atmospheric boundary layer downwind of Manaus. Measured particle number concentrations are plotted on a vertical axis on top of an image of land cover in the horizontal plane. Particle concentrations in the center of the plume ranged from 10,000 to 25,000 cm^{-3} nearby Manaus. Yellow pins indicate the locations of some of the GoAmazon2014/5 research sites, including T3 (Martin et al., [2016](#)[2016a](#)).

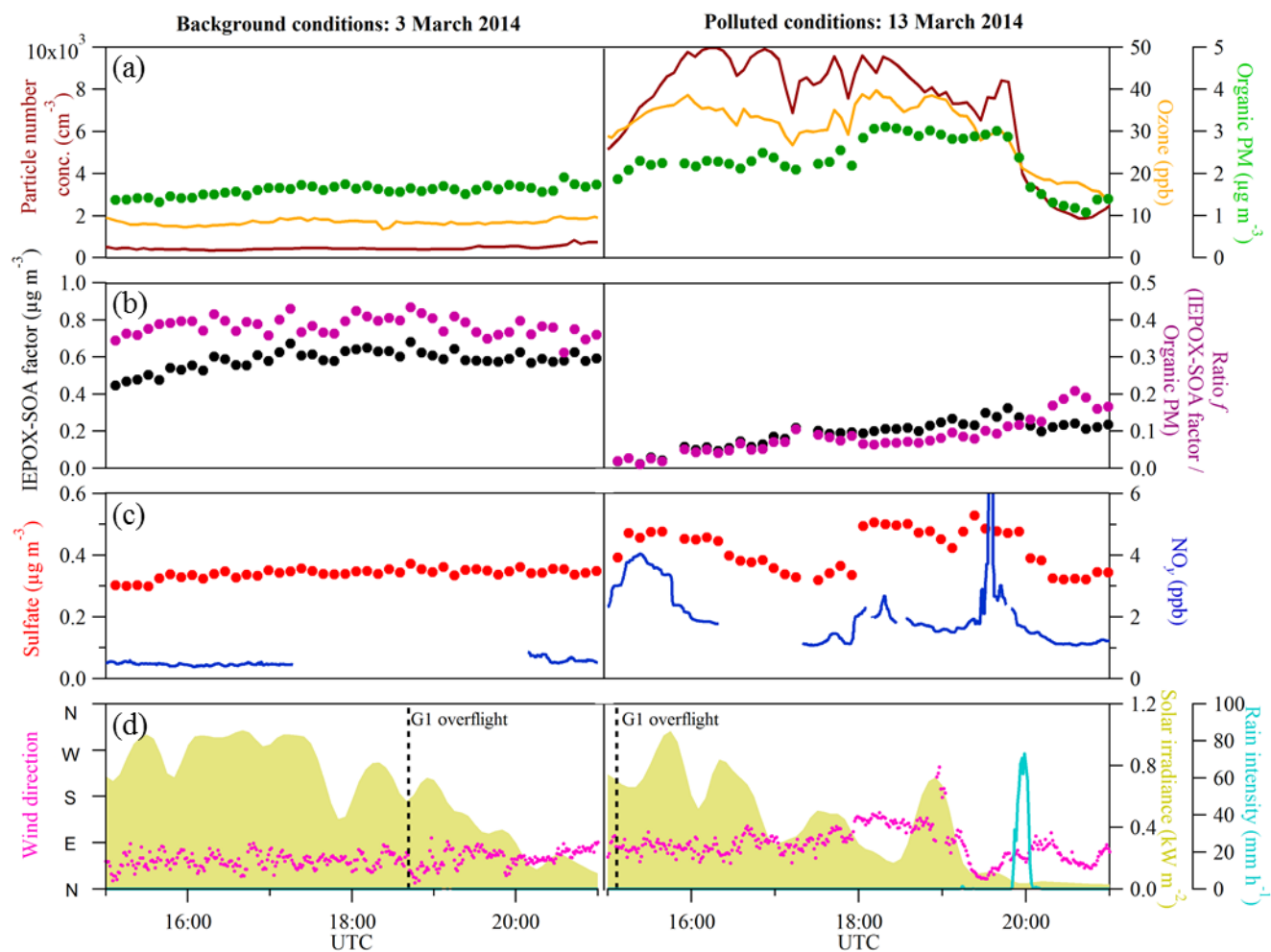


Figure 4. Case studies of (left) background and (right) polluted air masses passing over T3 on afternoons of March 3 and 13, 2014. (a) Ozone, particle number, and organic mass concentration. (b) IEPOX-SOA factor loading and the ratio f of the factor loading to the organic PM concentration. (c) Sulfate and NO_y concentrations. (d) Wind direction, rain intensity, and solar irradiance. Local time is UTC minus 4 h. Time points of overflights at 500 m by the G-1 research aircraft are marked by the dashed line (Martin et al., 2016a).

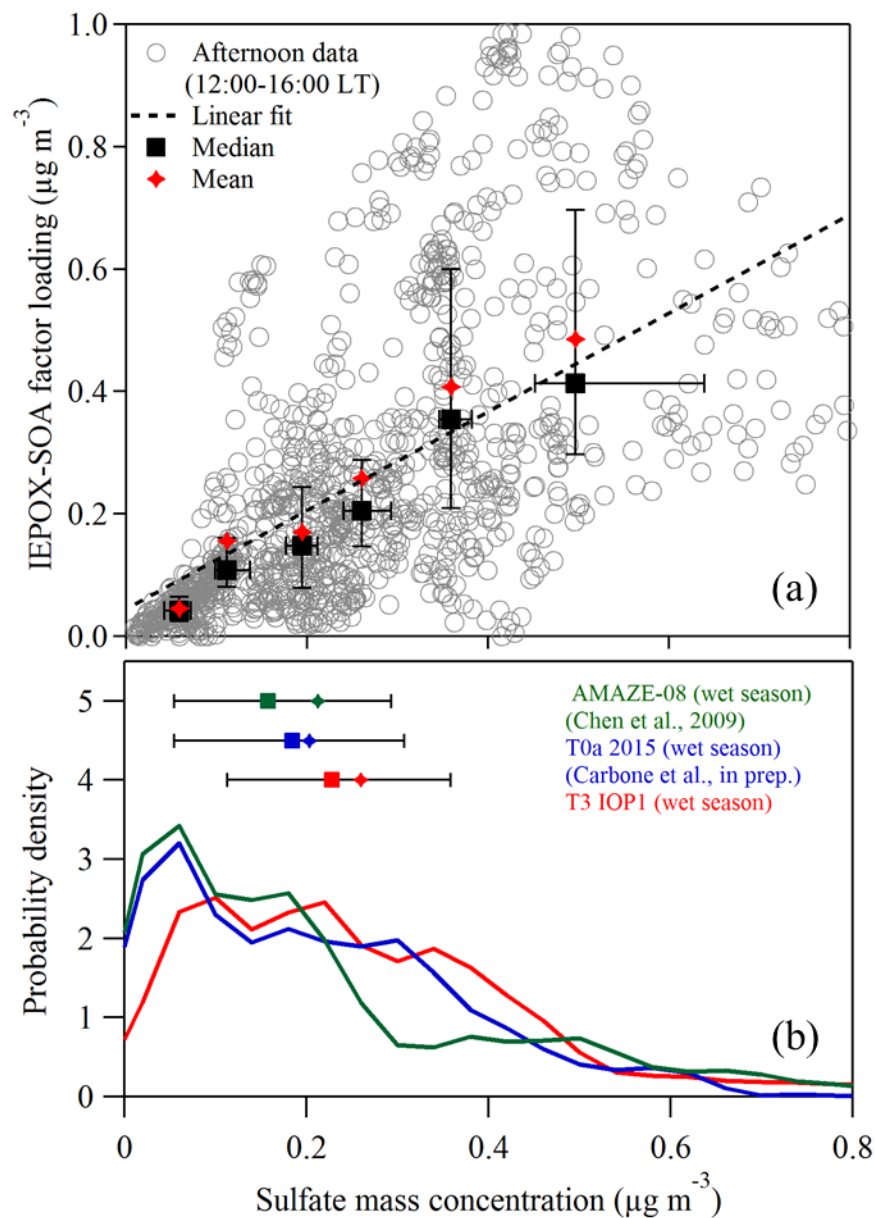


Figure 5. (a) Scatter plot of sulfate mass concentration and IEPOX-SOA factor loading. A least-squares linear fit is represented by the dashed line ($R^2 = 0.37$). The data set was collected into six subsets based on sulfate concentration to calculate statistics. Medians (squares) and means (diamonds) of each subset are plotted. Whiskers on the medians represent the interquartile ranges. (b) Probability density function of sulfate mass concentration at the background site T0t (“TT34”) north of Manaus in the wet season of 2008 (Chen et al., 2009; Martin et al., 2010b; Martin et al., 2016b), at the background site T0a (“ATTO”) northeast of Manaus in the wet season of 2015 (Andreae et al., 2015), and at T3 during the wet season of 2014 (IOP1). The plotted data sets were recorded during local afternoons (12:00-16:00 local time; 16:00-20:00 UTC). Means (diamonds), medians (squares), and interquartile range (whiskers) are shown for the probability density functions.

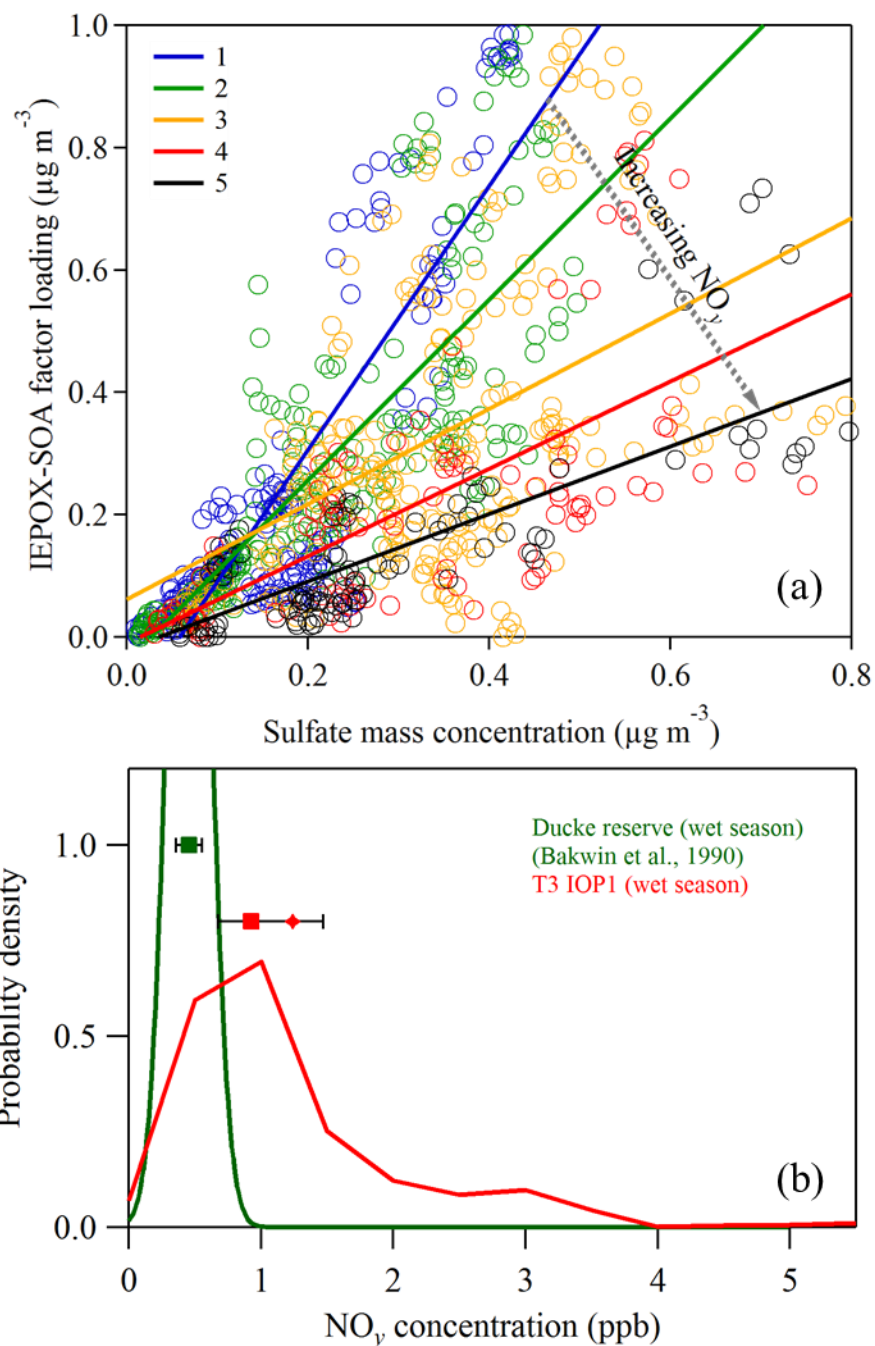


Figure 6. (a) Scatter plot of sulfate mass concentration and IEPOX-SOA factor loading for local afternoon (12:00-16:00 local time; 16:00-20:00 UTC). The data sets were collected into five subsets, colored and labeled 1 to 5, based on NO_y concentration. Table 1 presents the parameters of the five least-squares linear fits represented by the colored lines in the figure. (b) Probability density function of NO_y concentration at a background site nearby Manaus in the wet season of 1987 (Bakwin et al., 1990) and at T3 during the wet season of 2014 (IOP1) (afternoon data). Means (diamonds), medians (squares), and interquartile range (whiskers) are shown for the probability density functions. Additional analysis of panel (a) is discussed in the Supplement (Section S5) related to Figure S5.

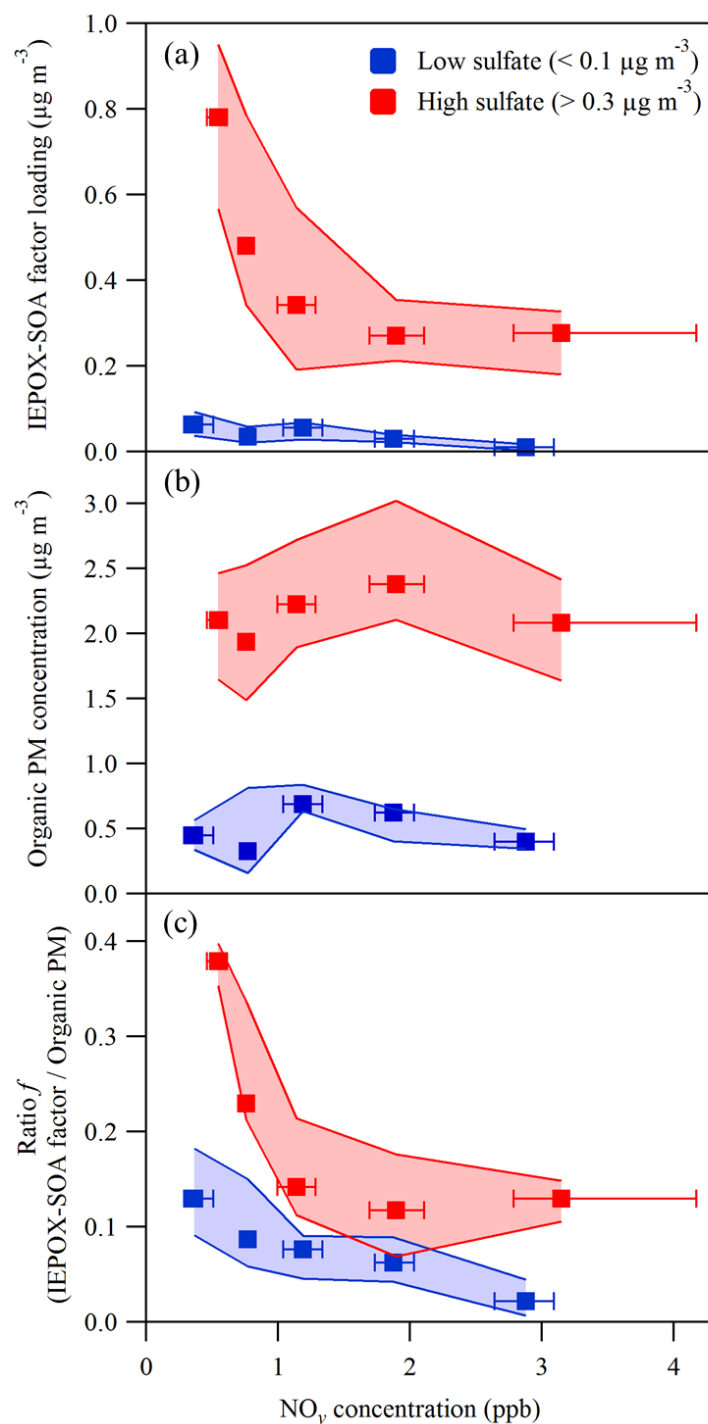


Figure 7. Dependence on NO_y concentration of (a) IEPOX-SOA factor loading, (b) organic mass concentration, and (c) the ratio f of the IEPOX-SOA factor loading to the organic PM concentration. Data are segregated by low ($< 0.1 \mu\text{g m}^{-3}$) and high ($> 0.3 \mu\text{g m}^{-3}$) sulfate mass concentration and grouped into five levels of NO_y concentration (Figure 6). Squares represent medians of each group. Interquartile ranges are represented by whiskers along the abscissa and shading along the ordinate. The plotted data sets were recorded during local afternoon (12:00-16:00 local time; 16:00-20:00 UTC).

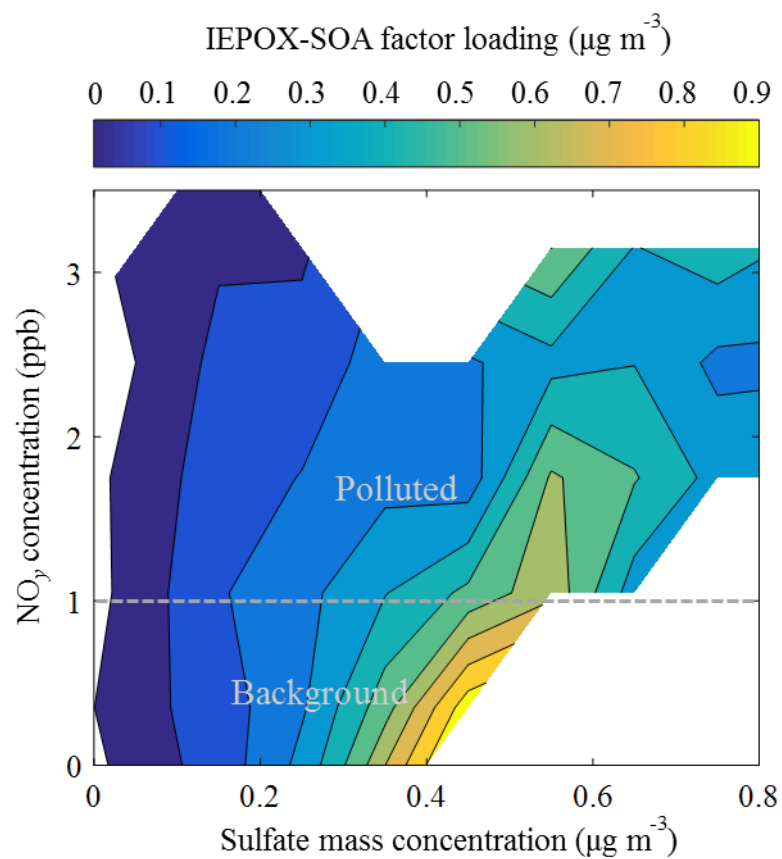


Figure 8. Contours of IEPOX-SOA factor loading for sulfate and NO_y concentrations. The plotted data were recorded during local afternoon (12:00-16:00 local time; 16:00-20:00 UTC). Typical transition between regimes of background and polluted conditions for the region downwind of Manaus are approximately represented by the dashed gray line.

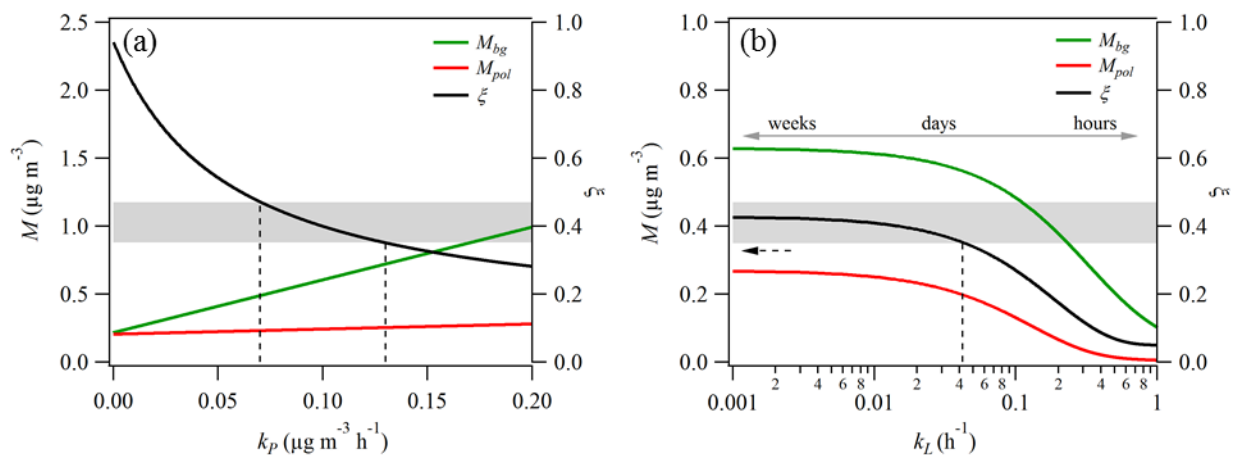


Figure 9. Modeled IEPOX-derived PM mass concentrations M_{pol} and M_{bg} at the T3 site under polluted compared to background conditions. The ratio ζ of concentrations (i.e., M_{pol}/M_{bg}) is also plotted. Panels a and b correspond to the two model Cases 1 and 2 listed in Table 4 and described in the text. Gray shading indicates the range of observed values of ζ across low and high sulfate concentrations. Dashed lines indicate the intersection of modeled and observed values of ζ and the corresponding constrained values of k_p or k_L along the abscissa. Labels above the double-headed arrow in panel b correspond to characteristic times (i.e., k_L^{-1}). The dashed black arrow in panel b communicates that the observed values of ζ provide no constraint on the lower limit of k_L .

Supplementary Material

Influence of urban pollution on the production of organic particulate matter from isoprene epoxydiols in central Amazonia

S.S. de Sá (1), B.B. Palm (2), P. Campuzano-Jost (2), D.A. Day (2), M.K. Newburn (3), W. Hu (2), G. Isaacman-VanWertz^a (4), L.D. Yee (4), R. Thalman (5), J. Brito^b (6), S. Carbone (6), P. Artaxo (6), A.H. Goldstein (4), A.O. Manzi (7), R.A.F. Souza (8), F. Mei (9), J. E. Shilling (3,9), S.R. Springston (5), J. Wang (5), J.D. Surratt (10), M.L. Alexander (3), J.L. Jimenez (2), S.T. Martin* (1, 11)

- (1) School of Engineering and Applied Sciences, Harvard University, Cambridge, Massachusetts, USA
- (2) Department of Chemistry & Biochemistry and Cooperative Institute for Research in Environmental Sciences, University of Colorado, Boulder, Colorado, USA
- (3) Environmental Molecular Sciences Laboratory, Pacific Northwest National Laboratory, Richland, Washington, USA
- (4) Dept. of Environmental Science, Policy, and Management, University of California, Berkeley, California, USA
- (5) Brookhaven National Laboratory, Upton, New York, USA
- (6) Departamento de Física Aplicada, Universidade de São Paulo, São Paulo, Brasil
- (7) Instituto Nacional de Pesquisas da Amazonia, Manaus, Amazonas, Brasil
- (8) Escola Superior de Tecnologia, Universidade do Estado do Amazonas, Manaus, Amazonas, Brasil
- (9) Atmospheric Sciences and Global Change Division, Pacific Northwest National Laboratory, Richland, WA, USA
- (10) Department of Environmental Sciences and Engineering, Gillings School of Global Public Health, The University of North Carolina at Chapel Hill, Chapel Hill, North Carolina, USA
- (11) Department of Earth and Planetary Sciences, Harvard University, Cambridge, Massachusetts, USA

^a Now at Massachusetts Institute of Technology, Cambridge, Massachusetts, USA

^b Now at: Laboratory for Meteorological Physics (LaMP), University Blaise Pascal, Aubière, France

1 **S1. Instrumentation**

2 **S1.1 Aerosol Mass Spectrometry: set up and operation**

3 Online measurements of organic and sulfate mass concentrations measured in this study
4 were made by a High-Resolution Time-of-Flight Aerosol Mass Spectrometer (AMS, Aerodyne
5 Research Inc.) (DeCarlo et al., 2006; Canagaratna et al., 2007). The AMS provided real-time
6 measurements of bulk non-refractory particle chemical composition (organic, sulfate, nitrate,
7 ammonium, chloride) and chemically resolved mass-diameter distribution. Air was sampled
8 through a critical orifice and enters an aerodynamic lens, which focused the submicron particles
9 into a narrow beam (Zhang et al., 2004). Particles traveled through a sizing chamber to reach a
10 porous tungsten inverted-cone vaporizer at 600 °C, and non-refractory components volatilized.
11 The gaseous molecules were then ionized through electron impact (70 eV), and the ions were
12 measured by time-of-flight mass spectrometry. The high mass resolution allowed for the
13 distinction of ions having the same nominal mass but different elemental composition. Data
14 analysis was performed using standard AMS software (*SQUIRREL* 1.56D, *PIKA* 1.14G)
15 (webpage: [http://cires1.colorado.edu/jimenez-](http://cires1.colorado.edu/jimenez-group/ToFAMSResources/ToFSoftware/index.html)
16 [group/ToFAMSResources/ToFSoftware/index.html](http://cires1.colorado.edu/jimenez-group/ToFAMSResources/ToFSoftware/index.html)).

17 Aerosol particles were sampled through a cyclone (URG-2000-30EH) which had a size
18 cut of 2.5 μm for a flow of 16.7 L min^{-1} . The sampled flow (14.9 to 16.3 L min^{-1}) traveled
19 through a stainless steel tube for about 1.5 m. The flow was then split in two: a 4-m line for
20 sampling (1.2 or 2.6 L min^{-1}) and a line (13.7 L min^{-1}) for exhaust. The sampling flow changed
21 between 1.2 and 2.6 L min^{-1} according to the flow set up of the Scanning Mobility Particle Sizer
22 (SMPS), which was sampling in parallel to the AMS. The sampling flow then entered a poly-
23 tube Nafion dryer (Perma Pure, model PD-100T). Drying prior to entering the instrument

24 container aimed at avoiding water condensation in the line inside the container, which was
25 always kept at lower temperatures than outside (i.e., trailer temperature was around 23 °C during
26 daytime). RH measured after the poly-tube dryer and inside the container was at 40 to 80%.
27 Within the container, a subflow (0.6 or 3 L min⁻¹) was passed through a mono-tube Nafion dryer
28 (Perma Pure, model MD-110) to reach RH < 40%. A flow of 0.09 L min⁻¹ was sampled by the
29 AMS, and the remaining flow of 0.5 or 2.9 L min⁻¹ was sampled by the SMPS. The ambient air
30 sampling line was integrated to a valve switching system, which alternated the AMS/SMPS
31 sampling between the unprocessed ambient air and air processed by oxidation flow reactors or a
32 thermal denuder. The unprocessed ambient air (used for this analysis) was sampled for 4 out of 8
33 min, constituting half of the total acquired data set.

34 Due to expected low mass concentrations and to secondary need for the low-sensitivity
35 high-resolution data, the AMS was operated for most of the time in medium-resolution V-mode
36 ($\Delta m/m = 2200$ at m/z 44), which was used for mass quantification. High-resolution W-mode
37 ($\Delta m/m = 4000$ at m/z 44) was acquired for one of every six days. These data were used to aid
38 choice of ions to fit. When only V-mode data were acquired, the instrument was operated in
39 “mass spectrum” sub-mode for 180 s and in “particle-time-of-flight” sub-mode for 60 s. When
40 W-mode data were also collected, the “W-mass-spectrum” sub-mode was operated for 60 s, the
41 “V-mass-spectrum” sub-mode ran for 120 s, and “V-particle-time-of-flight” sub-mode ran for 60
42 s. Both ways of operation corresponded to 4 min for each cycle, allowing for synchronization to
43 the valve switching system.

44 The AMS sensitivity and the ammonium relative ionization efficiency (RIE) were
45 calibrated every five days using dried ammonium nitrate particles having a mobility diameter of
46 400 nm. An interpolated curve of the obtained values, corresponding to $RIE = 4.3 \pm 0.2$, was

47 used for mass calculation corrections. The sulfate RIE was calibrated using ammonium sulfate a
48 few times during the campaign, and the average value of 0.9 ± 0.1 was applied to the entire
49 campaign. The collection efficiency (CE) was determined as 1.0 for IOP1 according to volume
50 comparison to the two co-located Scanning Mobility Particle Sizers (Figure S6). Volume of
51 black carbon (BC) accounted for 8 ± 6 % of the total volume measured by SMPS, for an
52 assumed density of 1.8 g cm^{-3} for BC. Since BC data were limited, the abscissa of Figure S6 was
53 not subtracted by BC contribution. This CE value was consistent with that used for the AMAZE-
54 08 in the wet season of 2008 (Chen et al., 2009).

55 **S1.2 Semi-Volatile Thermal desorption Aerosol Gas Chromatography: set up and** 56 **operation**

57 Online measurements of organic tracer compounds in the particle and gas phases were
58 made by a Semi-Volatile Thermal desorption Aerosol Gas chromatograph (SV-TAG). This
59 instrument is described in detail elsewhere (Isaacman et al., 2014). Its operation is briefly
60 presented here.

61 Air was sampled at 20 L min^{-1} from the center stream of a flow of 200 L min^{-1} through a
62 15.24 cm (OD) stainless steel duct at a height of approximately 5 m above ground level. The
63 flow was then divided into two channels, passing through a PM1 cyclone at 10 L min^{-1} , each
64 containing a custom Filter Collection and Thermal Desorption cell (F-CTD). The F-CTD
65 quantitatively collected and retained both particle- and gas-phase compounds. A multi-channel
66 carbon denuder (MAST Carbon) was used to remove all gases upstream of one collection cell. In
67 this way, two samples were simultaneously collected: a “particle” sample and a “total” gas-plus-
68 particle sample. Samples were thermally desorbed from the cells subjected to a ramping
69 temperature from 30 to $310 \text{ }^\circ\text{C}$ ($35 \text{ }^\circ\text{C min}^{-1}$) into a helium stream that was 80% saturated with

70 MSTFA (N-Methyl-N-(trimethylsilyl) trifluoroacetamide). Hydroxyl groups were converted into
71 silyl esters and ethers. Analytes were transferred to the GC column, and the sample was analyzed
72 through a commercially available GC/MS (7890A/5975C; Agilent Technologies). The
73 chromatographic data were analyzed using the publicly available software *TAG ExploreR and*
74 *iNtegration* (Isaacman-VanWertz and Sueper).

75 Compounds were quantified using isotopically labeled internal standards to correct for
76 run-to-run variability in sample transfer efficiency and instrument response. Regular multi-point
77 calibrations were made of approximately 100 authentic standards. Pentaerythritol-2-¹³C was used
78 for 2-methyltetrols and C₅-alkene triols. The uncertainty in mass concentration was
79 approximately 15% (Isaacman et al., 2014). C₅-alkene triols were quantified using the calibration
80 factor of 2-methyltetrols under the assumption of an identical total ion response. An absence of
81 an authentic standard results in unconstrained uncertainty in mass concentration of 30 of 50%
82 (Jaoui et al., 2005).

83 **S1.3 NO_y measurements**

84 The NO_y measured included the following species: NO, NO₂, HNO₃, particle nitrate,
85 RNO₃, and PAN. Measurements were made by a custom analyzer designed by Air Quality
86 Design (AQD; <http://www.airqualitydesign.com>). The analyzer was based on two commercial
87 oxides of nitrogen detectors made by Thermo Scientific (Model 42i TLE) and extensively
88 modified by AQD. An external, temperature-controlled inlet box was mounted at 10 m above
89 ground level.

90 The instrument contained both a research grade LED photolysis cell for converting NO₂
91 into NO and a heated molybdenum converter for converting total NO_y into NO. One channel,
92 leading from the photolysis cell to one 42i TLE detector, alternated every minute between NO

93 and NO_x by switching the LED photolysis cell on/off. The other channel, leading from the
94 molybdenum converter to the second 42i TLE detector, measured total NO_y . The detectors
95 internally measured zero based on pre-reaction of the sample with ozone. Instrument response
96 was measured by addition of NO in zero air at the sampling point (10 m). Converter efficiency
97 was measured by gas-phase titration of the NO standard to NO_2 . An HNO_3 source was sampled
98 every other day. The calibration unit was a Thermo Scientific Model 146i calibrator equipped
99 with gas-phase titration and a permeation oven. The raw NO_y measurements, reported at a
100 resolution of 10 s, were averaged into bins of 30 min to filter for local events not representative
101 of the larger scale chemical processes that form the scope of this study.

102 **S2. Positive Matrix Factorization and the IEPOX-SOA factor**

103 The time series of mass spectra of organic material measured by the AMS was analyzed
104 by positive matrix factorization (PMF) using a standard analysis toolkit (Ulbrich et al., 2009).
105 High-resolution, V-mode data were used. The PMF solution was based on minimization of the
106 “Q-value” or “PMF quality-of fit parameter”, meaning the sum of the weighed squared residuals
107 for a chosen number of factors. The interpretation of the physical significance of the AMS PMF
108 factors took into account correlations with quantities simultaneously measured by other
109 instruments. The solution consisted of six factors, and the present study focuses on one of the
110 derived factors, labeled “IEPOX-SOA”. de Sá (in preparation) focuses on presentation of the
111 other factors.

112 The profile of the resolved IEPOX-SOA factor is shown in Figure S1. A key
113 characteristic is intensity at $\text{C}_3\text{H}_6\text{O}^+$ (m/z 82) (Hu et al., 2015). In addition, a prominent signal at
114 C_4H_5^+ (m/z 53) is observed, which has also been reported as characteristic of the IEPOX-SOA
115 factor (Hu et al., 2015). The IEPOX-SOA factor is also relatively highly oxidized, as expressed

116 by $f_{44} = 0.15$ and oxygen to carbon atomic ratio O:C = 0.80, applying the calibration described in
117 Canagaratna et al. (2015).

118 Technical diagnostics of the six-factor solution are presented in Figure S2 and more
119 extensively described in (de Sá, in preparation). Panel b shows the quality of fit parameter
120 $Q/Q_{expected}$ (Ulbrich et al., 2009) as a function of the number of factors, suggesting that the
121 solution should have at least three factors. Panel a shows a great reduction in the structure of the
122 total residuals when going from the five-factor to the six-factor solution. The six-factor solution
123 also offered more meaningful factor profiles (“mass spectra”) (de Sá, in preparation). Panel c
124 shows $Q/Q_{expected}$ as a function of the rotational ambiguity parameter f_{peak} (Ulbrich et al., 2009)
125 for the six-factor solution. A plausible range for f_{peak} was determined according to the best
126 practice of limiting $Q/Q_{expected}$ to a value that does not exceed 0.1% of the minimum value
127 (occurring at $f_{peak} = 0$). The default value of $f_{peak} = 0$ was chosen for the final six-factor solution,
128 since no significant improvements in the external validation of the factors were observed.
129 Moreover, the IEPOX-SOA factor resolved in the six-factor solution had a very robust time trend
130 across a range of rotations in the solution (Figure S2d). As f_{peak} varied, the correlation of factor
131 loading with C5-alkene triols concentrations remained approximately constant, even as some
132 features of the factor profile changed significantly, such as the relative signals of $C_5H_6O^+$ and
133 CO_2^+ , respectively $f(C_5H_6O)$ and $f(CO_2)$, as well as the magnitude of factor loadings and
134 consequently the ratio f .

135 The loading of the IEPOX-SOA factor may be an overestimate or an underestimate of the
136 atmospheric concentration of the IEPOX-derived PM (brown dashed lines in Figure 1). In
137 respect to overestimate, the AMS mass spectrum observed in laboratory studies for the uptake of
138 IEPOX by acidic sulfate particles is statistically equal to that obtained for the uptake of isoprene

139 photo-oxidation products, yet IEPOX accounted for only half of those products (Liu et al., 2015).
140 The implication is that the uptake of non-IEPOX species can lead to a similar AMS spectrum.
141 Pathways of PM production from condensation of multifunctional hydroperoxides lead to a
142 distinct mass spectrum from IEPOX pathways, and are not expected to be highly active under the
143 acidic particle conditions of these experiments (Riva et al., 2016), leaving a large mass fraction
144 of produced PM unexplained. The combination of AMS vaporization at 600 °C and ionization by
145 electron impact at 70 eV may convert IEPOX-derived and non-IEPOX-derived molecules into
146 similar groups of ions, which then give rise to a similar mass spectrum. The SV-TAG, which
147 uses desorption temperatures up to 310 °C and thus can also induce thermal decomposition of
148 some molecules, might also result in an in-common analyte (i.e., tracer) between IEPOX-derived
149 and non-IEPOX-derived molecules, thereby precluding a constraint on any possible overestimate
150 by the AMS factor (Isaacman-VanWertz et al., 2016; Lopez-Hilfiker et al., 2016). For these
151 reasons, the loading of the IEPOX-SOA factor might overestimate IEPOX-derived PM
152 concentrations by accounting for other isoprene oxidation products that are not produced through
153 the IEPOX intermediate.

154 In respect to underestimate, the loading of the IEPOX-SOA factor may not capture the
155 entire particle-phase carbon footprint that originated from IEPOX uptake. Extensive atmospheric
156 processing, such as reactions with hydroxyl radicals or photolysis, can partly eliminate the initial
157 products of IEPOX uptake (Kroll et al., 2009; Bateman et al., 2011; Epstein et al., 2014; Hu et
158 al., 2015; Hu et al., 2016). The IEPOX-originated carbon can still be inside the particle, yet it no
159 longer contributes to the loading of the IEPOX-SOA factor because of an altered mass spectrum
160 for some molecules. Atmospheric reactions gradually homogenize particle composition and
161 properties, and the AMS spectra can become more uniform (Jimenez et al., 2009). Specifically,

162 the ratio of signal intensity at m/z 44 to that at m/z 43 increases, and the relative intensity of m/z
163 82 decreases (Ng et al., 2011; Hu et al., 2015). This modified organic material, which originally
164 entered the particle phase through IEPOX uptake, may then contribute to the loading of PMF
165 factors other than IEPOX-SOA, such as the oxidized organic factors broadly labeled as “OOA”
166 (Zhang et al., 2005). For these several reasons, the IEPOX-SOA factor loading might be an
167 underestimate of IEPOX-derived PM concentrations.

168 **S3. Comparison of background and polluted cases**

169 The presence of a pollution plume at T3 is indicated by a combination of several external
170 measured variables, including particle number, ozone, and NO_y concentrations. The definition of
171 background and polluted cases aimed at selecting afternoons that were associated with extreme
172 values of those variables. Conditions entailing concentration of ozone at around 10 ppb or less,
173 particle number concentration of less than 500 cm^{-3} , and NO_y concentrations of less than 1 ppb
174 were collectively a strong indicative of a background case. Conditions including ozone
175 concentrations upward of 30 ppb, particle number concentration above 2000 cm^{-3} , and NO_y
176 concentrations around 1.5 ppb or above indicated pollution. Measurements of these variables
177 onboard the G-1 aircraft confirmed what the ground measurements suggested on the several days
178 that the G-1 flew overhead.

179 Examples of these supporting data are illustrated in Figure 3 for the chosen background
180 and polluted days (March 3 and 13, 2014, respectively) composing the primary case study
181 analyzed in the main text. A few other afternoons, representative of these two extremes of
182 background and polluted cases, were selected from the campaign time series and are depicted in
183 Figure S4. The top panel shows cases of background conditions, and the bottom panel shows
184 cases of polluted conditions. The local wind direction observed for the polluted cases generally

185 characterized by easterlies, as consistent with Manaus direction, whereas for the background
186 cases it tends to diverge from that prevailing direction. The cases within each category are
187 ordered from left to right in ascending order of IEPOX-SOA factor loadings.

188 Sulfate concentrations had a wide range of values, even for background conditions
189 (Figure S4), as discussed in the main text. Meteorological conditions such as overcast (lower
190 photooxidation activity) and rain events (higher wet deposition), as seen on March 20 and March
191 23, are some of the factors that control particle number and mass concentration (sulfate and
192 organic compounds). These factors help to explain the natural variability in sulfate mass
193 concentration. By comparison, on a sunny day, with winds mostly coming from the northeast
194 direction, as exemplified by February 16 and March 3, sulfate mass concentrations can be around
195 $0.3 \mu\text{g m}^{-3}$ or more, values which are also typical of some polluted days (bottom panel). Both the
196 factor loading and the ratio f increased with increasing sulfate (rows 2 and 3 of top panel), when
197 NO_y levels were approximately the same. A comparison of February 16 and March 3 shows in
198 addition the importance of NO_y concentration: for similar concentrations of sulfate and organic
199 PM and similar meteorological conditions, the case having lower NO_y concentrations (0.4 to 0.5
200 ppb on March 3 as compared to 0.7 to 0.8 ppb on February 16) was associated with considerably
201 higher absolute and relative factor loadings.

202 For the polluted cases shown in Figure S4, NO_y concentrations were variable between
203 and within cases, ranging from 1 ppb up to 7 ppb. Larger sulfate mass concentrations (from left
204 to right) were associated with larger absolute and relative factor loadings, analogous to what was
205 observed for background cases. A comparison between March 3 and 13 (i.e., background and
206 polluted; Figure 4) shows that for similar sulfate concentrations but higher NO_y levels March 13
207 had considerably lower factor loadings. The case of February 9 (polluted) illustrates that the

208 factor loadings did not exceed $0.4 \mu\text{g m}^{-3}$ and f did not exceed 0.2 even at rarely high sulfate
209 concentrations in the wet season, reaching $0.9 \mu\text{g m}^{-3}$. This finding is attributed to the high NO
210 concentrations, as implied by NO_y concentrations of 3 ppb and greater, that suppressed IEPOX
211 production.

212 These cases illustrate the possible wide range of observed sulfate mass concentrations
213 under background conditions, in great part overlapping with typical values of polluted
214 conditions. The cases also demonstrate that the trend in observed IEPOX-SOA factor loadings
215 and ratio f , both within each category (background or polluted conditions) and between them, can
216 be consistently explained by the roles that sulfate and NO exert on the production of IEPOX-
217 derived PM.

218 **S4. Sulfate and particle acidity estimates in the context of field studies**

219 The underlying relative importance of direct compared to indirect roles of sulfate on the
220 formation of IEPOX-derived PM is not well understood. Sulfate can play a direct role as a
221 nucleophile in the reaction of formation of organosulfates from IEPOX (Surratt et al., 2007b;
222 Nguyen et al., 2014). Organosulfates, however, are believed to constitute only a fraction of the
223 IEPOX-derived PM (Hu et al., 2015). Particle acidity, an indirect effect of sulfate, has been
224 shown to drive IEPOX-derived PM production in several lab studies (Surratt et al., 2007a;
225 Kuwata et al., 2015; Lewandowski et al., 2015). Nevertheless, the acidity effect observed in
226 laboratories is not as clearly observed in field studies, wherein pH estimates have typically been
227 employed as a proxy for acidity (Budisulistiorini et al., 2013; Lin et al., 2013; Worton et al.,
228 2013; Budisulistiorini et al., 2015; Xu et al., 2015). The present study corroborates those findings
229 and further argues that this apparent conflict can be reasoned by taking into account that both the
230 estimate and the end-use of pH may be problematic in the context of field studies.

231 Firstly, a reliable estimate of pH is often hard to obtain. In the case of the present study,
232 some difficulties were imposed by data availability. Gas-phase measurements of NH_3 or HNO_3
233 were not available for performing “forward” mode calculations in thermodynamic models or gas-
234 particle phase partitioning calculations, which have been suggested as the best method to predict
235 pH (Hennigan et al., 2015). Co-located independent measurements of ion concentrations (e.g., by
236 chromatograph) were not available to confirm the ion balance obtained by AMS measurements
237 (Figure S7).

238 Bearing these caveats in mind, the analysis presented in the main text using sulfate as a
239 predictor for IEPOX-SOA was replicated here using pH in place of sulfate. Figure S8 is
240 analogous to Figure 6a. pH was estimated for IOP1 using AMS measurements of mass
241 concentrations of inorganic ions (sulfate, ammonium, nitrate, and chloride) and measurements of
242 RH and temperature. The E-AIM model II (Clegg et al., 1998) was employed. The final pH was
243 calculated taking into account both the inorganic water predicted by the model and the organic
244 water estimated from organic hygroscopicity κ_{org} values (Thalman, in preparation), in a similar
245 fashion as described by Guo et al. (2015). Figure S8 shows that pH, as calculated herein and for
246 the caveats herein, does not work well as a predictor for IEPOX-SOA factor loading. Figure S9
247 is analogous to Figure 7. Figure S9 shows that, although the overall dependencies on NO_y are
248 similar to analysis of the data by sulfate, the separation by pH yields groups that have less
249 distinct trends and ranges among them.

250 In addition to difficulties associated with generating accurate estimates of pH, there is an
251 inconsistency between the timescales of estimated particle acidity and IEPOX-SOA factor
252 loadings that may preclude underlying correlations to emerge. The estimated pH makes use of
253 instantaneous RH and temperature values and is therefore an instantaneous estimate of pH. They

254 can change in timescales of 15 min or less giving mixing in the boundary layer, for example. On
255 the other hand, sulfate mass concentrations and IEPOX-SOA factor loadings are variables
256 representative of processes of longer time scales of hours and days. By not containing any
257 information on the particle acidity history in the past hours or days, the calculated instantaneous
258 pH may fail in capturing the true effect of acidity on the chemical formation of IEPOX-derived
259 PM. The RH cycling history of sulfate particles has been demonstrated to mediate the extent of
260 IEPOX-derived PM production (Wong et al., 2015). Moreover, sulfate, by being intrinsically
261 related to particle acidity and at the same time a species of congruent lifetime with secondary
262 organic material, may in fact be a better proxy to capture the history of particle acidity than
263 estimates of pH. For these different reasons, sulfate rather than pH is used in the analysis herein.
264 The understanding, however, is that sulfate represents effects beyond those of the direct chemical
265 role of sulfate. In analogy to pH, this discussion also extends to the use of sulfate rather than
266 instantaneous particle water content as the predictor of IEPOX-SOA factor loadings.

267 **S5. Five subsets of data based on NO_y concentrations**

268 The data subsets and fits shown in Figure 6 are shown in separate panels in Figure S5.
269 Once a trend of decreasing fit slope with increasing NO_y concentration was identified, the
270 number of data subsets was defined as the minimum necessary to have subsets of at least 100
271 data points (of a total of 888) to allow for robust statistics and that were also cohesive (as
272 measured by R^2) and non-redundant (i.e., of different fit lines).

273 The coloring by date in Figure S5 shows that there is no apparent correlation between
274 levels of NO_y concentration or goodness of fit with different time periods within IOP1.
275 Meteorological variables such as solar radiation, temperature, and RH (not shown) are also not
276 able to delineate any clear pattern in the data, either within or among groups.

277 Although a linear bivariate statistical analysis for the IEPOX-SOA factor in sulfate and
278 NO_y concentrations at first appears attractive, the underlying chemical processes were not linear,
279 as reflected in the relationship between IEPOX-derived PM and NO_y concentrations. Moreover,
280 sulfate and NO_y concentrations were not independent variables. For these reasons, a linear
281 bivariate analysis is not appropriate, and a subset analysis was pursued instead.

282 **S6. Details and assumptions of the model**

283 The solution to the differential Equation 1 is as follows:

$$284 \quad M(t) = \frac{\alpha_P k_P}{\alpha_L k_L} + e^{\alpha_L k_L t} \left(M_0 - \frac{\alpha_P k_P}{\alpha_L k_L} \right) \quad (S1)$$

285 for which the subscript 0 indicates initial (background) conditions, i.e., immediately before the
286 air mass passes over Manaus. For the transport from Manaus to T3, $t = \tau_{tr}$, and the variable M
287 represents the IEPOX-derived PM mass concentrations at T3.

288 The zero-order production rate coefficient k_P and the first-order loss rate coefficient k_L
289 are lumped parameters representative of several production and loss processes, respectively. A
290 first assumption is that they are constant over the course of four hours. In hand with that
291 assumption, a constant boundary layer height throughout the integration time is assumed. The τ
292 values represent the time required under afternoon conditions to significantly affect the IEPOX-
293 derived PM mass concentration by the corresponding processes. For afternoon time periods,
294 observations show that $dM/dt > 0$ over tropical forests in the absence of pollution (Chen et al.,
295 2009; Chen et al., 2015). The parameter τ_P , corresponding to a first order process, therefore
296 represents an instantaneous quantity in the transient system. For simplicity of presentation, τ_P is
297 defined in reference to M_0 , although defining it in relation to M_{bg} or M_{pol} does not alter the main
298 conclusions presented herein.

299 In terms of loss processes, represented by the rate coefficient k_L , IEPOX-derived PM may
300 be lost by three main mechanisms: heterogeneous oxidation against OH, condensed-phase
301 reactions, and dry deposition. The lifetime of IEPOX-derived PM against heterogeneous
302 oxidation is estimated at around two weeks for an OH concentration of 10^6 molecules cm^{-3} (Hu et
303 al., 2016). Lifetime of IEPOX products against particle-phase reactions has not yet been reported
304 but is expected to be at least several days. A value of one week is used here. The lifetime of PM
305 against deposition is on the order of a week. The overall loss process is then approximated in the
306 model as the sum of these three processes, which leads to an estimate of overall loss rate
307 coefficient $k_L = 0.015 \text{ h}^{-1}$ (overall characteristic time of 2.8 days).

308 In respect to wet deposition along the track from Manaus to the T3 site, strong convection
309 imports background regional air, and for this reason strong wet deposition is mathematically
310 equivalent in the model developed herein to a trajectory that does not pass over Manaus, i.e.,
311 background conditions. Weak wet deposition represents a mixing of polluted and background air
312 masses, giving rise to intermediate NO_y concentrations. Entrainment on the plume edges as well
313 as with the free troposphere is mathematically similar to wet deposition in the model framework.
314 Thus entrainment and wet deposition, without directly contributing to k_L , are indirectly
315 incorporated in the developed model based on their effects on NO_y concentration.

316 In terms of production processes, represented by the rate coefficient k_P , IEPOX-derived
317 PM is produced by multigenerational chemistry of isoprene photooxidation and reactive uptake.
318 Model Case 1 investigated the sensitivity of pollution enhancement ratio and absolute mass
319 concentration of IEPOX-derived PM to its production rate coefficient. After constrained by
320 observations, the estimated interval for k_P was $[0.07, 0.13] \mu\text{g m}^{-3} \text{ h}^{-1}$. In addition, values of $k_P >$
321 $0.2 \mu\text{g m}^{-3} \text{ h}^{-1}$ are unlikely given the rare observation ($<1\%$) of $M_{bg} > 1 \mu\text{g m}^{-3}$.

322 The obtained range can be compared to estimates of total production rate of organic
323 material from diameter growth rates. Firstly, a relative production rate of 1:3 for IEPOX-derived
324 PM to total organic PM is assumed based on the following. IEPOX-derived PM is estimated to
325 contribute 34% on average to total organic PM in central Amazonia under background
326 conditions (Chen et al., 2015). For assumptions of equal first order loss rate coefficients for all
327 organic material, a mass concentration ratio of 1:3 for IEPOX-derived PM to total organic
328 material implies a ratio of 1:3 in their production rate coefficients k_p . As a consequence, the
329 estimated range for total organic material is $[0.21, 0.39] \mu\text{g m}^{-3} \text{h}^{-1}$. For the estimate of organic
330 material production based on growth rates, an average growth rate of 10 nm h^{-1} (Kulmala et al.,
331 2004) is assumed. Further assumptions are a range of particle number concentration of 500 to
332 1000 cm^{-3} and of initial diameter of 20 to 100 nm, typical of background conditions in the
333 Amazon. The obtained range of organic material production from growth rate estimates is
334 therefore 0.02 to $0.32 \mu\text{g m}^{-3} \text{h}^{-1}$, which is comparable to the range constrained by the model.

335 In terms of the influence of Manaus plume on the production and loss processes, the
336 following assumptions were made. The acceleration of the oxidant cycle in the plume implies
337 that $\alpha_L > 1$. Under plume conditions, OH concentrations observed at the T3 site increased by a
338 factor of three compared to background conditions (Martin et al., 2017a; Kim, in preparation).
339 A proportional increase in the loss rate of IEPOX-derived PM by OH heterogeneous chemistry in
340 the plume is expected. While the OH loss mechanism (of characteristic time of two weeks) is
341 accelerated by three fold in the plume, dry deposition and condensed phase reactions (both of
342 assumed characteristic times of a week) are held constant. As a result, the overall loss rate is
343 enhanced by two fold, i.e., $\alpha_L = 2$ is assumed.

344 Concerning the production enhancement factor, the interception of ISOPOO radicals by
345 NO in the pollution plume as well as the faster consumption of intermediate gas-phase species by
346 the enhanced OH and O₃ concentrations implies $\alpha_P < 1$. The assumption is that the production of
347 IEPOX almost halts in the plume, and $\alpha_P = 0.1$. This assumption is supported by measured gas-
348 phase concentrations of ISOPOOH at the T3 site, which dropped by 90% when NO_y
349 concentrations increased from 0.5 ppb to 2 ppb (Liu et al., 2016). This observation and the
350 associated model assumption are a reflection of the lifetimes of the chemical species discussed:
351 in contrast to the abovementioned lifetimes on order of a week for organic particle material
352 against loss processes, the lifetimes of the gaseous species are significantly shorter. Isoprene and
353 ISOPOOH have a lifetime on the order of a few hours (Eddingsaas et al., 2010; St. Clair et al.,
354 2015), and IEPOX has a lifetime of a few hours to a day for an OH concentration of 10⁶
355 molecules cm⁻³ (Jacobs et al., 2013; Bates et al., 2014).

Supplementary References

- Bateman, A. P., Nizkorodov, S. A., Laskin, J., and Laskin, A.: Photolytic processing of secondary organic aerosols dissolved in cloud droplets, *Phys. Chem. Chem. Phys.*, 13, 12199-12212, 2011, 10.1039/C1CP20526A.
- Bates, K. H., Crouse, J. D., St. Clair, J. M., Bennett, N. B., Nguyen, T. B., Seinfeld, J. H., Stoltz, B. M., and Wennberg, P. O.: Gas phase production and loss of isoprene epoxydiols, *J. Phys. Chem. A*, 118, 1237-1246, 2014, 10.1021/jp4107958.
- Budisulistiorini, S. H., Canagaratna, M. R., Croteau, P. L., Marth, W. J., Baumann, K., Edgerton, E. S., Shaw, S. L., Knipping, E. M., Worsnop, D. R., Jayne, J. T., Gold, A., and Surratt, J. D.: Real-time continuous characterization of secondary organic aerosol derived from isoprene epoxydiols in downtown Atlanta, Georgia, using the Aerodyne Aerosol Chemical Speciation Monitor, *Environ. Sci. Technol.*, 47, 5686-5694, 2013, 10.1021/es400023n.
- Budisulistiorini, S. H., Li, X., Bairai, S. T., Renfro, J., Liu, Y., Liu, Y. J., McKinney, K. A., Martin, S. T., McNeill, V. F., Pye, H. O. T., Nenes, A., Neff, M. E., Stone, E. A., Mueller, S., Knote, C., Shaw, S. L., Zhang, Z., Gold, A., and Surratt, J. D.: Examining the effects of anthropogenic emissions on isoprene-derived secondary organic aerosol formation during the 2013 Southern Oxidant and Aerosol Study (SOAS) at the Look Rock, Tennessee ground site, *Atmos. Chem. Phys.*, 15, 8871-8888, 2015, 10.5194/acp-15-8871-2015.
- Canagaratna, M. R., Jayne, J. T., Jimenez, J. L., Allan, J. D., Alfarra, M. R., Zhang, Q., Onasch, T. B., Drewnick, F., Coe, H., Middlebrook, A., Delia, A., Williams, L. R., Trimborn, A. M., Northway, M. J., DeCarlo, P. F., Kolb, C. E., Davidovits, P., and Worsnop, D. R.: Chemical and microphysical characterization of ambient aerosols with the aerodyne

aerosol mass spectrometer, *Mass Spectrom. Rev.*, 26, 185-222, 2007,

10.1002/mas.20115.

Canagaratna, M. R., Jimenez, J. L., Kroll, J. H., Chen, Q., Kessler, S. H., Massoli, P., Hildebrandt Ruiz, L., Fortner, E., Williams, L. R., Wilson, K. R., Surratt, J. D., Donahue, N. M., Jayne, J. T., and Worsnop, D. R.: Elemental ratio measurements of organic compounds using aerosol mass spectrometry: characterization, improved calibration, and implications, *Atmos. Chem. Phys.*, 15, 253-272, 2015, 10.5194/acp-15-253-2015.

Chen, Q., Farmer, D. K., Schneider, J., Zorn, S. R., Heald, C. L., Karl, T. G., Guenther, A., Allan, J. D., Robinson, N., Coe, H., Kimmel, J. R., Pauliquevis, T., Borrmann, S., Pöschl, U., Andreae, M. O., Artaxo, P., Jimenez, J. L., and Martin, S. T.: Mass spectral characterization of submicron biogenic organic particles in the Amazon Basin, *Geophys. Res. Lett.*, 36, L20806, 2009, 10.1029/2009GL039880.

Chen, Q., Farmer, D. K., Rizzo, L. V., Pauliquevis, T., Kuwata, M., Karl, T. G., Guenther, A., Allan, J. D., Coe, H., Andreae, M. O., Pöschl, U., Jimenez, J. L., Artaxo, P., and Martin, S. T.: Submicron particle mass concentrations and sources in the Amazonian wet season (AMAZE-08), *Atmos. Chem. Phys.*, 15, 3687-3701, 2015, 10.5194/acp-15-3687-2015.

Clegg, S. L., Brimblecombe, P., and Wexler, A. S.: Thermodynamic model of the system H^+ - NH_4^+ - SO_4^{2-} - NO_3^- - H_2O at tropospheric temperatures, *J. Phys. Chem. A*, 102, 2137-2154, 1998, 10.1021/jp973042r.

de Sá, S. S.: [Anthropogenic emissions affect the S_s sources and composition of submicron particulate matter in central Amazonia as affected by anthropogenic emissions during in the wet and dry season](#), in preparation.

- DeCarlo, P. F., Kimmel, J. R., Trimborn, A., Northway, M. J., Jayne, J. T., Aiken, A. C., Gonin, M., Fuhrer, K., Horvath, T., Docherty, K. S., Worsnop, D. R., and Jimenez, J. L.: Field-deployable, high-resolution, time-of-flight aerosol mass spectrometer, *Anal. Chem.*, 78, 8281-8289, 2006, 10.1021/ac061249n.
- Eddingsaas, N. C., VanderVelde, D. G., and Wennberg, P. O.: Kinetics and products of the acid-catalyzed ring-opening of atmospherically relevant butyl epoxy alcohols, *J. Phys. Chem. A*, 114, 8106-8113, 2010, 10.1021/jp103907c.
- Epstein, S. A., Blair, S. L., and Nizkorodov, S. A.: Direct photolysis of α -pinene ozonolysis secondary organic aerosol: effect on particle mass and peroxide content, *Environ. Sci. Technol.*, 48, 11251-11258, 2014, 10.1021/es502350u.
- Guo, H., Xu, L., Bougiatioti, A., Cerully, K. M., Capps, S. L., Hite Jr, J. R., Carlton, A. G., Lee, S. H., Bergin, M. H., Ng, N. L., Nenes, A., and Weber, R. J.: Fine-particle water and pH in the southeastern United States, *Atmos. Chem. Phys.*, 15, 5211-5228, 2015, 10.5194/acp-15-5211-2015
- Hu, W. W., Campuzano-Jost, P., Palm, B. B., Day, D. A., Ortega, A. M., Hayes, P. L., Krechmer, J. E., Chen, Q., Kuwata, M., Liu, Y. J., de Sá, S. S., McKinney, K., Martin, S. T., Hu, M., Budisulistiorini, S. H., Riva, M., Surratt, J. D., St. Clair, J. M., Isaacman-Van Wertz, G., Yee, L. D., Goldstein, A. H., Carbone, S., Brito, J., Artaxo, P., de Gouw, J. A., Koss, A., Wisthaler, A., Mikoviny, T., Karl, T., Kaser, L., Jud, W., Hansel, A., Docherty, K. S., Alexander, M. L., Robinson, N. H., Coe, H., Allan, J. D., Canagaratna, M. R., Paulot, F., and Jimenez, J. L.: Characterization of a real-time tracer for isoprene epoxydiols-derived secondary organic aerosol (IEPOX-SOA) from aerosol mass

- spectrometer measurements, *Atmos. Chem. Phys.*, 15, 11807-11833, 2015, 10.5194/acp-15-11807-2015.
- Hu, W. W., Palm, B., Day, D., Campuzano-Jost, P., Krechmer, J., Peng, Z., De Sá, S. S., Martin, S. T., Alexander, M. L., Baumann, K., Hacker, L., Kiendler-Scharr, A., Koss, A., De Gouw, J., Goldstein, A. H., Seco, R., Sjostedt, S., Park, J.-H., Guenther, A., Kim, S., Canonaco, F., Prevot, A., Brune, W., and Jimenez, J. L.: Long lifetime of ambient isoprene epoxydiols-derived Secondary Organic Aerosol (IEPOX-SOA) against OH oxidation and evaporation, *Atmos. Chem. Phys. Disc.*, 2016, doi: 10.5194/acp-2016-418.
- Isaacman-VanWertz, G. and Sueper, D.: TERN: TAG ExploreR and iNtegration
<https://sites.google.com/site/terninigor/>.
- Isaacman-VanWertz, G., Yee, L. D., Kreisberg, N. M., Wernis, R., Moss, J. A., Hering, S. V., de Sá, S. S., Martin, S. T., Alexander, M. L., Palm, B. B., Hu, W., Campuzano-Jost, P., Day, D. A., Jimenez, J. L., Riva, M., Surratt, J. D., Viegas, J., Manzi, A., Edgerton, E., Baumann, K., Souza, R., Artaxo, P., and Goldstein, A. H.: Ambient Gas-Particle Partitioning of Tracers for Biogenic Oxidation, *Env. Sci. Technol.*, 2016, 10.1021/acs.est.6b01674.
- Isaacman, G., Kreisberg, N., Yee, L., Worton, D., Chan, A., Moss, J., Hering, S., and Goldstein, A.: Online derivatization for hourly measurements of gas-and particle-phase semi-volatile oxygenated organic compounds by thermal desorption aerosol gas chromatography (SV-TAG), *Atmos. Meas. Tech.*, 7, 4417-4429, 2014, 10.5194/amt-7-4417-2014.
- Jacobs, M. I., Darer, A. I., and Elrod, M. J.: Rate constants and products of the OH reaction with isoprene-derived epoxides, *Environ. Sci. Technol.*, 47, 12868-12876, 2013, 10.1021/es403340g.

Jaoui, M., Kleindienst, T., Lewandowski, M., Offenberg, J., and Edney, E.: Identification and quantification of aerosol polar oxygenated compounds bearing carboxylic or hydroxyl groups. 2. Organic tracer compounds from monoterpenes, *Environ. Sci. Technol.*, 39, 5661-5673, 2005, 10.1021/es048111b.

Jimenez, J. L., Canagaratna, M. R., Donahue, N. M., Prevot, A. S. H., Zhang, Q., Kroll, J. H., DeCarlo, P. F., Allan, J. D., Coe, H., Ng, N. L., Aiken, A. C., Docherty, K. S., Ulbrich, I. M., Grieshop, A. P., Robinson, A. L., Duplissy, J., Smith, J. D., Wilson, K. R., Lanz, V. A., Hueglin, C., Sun, Y. L., Tian, J., Laaksonen, A., Raatikainen, T., Rautiainen, J., Vaattovaara, P., Ehn, M., Kulmala, M., Tomlinson, J. M., Collins, D. R., Cubison, M. J., Dunlea, J., Huffman, J. A., Onasch, T. B., Alfarra, M. R., Williams, P. I., Bower, K., Kondo, Y., Schneider, J., Drewnick, F., Borrmann, S., Weimer, S., Demerjian, K., Salcedo, D., Cottrell, L., Griffin, R., Takami, A., Miyoshi, T., Hatakeyama, S., Shimo, A., Sun, J. Y., Zhang, Y. M., Dzepina, K., Kimmel, J. R., Sueper, D., Jayne, J. T., Herndon, S. C., Trimborn, A. M., Williams, L. R., Wood, E. C., Middlebrook, A. M., Kolb, C. E., Baltensperger, U., and Worsnop, D. R.: Evolution of organic aerosols in the atmosphere, *Science*, 326, 1525-1529, 2009, 10.1126/science.1180353.

Kim, S., in preparation.

Kroll, J. H., Smith, J. D., Che, D. L., Kessler, S. H., Worsnop, D. R., and Wilson, K. R.: Measurement of fragmentation and functionalization pathways in the heterogeneous oxidation of oxidized organic aerosol, *Phys. Chem. Chem. Phys.*, 11, 8005-8014, 2009, 10.1039/B905289E.

Kulmala, M., Vehkamäki, H., Petäjä, T., Dal Maso, M., Lauri, A., Kerminen, V. M., Birmili, W., and McMurry, P. H.: Formation and growth rates of ultrafine atmospheric particles: a

- review of observations, *J. Aerosol Sci.*, 35, 143-176, 2004,
<http://dx.doi.org/10.1016/j.jaerosci.2003.10.003>.
- Kuwata, M., Zorn, S. R., and Martin, S. T.: Using elemental ratios to predict the density of organic material composed of carbon, hydrogen, and oxygen, *Environ. Sci. Technol.*, 46, 787-794, 2011, 10.1021/es202525q.
- Kuwata, M., Liu, Y., McKinney, K., and Martin, S. T.: Physical state and acidity of inorganic sulfate can regulate the production of secondary organic material from isoprene photooxidation products, *Phys. Chem. Chem. Phys.*, 17, 5670-5678, 2015, 10.1039/C4CP04942J.
- Lewandowski, M., Jaoui, M., Offenberg, J., Krug, J., and Kleindienst, T.: Atmospheric oxidation of isoprene and 1, 3-butadiene: influence of aerosol acidity and relative humidity on secondary organic aerosol, *Atmos. Chem. Phys.*, 15, 3773-3783, 2015, 10.5194/acp-15-3773-2015.
- Lin, Y.-H., Knipping, E., Edgerton, E., Shaw, S., and Surratt, J. D.: Investigating the influences of SO₂ and NH₃ levels on isoprene-derived secondary organic aerosol formation using conditional sampling approaches, *Atmos. Chem. Phys.*, 13, 8457-8470, 2013, 10.5194/acp-13-8457-2013.
- Liu, Y., Kuwata, M., Strick, B. F., Geiger, F. M., Thomson, R. J., McKinney, K. A., and Martin, S. T.: Uptake of epoxydiol isomers accounts for half of the particle-phase material produced from isoprene photooxidation via the HO₂ pathway, *Environ. Sci. Technol.*, 49, 250-258, 2015, 10.1021/es5034298.
- Liu, Y., Brito, J., Dorris, M. R., Rivera-Rios, J. C., Seco, R., Bates, K. H., Artaxo, P., Duvoisin, S., Keutsch, F. N., Kim, S., Goldstein, A. H., Guenther, A. B., Manzi, A. O., Souza, R. A.

F., Springston, S. R., Watson, T. B., McKinney, K. A., and Martin, S. T.: Isoprene photochemistry over the Amazon rain forest, *Proc. Natl. Acad. Sci. USA*, 113, 6125-6130, 2016, 10.1073/pnas.1524136113.

Lopez-Hilfiker, F. D., Mohr, C., D'Ambro, E. L., Lutz, A., Riedel, T. P., Gaston, C. J., Iyer, S., Zhang, Z., Gold, A., Surratt, J. D., Lee, B. H., Kurten, T., Hu, W. W., Jimenez, J., Hallquist, M., and Thornton, J. A.: Molecular composition and volatility of organic aerosol in the Southeastern US: implications for IEPOX derived SOA, *Environ. Sci. Technol.*, 2200–2209, 2016, 10.1021/acs.est.5b04769.

~~Martin, S. T., Artaxo, P., Machado, L., Manzi, A. O., Souza, R. A. F., Schumacher, C., Wang, J., Biscaro, T., Brito, J., Calheiros, A., Jardine, K., Medeiros, A., Portela, B., Sá, S. S. d., Adachi, K., Aiken, A. C., Albrecht, R., Alexander, L., Andreae, M. O., Barbosa, H. M. J., Buseck, P., Chand, D., Comstock, J. M., Day, D. A., Dubey, M., Fan, J., Fast, J., Fisch, G., Fortner, E., Giangrande, S., Gilles, M., Goldstein, A. H., Guenther, A., Hubbe, J., Jensen, M., Jimenez, J. L., Keutsch, F. N., Kim, S., Kuang, C., Laskin, A., McKinney, K., Mei, F., Miller, M., Nascimento, R., Pauliquevis, T., Pekour, M., Peres, J., Petäjä, T., Pöhlker, C., Pöschl, U., Rizzo, L., Schmid, B., Shilling, J. E., Dias, M. A. S., Smith, J. N., Tomlinson, J. M., Tóta, J., and Wendisch, M.: The Green ocean Amazon Experiment (GoAmazon2014/5) observes pollution affecting gases, aerosols, clouds, and rainfall over the rain forest, *B. Am. Meteorol. Soc.*, 2016a, doi:10.1175/BAMS-D-15-00221.1.~~

Martin, S. T., Artaxo, P., Machado, L. A. T., Manzi, A. O., Souza, R. A. F., Schumacher, C., Wang, J., Andreae, M. O., Barbosa, H. M. J., Fan, J., Fisch, G., Goldstein, A. H., Guenther, A., Jimenez, J. L., Pöschl, U., Silva Dias, M. A., Smith, J. N., and Wendisch, M.: Introduction: observations and modeling of the green ocean Amazon

(GoAmazon2014/5), Atmos. Chem. Phys., 16, 4785-4797, 2016^b, 10.5194/acp-16-4785-2016.

Martin, S. T., Artaxo, P., Machado, L., Manzi, A. O., Souza, R. A. F., Schumacher, C., Wang, J., Biscaro, T., Brito, J., Calheiros, A., Jardine, K., Medeiros, A., Portela, B., Sá, S. S. d., Adachi, K., Aiken, A. C., Albrecht, R., Alexander, L., Andreae, M. O., Barbosa, H. M. J., Buseck, P., Chand, D., Comstock, J. M., Day, D. A., Dubey, M., Fan, J., Fast, J., Fisch, G., Fortner, E., Giangrande, S., Gilles, M., Goldstein, A. H., Guenther, A., Hubbe, J., Jensen, M., Jimenez, J. L., Keutsch, F. N., Kim, S., Kuang, C., Laskin, A., McKinney, K., Mei, F., Miller, M., Nascimento, R., Pauliquevis, T., Pekour, M., Peres, J., Petäjä, T., Pöhlker, C., Pöschl, U., Rizzo, L., Schmid, B., Shilling, J. E., Dias, M. A. S., Smith, J. N., Tomlinson, J. M., Tóta, J., and Wendisch, M.: The Green ocean Amazon Experiment (GoAmazon2014/5) observes pollution affecting gases, aerosols, clouds, and rainfall over the rain forest, B. Am. Meteorol. Soc., 2017, doi:10.1175/BAMS-D-15-00221.1.

Ng, N., Canagaratna, M., Jimenez, J., Chhabra, P., Seinfeld, J., and Worsnop, D.: Changes in organic aerosol composition with aging inferred from aerosol mass spectra, Atmos. Chem. Phys., 11, 6465-6474, 2011, 10.5194/acp-11-6465-2011.

Nguyen, T. B., Coggon, M. M., Bates, K. H., Zhang, X., Schwantes, R. H., Schilling, K. A., Loza, C. L., Flagan, R. C., Wennberg, P. O., and Seinfeld, J. H.: Organic aerosol formation from the reactive uptake of isoprene epoxydiols (IEPOX) onto non-acidified inorganic seeds, Atmos. Chem. Phys., 14, 3497-3510, 2014, 10.5194/acp-14-3497-2014.

Riva, M., Budisulistiorini, S. H., Chen, Y., Zhang, Z., D'Ambro, E. L., Zhang, X., Gold, A., Turpin, B. J., Thornton, J. A., Canagaratna, M. R., and Surratt, J. D.: Chemical

- characterization of secondary organic aerosol from oxidation of isoprene hydroxyhydroperoxides, *Environ. Sci. Technol.*, 2016, 10.1021/acs.est.6b02511.
- St. Clair, J. M., Rivera-Rios, J. C., Crouse, J. D., Knap, H. C., Bates, K. H., Teng, A. P., Jørgensen, S., Kjaergaard, H. G., Keutsch, F. N., and Wennberg, P. O.: Kinetics and products of the reaction of the first-generation isoprene hydroxy hydroperoxide (ISOPOOH) with OH, *J. Phys. Chem. A*, 2015, 10.1021/acs.jpca.5b06532.
- Surratt, J. D., Lewandowski, M., Offenberg, J. H., Jaoui, M., Kleindienst, T. E., Edney, E. O., and Seinfeld, J. H.: Effect of acidity on secondary organic aerosol formation from isoprene, *Environ. Sci. Technol.*, 41, 5363-5369, 2007a, 10.1021/es0704176.
- Surratt, J. D., Kroll, J. H., Kleindienst, T. E., Edney, E. O., Claeys, M., Sorooshian, A., Ng, N. L., Offenberg, J. H., Lewandowski, M., Jaoui, M., Flagan, R. C., and Seinfeld, J. H.: Evidence for organosulfates in secondary organic aerosol, *Environ. Sci. Technol.*, 41, 517-527, 2007b, 10.1021/es062081q.
- Thalman, R., in preparation.
- Ulbrich, I., Canagaratna, M., Zhang, Q., Worsnop, D., and Jimenez, J.: Interpretation of organic components from Positive Matrix Factorization of aerosol mass spectrometric data, *Atmos. Chem. Phys.*, 9, 2891-2918, 2009, 10.5194/acp-9-2891-2009.
- Wong, J. P., Lee, A. K., and Abbatt, J. P.: Impacts of Sulfate Seed Acidity and Water Content on Isoprene Secondary Organic Aerosol Formation, *Environ. Sci. Technol.*, 49, 13215-13221, 2015, 10.1021/acs.est.5b02686.
- Worton, D. R., Surratt, J. D., LaFranchi, B. W., Chan, A. W. H., Zhao, Y., Weber, R. J., Park, J.-H., Gilman, J. B., de Gouw, J., Park, C., Schade, G., Beaver, M., Clair, J. M. S., Crouse, J., Wennberg, P., Wolfe, G. M., Harrold, S., Thornton, J. A., Farmer, D. K., Docherty, K.

- S., Cubison, M. J., Jimenez, J.-L., Frossard, A. A., Russell, L. M., Kristensen, K., Glasius, M., Mao, J., Ren, X., Brune, W., Browne, E. C., Pusede, S. E., Cohen, R. C., Seinfeld, J. H., and Goldstein, A. H.: Observational insights into aerosol formation from isoprene, *Environ. Sci. Technol.*, 47, 11403-11413, 2013, 10.1021/es4011064.
- Xu, L., Guo, H., Boyd, C. M., Klein, M., Bougiatioti, A., Cerully, K. M., Hite, J. R., Isaacman-VanWertz, G., Kreisberg, N. M., Knote, C., Olson, K., Koss, A., Goldstein, A. H., Hering, S. V., de Gouw, J., Baumann, K., Lee, S.-H., Nenes, A., Weber, R. J., and Ng, N. L.: Effects of anthropogenic emissions on aerosol formation from isoprene and monoterpenes in the southeastern United States, *Proc. Natl. Acad. Sci. USA*, 112, 37-42, 2015, 10.1073/pnas.1417609112.
- Zhang, Q., Alfarra, M. R., Worsnop, D. R., Allan, J. D., Coe, H., Canagaratna, M. R., and Jimenez, J. L.: Deconvolution and quantification of hydrocarbon-like and oxygenated organic aerosols based on aerosol mass spectrometry, *Environ. Sci. Technol.*, 39, 4938-4952, 2005, 10.1021/es048568l.
- Zhang, X., Smith, K. A., Worsnop, D. R., Jimenez, J. L., Jayne, J. T., Kolb, C. E., Morris, J., and Davidovits, P.: Numerical characterization of particle beam collimation: part II integrated aerodynamic-lens–nozzle system, *Aerosol Sci. Technol.*, 38, 619-638, 2004, 10.1080/02786820490479833.

List of Supplementary Figures

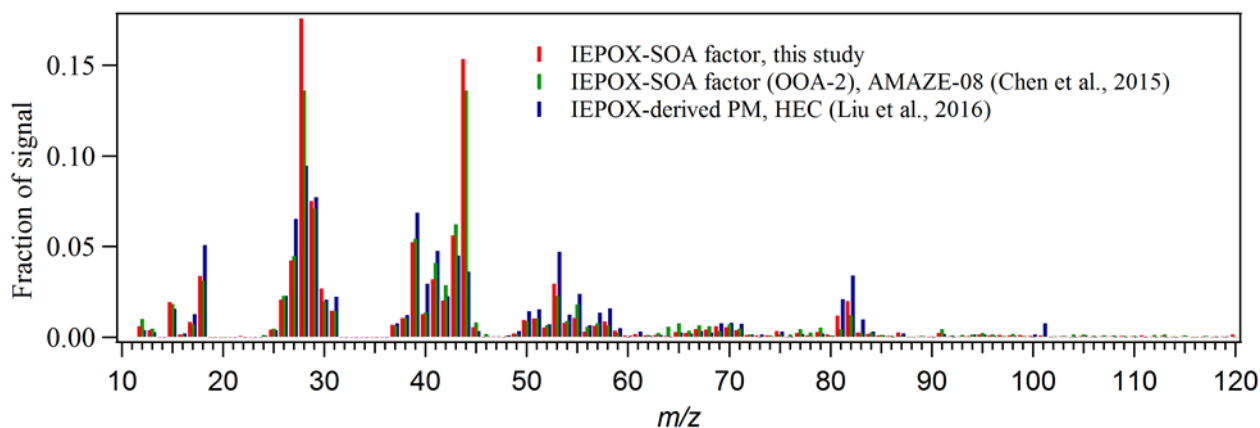


Figure S1. Profile of the IEPOX-SOA factor resolved by PMF analysis of the time series of AMS organic mass spectra collected in the wet season of 2014 (IOP1) at the T3 site (red), and in the wet season of 2008 (green) as part of AMAZE-08 experiment at the T0t site (Chen et al., 2015). Also plotted is the mass spectrum of secondary organic material produced in the Harvard Environmental Chamber from β -IEPOX photooxidation onto acidic ammonium sulfate seed particles under HO_2 -dominant conditions and $\text{RH} < 5\%$ (blue) (Liu et al., 2015). Pearson correlation coefficients R between the PMF factor of this study and the other spectra were: $R = 0.99$ for the AMAZE-08 PMF factor, $R = 0.81$ for the chamber spectrum with all ions included, and $R = 0.95$ for the chamber spectrum with m/z 44 and 28 excluded.

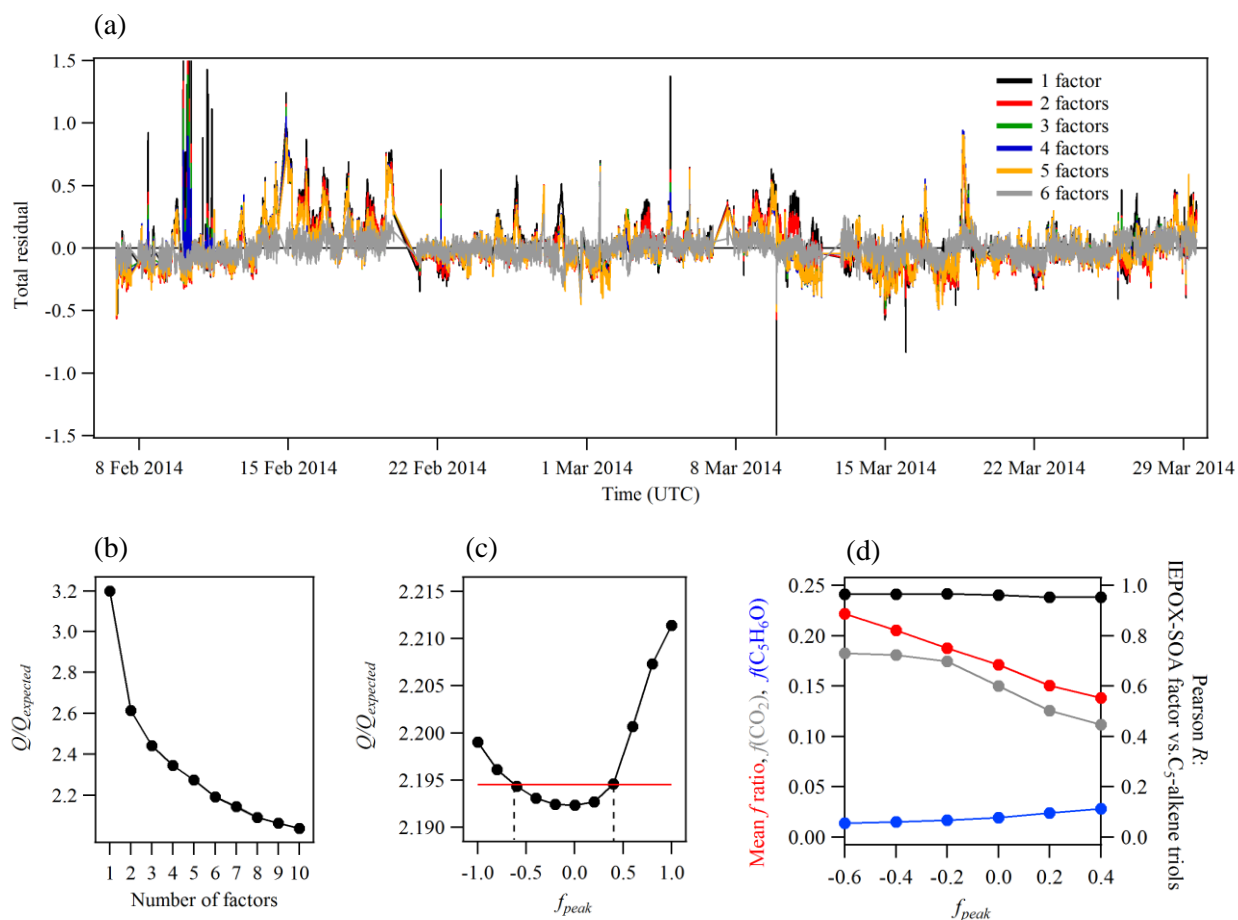
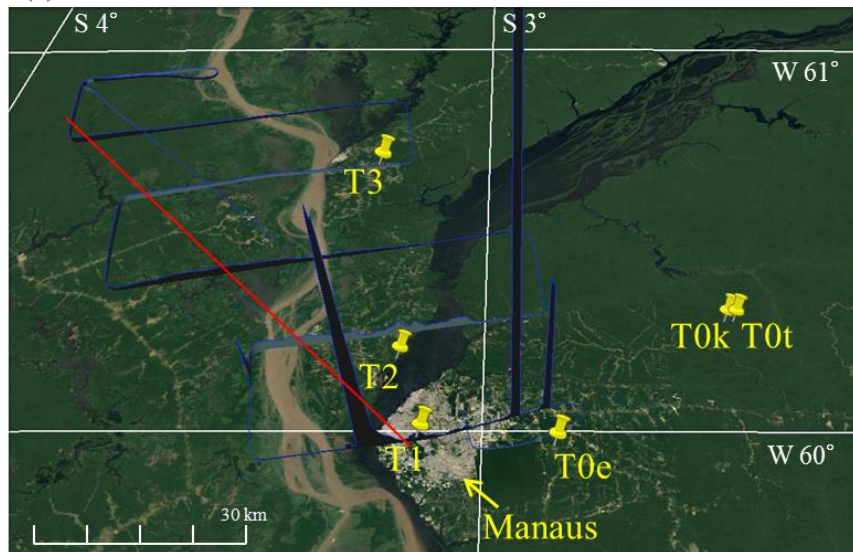


Figure S2. (a) Time series of total ion residuals of PMF solutions from one to six factors, (b) Dependence of the quality-of-fit parameter $Q/Q_{expected}$ on the number of factors for $f_{peak} = 0$, (c) Dependence of the quality-of-fit parameter $Q/Q_{expected}$ on f_{peak} for number of factors = 6. The red line represents $Q/Q_{expected}$ that exceeds in 0.1% the minimum value at $f_{peak} = 0$. This limit determines the range of plausible f_{peak} values as indicated by the dashed black lines, (d) For the six-factor solution, dependence on the f_{peak} parameter of the Pearson correlation coefficient R between the IEPOX-SOA factor loadings and independently measured C_5 -alkene triols (on the right vertical axis), the mean f ratio of IEPOX-SOA factor loading to total organic PM mass concentration, and the relative intensities $f(CO_2)$ and $f(C_5H_6O)$ of the ions CO_2^+ and $C_5H_6O^+$, respectively (on the left vertical axis).

(a) 3 March 2014



(b) 13 March 2014

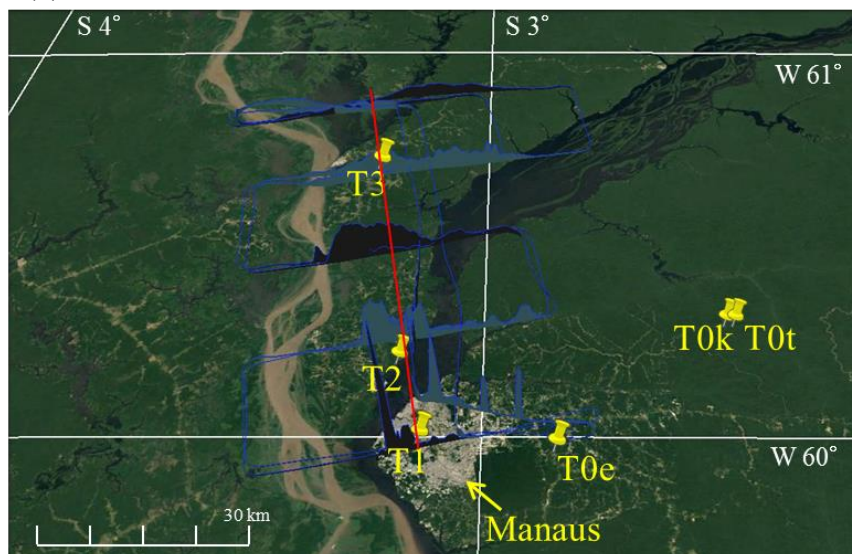


Figure S3. Visualization of the Manaus pollution plume for (a) March 3, 2014, 17:45 – 19:26 UTC, and (b) March 13, 2014, 14:14 – 17:21 UTC. The direction and extent of the plume observed within the boundary layer in the Manaus environs by the G-1 aircraft is represented by plotting NO_2 concentrations on a vertical axis (0.13 to 369 ppb on March 3 and 0.10 to 75 ppb on March 13). The red lines guide the eye through the central axis of the plume. An image of land cover is in the horizontal plane. Yellow pins indicate the locations of some of the GoAmazon2014/5 research sites, including T3 (Martin et al., 2016b).

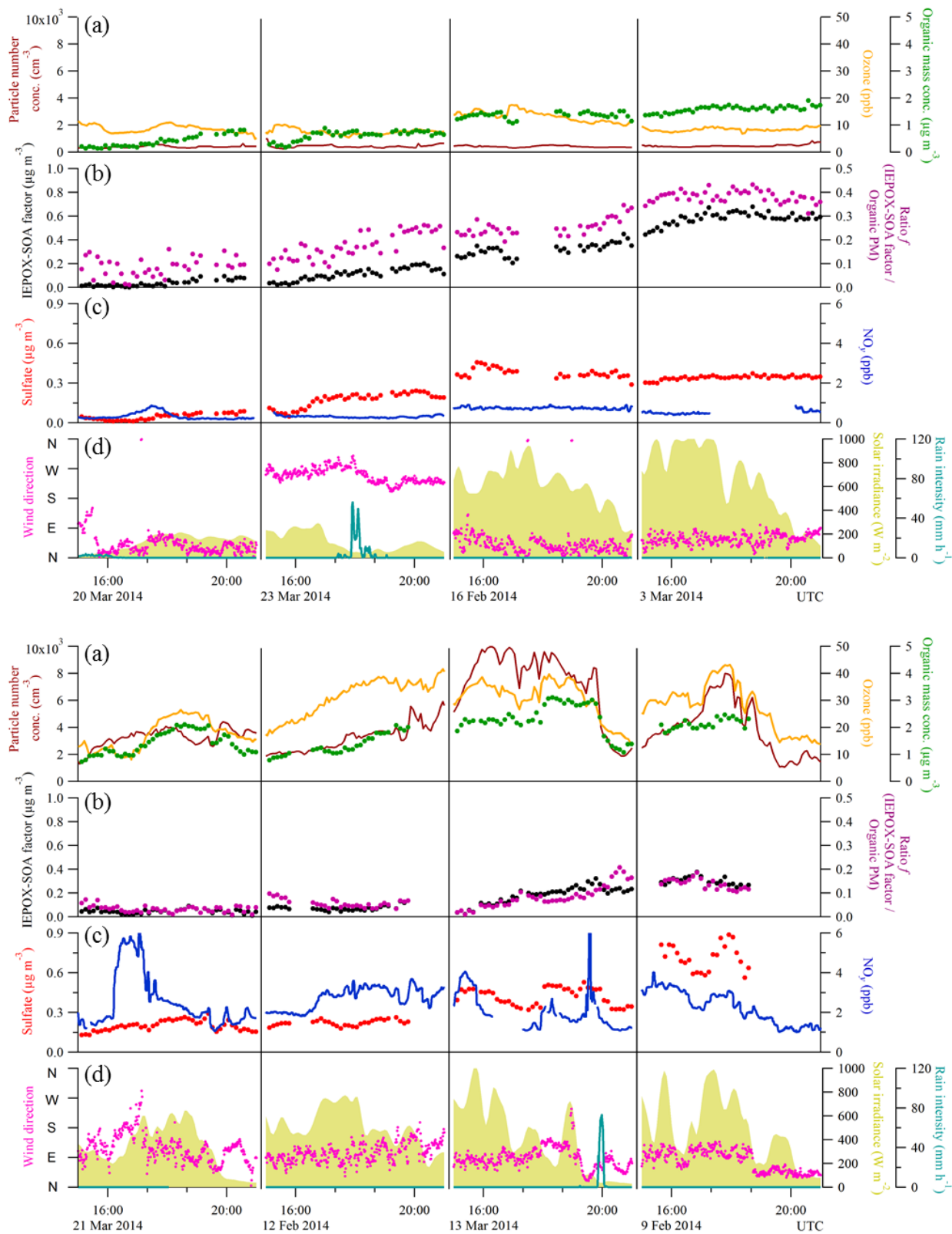


Figure S4. Selected cases of data sets collected during background and polluted conditions (top and bottom panels, respectively) as observed during afternoons at the T3 site.

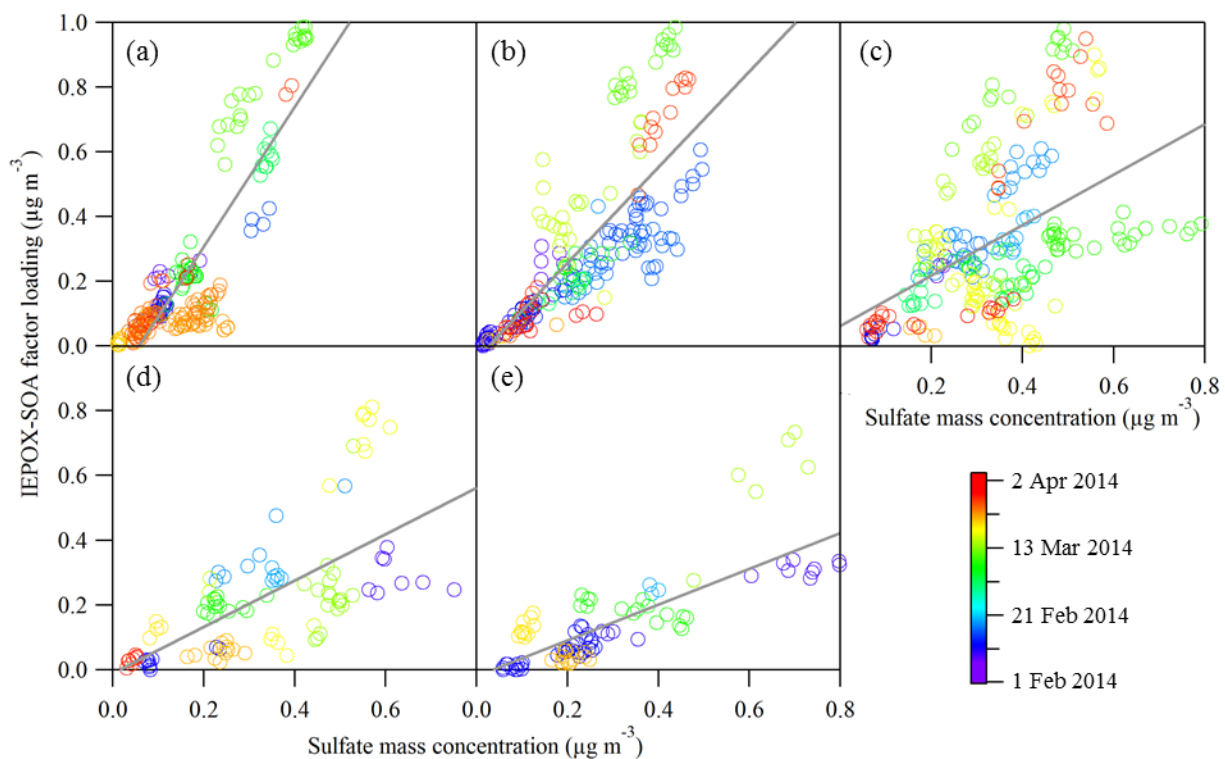


Figure S5. Scatter plots of sulfate mass concentration and IEPOX-SOA factor loading for local afternoon (12:00-16:00 local time; 16:00-20:00 UTC) for five different ranges of NO_y concentrations. Panels a-e correspond to groups labeled 1-5 according to Table 1. Table 1 presents the parameters of the six least-squares linear fits represented by the lines in the figure. Data is colored by date.

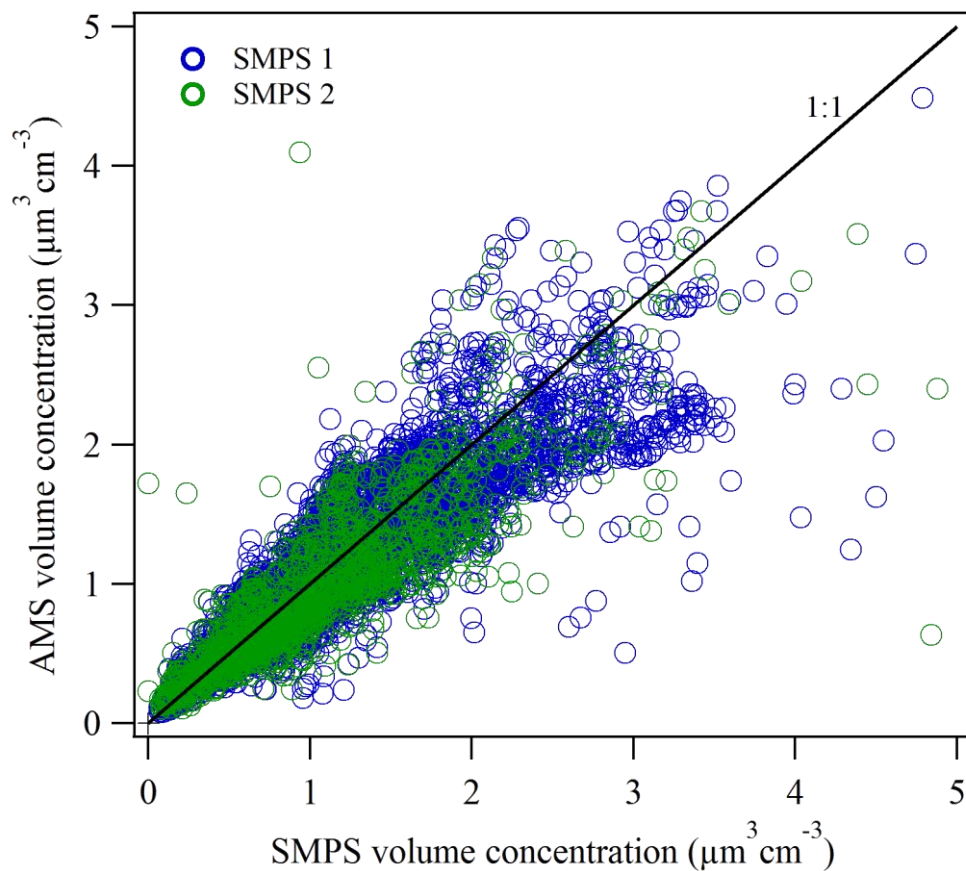


Figure S6. Scatter plot of AMS PM volume concentrations and SMPS PM volume concentrations. SMPS1 measured particles having mobility diameters of 10 to 461 nm from February 7 to March 28, 2014. SMPS2 measured particles having mobility diameters of 10 to 510 nm from February 24 to March 30. Material densities used in the calculation of AMS volume from AMS mass were based on a mixing rule for the five AMS-measured species. The material density of the organic component was calculated following the method of Kuwata et al. (2011) based on O:C and H:C values, which in turn were calculated following the method of Canagaratna et al. (2015).

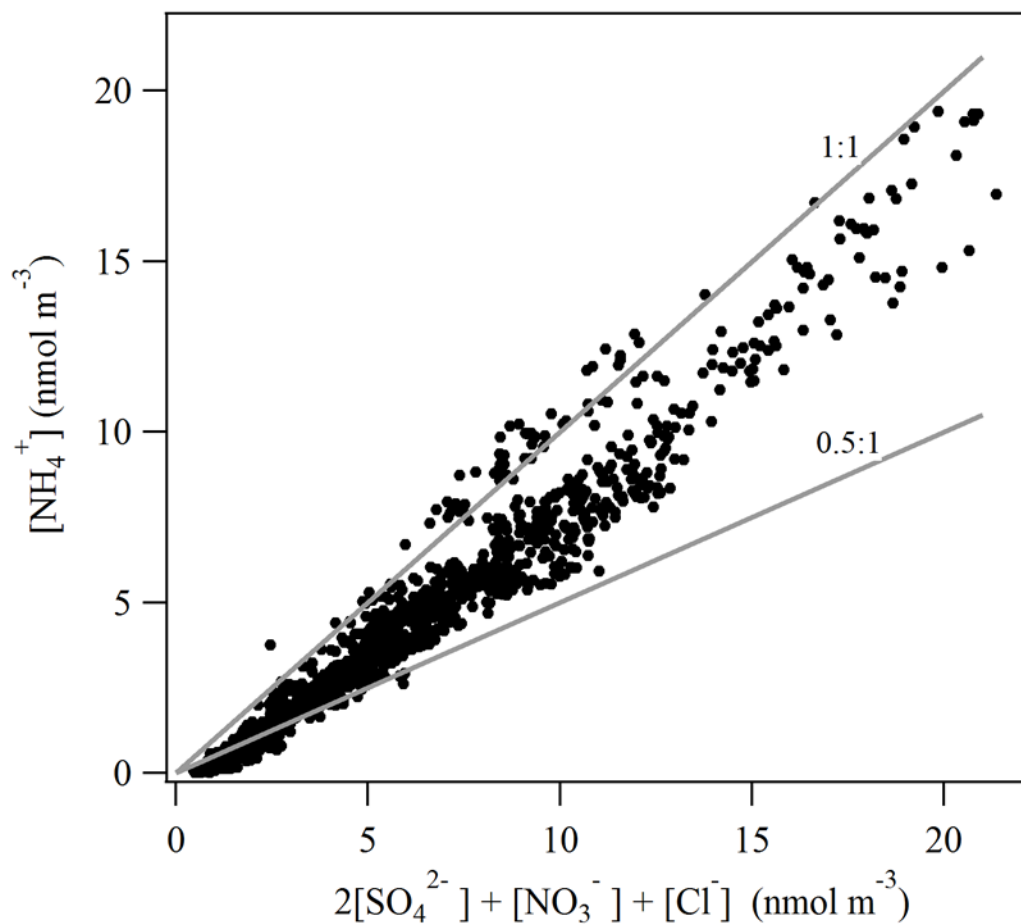


Figure S7. Ion balance for AMS measured species. A scatter plot is shown of mass concentrations of cations on the ordinate and of anions on the abscissa. Solid gray lines indicate relationships of 1:1 and 0.5:1.

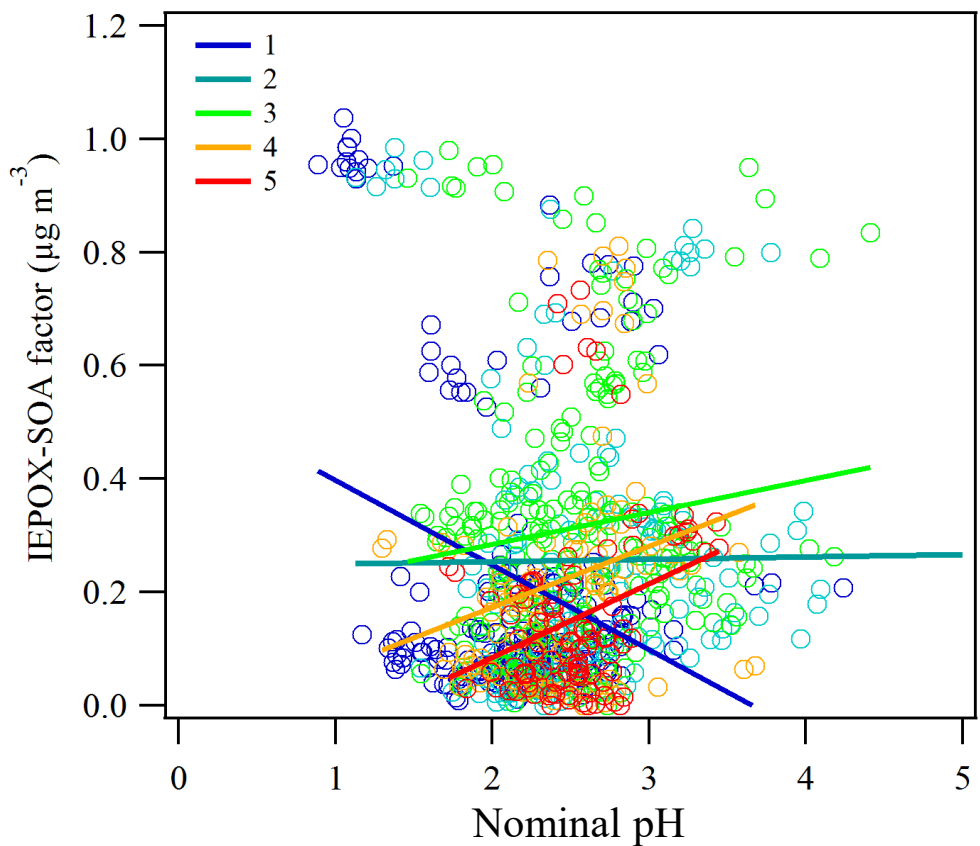


Figure S8. Scatter plot of estimated pH and IEPOX-SOA factor loading for local afternoon (12:00-16:00 local time; 16:00-20:00 UTC). The data sets were collected into five subsets, colored and labeled 1 to 5, based on NO_y concentration (analogous to analysis shown in Figure 6a).

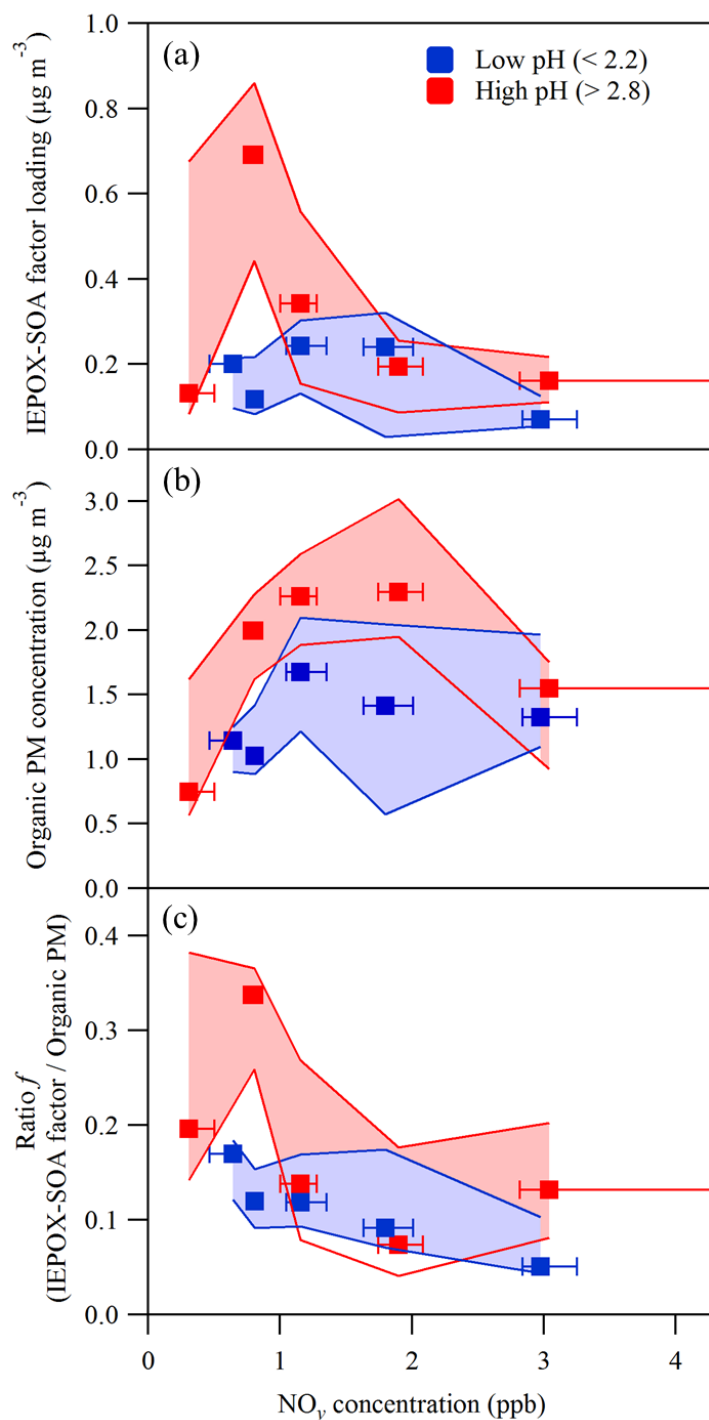


Figure S9. Dependence on NO_y concentration of (a) IEPOX-SOA factor loading, (b) organic mass concentration, and (c) the ratio f of the IEPOX-SOA factor loading to the organic PM concentration. Data are segregated by low (< 2.2) and high (> 2.8) pH and grouped into five levels of NO_y concentration (Figure 7). Squares represent medians of each group. Interquartile ranges are represented by whiskers along the abscissa and shading along the ordinate. The plotted data sets were recorded during local afternoon (12:00-16:00 local time; 16:00-20:00 UTC).